PHOTOPHYSICAL STUDIES ON SOME PORPHYRINS AND CYTOCHROME-C

A THESIS SUBMITTED
IN

FULFILMENT OF THE REQUIREMENT FOR
THE DEGREE OF

DOCTOR OF PHILOSOPHY

BY

HRANGHMINGTHANGA

TO

THE NORTH EASTERN HILL UNIVERSITY
SHILLONG - 793022
INDIA
APRIL 2002

TO

MY

MOTHER

NORTH EASTERN HILL UNIVERSITY
SHILLONG
(April, 2002)

I Hranghmingthanga, hereby declare that the subject matter of this thesis is the record of work done by me, that the contents of this thesis did not form basis of the award of any previous degree to me or to the best of my knowledge to anybody else, and that the thesis has not been submitted by me for any research degree in any other University/Institute.

This is being submitted to the North Eastern Hill University, Shillong for the degree of Doctor of Philosophy in Physics.

(HRANGHMINGTHANGA)

(Candidate)

9.4.02

(Prof. M.K. Panda)
Professor & Head,
Department of Physics,
North Eastern Hill Unversity,
Shillong-793022.
(Head)

1.4.2002

(Prof. A.L. Verma)

(Supervisor)

ACKNOWLEDGEMENT

It is with great pleasure that I wish to express my deepest sense of gratitude to Prof. ***A.L. Verma*** *for introducing me to this subject, his untiring supervision and guidance in carrying out this work. I am grateful to his constant patience with me during the time this work underway till its successful completion and indebted to him for his encouragement, advice, help and care.*

I am happy to record here my indebtedness and very special thanks to Mr. ***A. Bhattacharjee*** *and Mr.* ***A.K Rathore*** *for the most valuable help, support and affection I received from them throughout these years.*

I wish to thank Prof. ***D.T. Khathing*** *for his kind and invaluable help, all amidst his own busy schedule.*

I am grateful to many friends and colleagues who have directly or indirectly helped me in completing this work. My thanks are also due to Mr. ***B. Gogoi****, Dr.* ***A.K. Thakur****, Dr.* ***P.R Alapati****, Dr.* ***S.A. Hashmi*** *of NERIST for their wishes and supports.*

Words are inadequate to convey my very special thanks, love and appreciation to my parents for bearing with extraordinary patience and understanding the many hardships and inconveniences during these many years and for being a constant source of love, comfort and care.

I express my deep appreciation to NEHU for giving me the opportunity to undertake and complete this work successfully, to the Department of Science and Technology (DST) and to the Council of Scientific Industrial Research (CSIR), New Delhi, for providing the necessary financial assistance.

And thanks to Almighty God for being with me throughout these years and endow me with all His blessings.

Date: 9.01.02

Place: Shillong

(HRANGHMINGTHANGA)
Department of Physics
North-Eastern Hill University

CONTENTS

SYNOPSIS

SYNOPSIS

Porphyrins and their derivatives form an important class of compounds because of their very interesting physico-chemical properties as well as their crucial role in many biological functions. They constitute the chromophore of many biological molecules like hemoglobin, myoglobin, cytochromes, catalases, etc. Apart from their great biological importance, study of physical and chemical properties of these systems is also important in the fields like catalysis,[1] photoconductors, organic semiconductors,[2,3] superconductors, etc.

Because of their strong absorption in the visible and near UV region, resonance Raman (RR) spectroscopy provides a promising tool for studying molecular and electronic structure of porphyrins and their radicals. Under RR conditions the wavenumbers of the Raman bands exhibit sensitivity to changes in bonding arrangement, central metal, variation in its spin, oxidation and coordination states, etc., while the intensities of the bands are sensitive to the nature of the resonant excited electronic states.

The oxidized or reduced metalloporphyrins (π-cation or anion radicals) serve as transient intermediates in a variety of biological redox processes including light harvesting photosynthetic reaction center in chlorophylls and heme-protein reaction sequences.[4] The basic process of oxidation and reduction involves electron transfer. Oxidation is the process whereby a substance in a chemical reaction loses one or more electrons. This lost electron by one compound when taken up by another

compound or element leads to the complementary process of oxidation, which is called reduction.

Apart from usual chemical[5] or electrochemical[6] methods, porphyrin radicals can also be generated photochemically[7] by irradiation of the porphyrin solution by selected laser lines in the presence of external electron acceptors or donors. The addition or removal of electron from metalloporphyrins could involve both the porphyrin π-system and the central metal ion. The site of oxidation/reduction is influenced by many factors such as the electronegativity and oxidation state of the central metal,[8] peripheral substituents at the porphyrin ring,[9] axial ligands,[10] solvent, temperature and electronic interactions which govern the overlap of electron clouds of the donor and acceptor molecules.[11]

The current efforts are directed at understanding the electron transfer processes mediated by heme-related proteins in different biological systems. One such heme-protein is cytochrome-c (cyt-c), which shuttles electrons between two membrane-bound proteins, cytochrome-bc_1 complex and cytochrome-c oxidase, of the mitochondrial electron transfer chain. The active site is a mesoheme, which is covalently bound to the protein via two thioether linkages. At pH = 7, the heme iron adopts the Fe^{II}-, or Fe^{III}- low spin state and its two axial positions are occupied by methionyl (Met-80) and histidyl nitrogen (His-18).[12] Since the heme group is buried within the protein, several physicochemical studies have been conducted for delineating various pathways for movement of electron to the heme. Met-80 has been considered to play a crucial role in the redox process,[13,14] while according to other views, electrons may tunnel to the heme through some aromatic residues,[15,16] or through the exposed front portion of the heme edge.[17,18] A mixing of the iron t_{2g}

orbitals with the porphyrin π orbitals may extend the effective metal redox orbital density to the heme edge which may facilitate electron transfer to the metal. However there is no clear mechanism available for electron transfer mediated by cyt-c in spite of so many studies.

Although occurrence of photoreduction and photooxidation has been noticed in some other heme proteins upon laser irradiation at selected wavelengths,[19] nothing is known about their mechanisms, nature of electron donors and acceptors, etc. Ferri-cytochrome-c undergoes five distinct pH – dependent structural changes with pK_α values of 0.42, 2.50, 9.35 and 12.76 producing species with changed axial ligands, unfolding of protein or conversion to dimeric or polymeric forms under different conditions. We, therefore, undertook detailed investigations of the mechanism of photoreduction of cyt-c as a function of pH, oxygen, nitrogen or other inert gases, salt and buffer concentrations, etc. on the yield of photoreduction, using laser excited resonance Raman, UV-visible absorption and fluorescence emission studies. Such studies may help in identifying the possible electron donor to the heme during the electron transfer process, role of excited electronic states, information about transient intermediate species, state of the protein and other factors, which may help in establishing the mechanistic details of photoreduction of cyt-c.

In order to aid and understand the mechanism of photoreduction of cyt-c, we have also investigated the photophysical processes in some porphyrins initiated by selective laser irradiation in the presence of external electron acceptors like quinone, alkylchlorides, tetracyanoethylene or electron donor like substituted imidazoles using

resonance Raman and optical absorption techniques. Attempts have also been made to identify the transient intermediate species.

This thesis describes systematic RR and optical absorption studies carried out on free-base octaethylporphyrin (H_2OEP) and cobalt(II) *meso*-tetraphenylporphyrin ($Co^{II}TPP$) in the presence of external electron acceptors such as chloranil and quinone, and on cytochrome-c, in an effort to understand the mechanism of photoinduced redox reactions in the systems under selective laser irradiation. With free-base octaethylporphyrin, we carried out systematic studies to explore the detailed mechanism of photo-induced diacid formation in the presence of chloranil and p-benzoquinone as electron acceptors. Our detailed RR studies have revealed that protonation of the neutral free-base to yield the acid derivatives occurs through abstraction of proton from the solvent by an intermediate species formed during the process. When similar experiments were performed on $Co^{II}TPP$ sample, we observed occurrence of photooxidation. The photooxiadtion of $Co^{II}TPP$ was found to be sensitive to the presence or absence of molecular oxygen in the system. Depending on whether oxygen is present or not, oxidation occurred at the porphyrins ring or at the metal center. The study on cytochrome-c has been initiated with the aim of understanding the specific role of protein environment, conformation and axial ligands on the photoreduction of the hemeprotein. We monitored the photoreduction as a function of pH, excitation wavelengths, laser power, salt and buffer concentrations.

This thesis consists of seven chapters.

Chapter 1 presents a general review of resonance Raman studies, absorption spectra of porphyrins and other related studies on porphyrins and metalloporphyrins. Some of the important studies on oxidation-reduction products of porphyrins have been discussed in this chapter because of their relevance with this study. Importance of the photon-induced technique employed here for obtaining oxidation/reduction of porphyrin and metalloporphyrin complexes using selective laser irradiation and *in situ* monitoring of these processes by RR technique have been described.

Relevant theoretical aspects for an understanding of the electronic absorption and resonance Raman spectra of porphyrins and their metal derivatives are given in Chapter 2. Basic ideas about the principle of photophysical process are also given in this chapter.

Chapter 3 presents details of various experimental techniques employed in this study along with a brief description of the sample preparation, the lasers and laser Raman spectrometer, apart from details of other instruments and accessories used in conducting various experiments.

In Chapter 4, detailed studies on photo-induced formation of acid derivatives of free-base octaethylporphyrin under selective laser excitation in the presence of external electron acceptors like p-benzoquinone (p-BQ) and chloranil are presented. When laser line (406 or 441.6 nm) under aerobic or anaerobic conditions excites a solution of H_2OEP in CH_2Cl_2 containing p-BQ or chloranil, certain RR bands of H_2OEP shift to new positions. For example, the wavenumber for the ν_4 and ν_{11} modes shifted from 1369 and 1546 cm^{-1} to 1388 and 1561 cm^{-1}, respectively. The RR spectral profile of the photo-induced reaction product is similar to one obtained

with chemically prepared H_2OEP diacid. This observation confirms occurrence of photo-induced OEP diacid formation in the system. Other reaction products are generated due to porphyrin degradations irrespective of the presence or absence of molecular oxygen. Diacid formation also occurs in solvents like $CHCl_3$, $C_2H_4Cl_2$ and $C_2H_2Cl_4$, but not in others like CCl_4, CS_2 and C_6H_6. An unexpected observation is that H_2OEP shows no photooxidation in CCl_4 while H_2TPP shows very clean photooxidation , especially considering the similarity between the two compounds. On the other hand, in the simultaneous presence of p-BQ and methanol or ethanol, formation of OEP diacid was observed in CCl_4. In CH_2Cl_2 presence of methanol or ethanol greatly inhibits the formation of diacid. However, with excess concentration of the primary alcohol, we observed formation of OEP monoacid, which shows characteristic wavenumbers at 1385 and 1555 cm^{-1} for the ν_4 and ν_{11} modes. From the solvent dependent study, we are able to conclude that proton originates from the solvent used and the π-cation radical of OEP generated as transient species is believed to play crucial role in the abstraction of this proton from the solvent, in analogy with the photochemical formation of H_2TPP diacids. [20,21] The wavenumber shift pattern of the ν_{11} mode (10-16 cm^{-1}), involving mainly C_β–C_β bond, is in accord with the antibonding character of the a_u (a_{1u} in D_{4h} symmetry) orbital with respect to the C_β–C_β bond as expected for OEP complexes. However, a large upshift, 15-20 cm^{-1} in the wavenumber of the ν_4 (pyrrole half-ring stretch)$_{sym}$ mode in which the C_α–N and C_α–C_β bonds stretch out-of-phase, is inconsistent with these expectations since the a_u orbital is nonbonding and bonding, respectively, with respect to the C_α–N and C_α–C_β bonds. From an NMR study,[22] it was shown that protonation of

H_2OEP results in deshielding of the N-H protons and hence in a higher electron density on the methine C atom due to migration of negative charge from the anion counter ions to the positively charged porphyrin core. Accordingly, it is suggested that deshielding effect also increases electron densities in the C_α–N and C_α–C_β bonds of the acid derivatives, which get reflected in the large upshift of the ν_4 mode.

In Chapter 5, we report photooxidation of $Co^{II}TPP$ in the presence of p-BQ as electron acceptor probed by resonance Raman and absorption techniques. In CH_2Cl_2 solution, 441.6 nm laser excitation of $Co^{II}TPP$ in the presence of p-BQ under anaerobic conditions results in changes of absorption and RR spectra which are characteristics of $Co^{III}TPP^+$. No appreciable formation of the π-cation product was observed under these conditions. However, on allowing molecular oxygen in the system, other spectral changes were observed, which by comparing with chemically prepared $Co^{III}(TPP)^{2+\bullet}$ species, could be identified due to two-electron oxidation product of $Co^{II}TPP$. Since the formation of $Co^{III}(TPP)^{2+\bullet}$ was observed only in the presence of molecular oxygen, alkylchloride peroxy radicals are suggested to facilitate electron removal from the porphyrin ring. As expected for TPP radical complexes, the ν_2 mode shows downward shift by about 27 cm^{-1}, which is consistent with the a_{2u} character of the radical. Similar π-cation radical formation was also observed in other alkyl chloride solvents such as $C_2H_2Cl_4$ and $C_2H_4Cl_2$, but not in $CHCl_3$, CCl_4 and CS_2. The non-observation of photooxidation in the later group of solvents was attributed to (a) decrease in radical reactivity with increasing number of chloride substituents in the molecules;[23] (b) lower relative dielectric constants which decrease the efficiency of charge separation in the electron transfer process. [24]

Chapter 6 presents resonance Raman study of photoreduction of ferri-cytochrome-c as a function of excitation wavelengths, laser power, pH, salt and buffer concentrations. During the course of our resonance Raman (RR) studies we had noticed that purified monomeric cyt-c at neutral pH exhibits extensive photoreduction under anaerobic conditions upon laser irradiation in the 400-450 nm region. However, only partial photoreduction occurred at pH 10.1 where the sixth axial methionine ligand is replaced by lysine, and no photoreduction took place after the transitions with pK_a = 12.76 and 2.5 where the fifth axial histidine ligand is replaced by other residues. Observation of photoreduction of cyt-c only when it retains its folded conformation suggests that either the histidine ligand or the non-bonding aromatic amino acids, viz., Phe-82 or Tyr-67 could be the possible electron donors in the photoreduction process. Since ionization potential of such aromatic residues is much higher than the energy of the light at 400-440 nm, special mechanism involving a hole-induced electron transfer is proposed. The photoreduction of cyt-c was completely inhibited in the presence of oxygen suggesting active participation of a triplet state in this process. Presence of chloride or phosphate ion also produces inhibiting effect on the photoreduction process, and the effect is related to the type of anion rather than the cation counter part. The dependence of photoreduction on the nature of anion is expected to be a consequence of binding of the ion to some specific cationic amino acids like lysines on the surface and in the proximal part of the protein. Apart from these, detailed experiments were also conducted on the photoreduction as a function of excitation wavelength with constant photon flux. We find that the relative quantum yield for photoreduction of pure cyt-c at neutral pH as a function of excitation wavelengths shows a weak

maximum centered around 410 nm while it increases almost exponentially when excitation wavelength is moved from 380 to 330 nm. This type of behavior is a manifestation of different mechanisms of photoreduction: direct participation of non-bonding aromatic amino acid of the protein in the excitation region below 360 nm and active participation of excited states of the heme group in the 400-440 nm region. During the process of photoreduction, there always exists photo-oxidation, which competes strongly with the photoreduction even under anaerobic condition.

Chapter 7 gives summary and conclusions drawn from our spectroscopic studies in this thesis for understanding the mechanism of photo-induced redox reactions in simple model compounds and in a hemeprotein. Suggestion for extension of this work for future studies are also made which may help in confirmation of the proposed mechanism and other aspects discussed in this thesis.

References

1. Fleischer, E.B.; Krishnamurthy, M. *J. Am. Chem. Soc.* 1972, 94, 1382.

2. Wolf, M. *Electronics* 1963, 36, 35.

3. Haak, F.; Molta, J. *J. Chem. Phys.* 1967, 38, 2648.

4. Chang, C.K.; Dolphin, D. in *Bioinorganic Chemistry*; Tamolen E.E.V., Ed.; Acad. Press: New York, 1978; Vol. II, pp. 37.

5. Reddy, D.; Reddi, N.S.; Chandrashekar, T.K. *Inorg. Chem. Acta* 1989, 166, 147.

6. Kadish, K.M. in *Iron Porphyrins*, Lever, A.B.P.; Gray, H.B., Eds.; Addison-Wesley Publishing Company Inc.: Massachusetts (USA), 1983; Part II, pp.161-249.

7. Gasyna, Z.; Browett, W.R.; Stillman, M.J. *Inorg. Chem.* 1985, 24, 2440.

8. Bucher, J.W.; Kodish, W.; Smith, P.D. in *Structure and Bonding (Berlin)* 1978, 34, 79.

9. Kadish, K.M.; Morrison, M.M. *Bioinorg. Chem.* 1977, 1, 107.

10. Whitten, D.G.; Meyer, T.J. *J. Am. Chem. Soc.*, 1973, 95, 5939.

11. Mataya, N.; Kubota in *Molecular Interactions and Electronic Spectra*; Marcel Dekker: New York, 1970; chapter 6, pp. 201-291.

12. Dickerson, R.E.; Timkovick, R. in *Enzymes*; 3rd Ed.; 1975.

13. Takano, T.; Dicherson, R.E. *Proc. Natl. Acad. Sci. USA* 1980, 77, 6371.

14. Lambeth, D.O.; Capbell, K.L.; Zand, R.; Palmer, G. *J. Biol. Chem,* 1973, 248, 8130.

15. Iseid, S.S.; Vassilian, A. *J. Am. Chem. Soc.* 1984, 106, 1726.

16. Salemme, F.R. in *Tunneling in Biological Systems*, Chance, B.; Marcus, R.; Devault, D.; Schrieffer, J.R.; Frauenfelder, H.; Sutin, N., Eds.; Acad. Press: New York, 1979; pp. 523-541.

17. Chance, B.; Devault, D.; Legallais, V.; Melta, L.; Yanetani, T. in Nobel Symposium 5; Claesson, S., Ed.; Interscience: New York, 1967; pp. 437-468.

18. (a) Butler, J.; Davies, D.M.; Sykes, A.G.; Koppenol, W.H.; Osheroff, N.; Margoliash, E. *J. Am. Chem. Soc.* 1981, 103, 469. (b) Armstrong, F.A.; Hill. H.A.O.; Walton, N.J., in *Quart. Rev. Biophys.* 1985, 18, 261.

19. (a) Adar, F.; Yonetani, T. *Biochim. Biophys. Acta,* 1978, 502, 80. (b) Salmeen, F.; Rimai, L.; Babcock, G.T. *Biochemistry* 1978, 17, 800. (c) Kitagawa, T.; Nagai. K. *Nature (London)* 1979, 281, 503. (d) Ogura, T.; Sone, N.; Tagawa, K.; Kitagawa, T. *Biochemistry*, 1984, 23, 2826. (e) Kitagawa, T.; Chihara, S.; Fushitani, K.; Morimoto, H. *J. Am. Chem. Soc.* 1984, 106, 1860. (f) Verma, A.L. et al. *J. Am. Chem. Soc.* 1988, 110, 6617.

20. Varani, G.; . Maldotti, A.; C. Bartocci, C. *New J. Chem.*, 1992, 16, 827.

21. Saini, G.S.S.; Mehdi, O.K.; Verma, A.L. *Chem. Phys. Lett.*, 2000, 322, 293.

22. Ogoshi, H.; Watanabe, E.; Yoshida, Z. *Tetrahedron*, 1973, 29, 3241.

23. Bansal, R.K. *Organic Reaction Mechanism*, 2nd Ed.; TATA McGraw-Hill Publishing Co. Ltd.: New Delhi, 1986; pp. 207-258.

24. O'Driscoll, E.; Simon, J.D.; Peters, K.S. *J. Am. Chem. Soc.* 1990, 112, 7091.

CHAPTER 1

INTRODUCTION

Porphyrins and their metal derivatives, which form the chromophore in such important natural complexes as chlorophylls, vitamin B_{12}, haem of the blood and others, represent a vast and unique group of intercomplex compounds. Scientists in the fields like Mathematics, Physics, Chemistry, Biochemistry, Biology and medicine are currently involved in different type of investigations of these systems and their numerous analogues and derivatives. The specific features and great diversity of porphyrins, particularly metalloporphyrins, are the factors responsible for their importance and wide distribution in nature, their extensive use in various physical, physicochemical, quantum-chemical, and biological studies, as well as in the production of dyes, semiconductors, and catalysts.

A large number of biological systems are known in which metalloporphyrins act as initiators of a particular biological process. Owing to their great biological importance, a large group of metalloporphyrins has been synthesized because of their obvious relevance as biological models.[1,2] Most of these investigations have involved chlorophyll[3-7] which, being a part of the protein-lipid system, initiates photosynthesis in green plants and in photosynthetic bacteria. The chloropylls found in green plants are magnesium complexes of derivatives of dihydroporphins known as chlorin, while in photosynthetic bacteria the function of chlorophyll is performed by its structural analogue related to the terahyroporphin known as bacteriochlorophyll.

Another biologically important metalloporphyrin, which received many theoretical and experimental studies, is iron-protoporphyrin.[8-11] Being part of the

protein complex of haemoglobin, it is known as haem of the blood. Other biological systems containing iron-porphyrins include myoglobin, cytochromes, catalases, and peroxidases. Altogether, the biological importance of these hemoproteins are due to their three distinct functions: myoglobin and hemoglobin serve as reversible oxygen transport proteins;[12] the cytochrome b's and c's function as reversible one-electron transfer agents;[13] and the cytochrome-P_{450}, peroxidases and catalases are involved in irreversible, covalent transformation of substrates.[14] In spite of these diverse functions, all hemoproteins have the unifying feature of a common active site or "prosthetic" group composed of an iron-porphyrin complex, namely iron-protoheme IX. It is this " chromophore" which is the center of all the diverse functions of hemoproteins.

The oxygen that is reversibly transported binds directly to the iron in competition with other small molecules. The one-electron transfer in cytochrome occurs by reversible oxidation-reduction between ferrous and ferric states of iron. Cytochrome-P_{450} catalyzes the necessary function of substrate hydroxylation in living organism.[15] Hydroxylation of substrate molecules by cytochrome-P_{450} occurs by transfer of an oxygen atom directly bound to the iron. Peroxidases and catalases catalyze a wide variety of organic or inorganic compounds by hydrogen or alkyl peroxides.[12b,16] These enzymes react with peroxides to produce an oxidized enzyme intermediate referred to as compound I. The intermediates formed by peroxidases and catalases are thought to involve oxygen atom binding directly to the iron of the heme groups itself.[17,18] While the remainder of the protein obviously plays a large role in modulating their biological activity, there is a great deal of evidence that the

biological function of hemoproteins is determined to a large extent by the conformational and electronic properties of the heme group.

Apart from their great biological importance, natural porphyrins and their synthetic analogues are finding a host of biomedical and industrial uses. It has been suggested that disturbances in porphyrin metabolism causes diseases[19] related to drug metabolism, porphyria and cancer, while hematoporphyrin derivatives[20,21] in combination with laser irradiation have been used in photodynamic cancer therapies. On the other hand, broad possibilities for using porphyrin complexes are being opened up in the fields like catalysis,[22] photoconductors, organic semiconductors,[23,24] superconductors,[25] solar and fuel cells,[26] lasers,[27] and as chemical shift reagents.[28] For example, porphyrins have been used for solar energy conversion, because of their good light-absorbing properties and favorable redox potential for photochemical water splitting.[29] Stacks of metalloporphyrins and metallophthalocyanines are good organic conductors,[30] and the liquid crystalline properties of porphyrins have been studied extensively.[31,32] Besides these, several porphyrin related compounds, particularly, phthalocyanines have been used in photovoltaic and photoelectrochemical cells, as a high density optical storage material, as dyes in textile, painting, printing and paper industries, as well as in producing heavy isotopes of some elements and oxidation-reduction indicators.[27, 33-35]

The basic structure of the free base porphin (H_2P) is shown in Fig 1.1. The porphin nucleus consists of four pyrrole rings, fused together by methine bridges to form a macrocycle. In general, the peripheral positions are numbered from 1 to 8 and interpyrrolic methine positions are designated as α, β, γ, δ and usually term as *meso*

position. Carbon atoms designations C_α, C_β and C_m are also shown in Fig. 1.1. If all the positions labeled 1 to 8, and α to δ are occupied by hydrogen atoms and if there are two hydrogen atoms at the center, we get the simplest derivative of porphyrin, called "free base porphin" or H_2P. If the central core hydrogen atoms are replaced by a metal ion, the system is known as metalloporphyrin (MP). Porphyrins are formally derived from porphin by substitution of some or all the peripheral hydrogens with various side-chains. Depending on the nature of the substituents at the periphery of the ring and at the methine positions, the complexes are known by specific nomenclature. Fig. 1.1 gives the structure and nomenclature of some of the commonly known porphyrins. The basic molecular structures of free base octaethylporphyrin, cobalt tetrapheylporphyrin and iron protoporphyrin IX (prosthetic group of cytochrome-c) are shown in Fig. 1.2.

In the metal derivative, the central metal atom finds itself in a symmetrical electrostatic field of four nitrogen atoms with which it may form four equivalent, or almost equivalent, coordinate donor-acceptor bonds. If the interaction between the metal and the porphyrin anion is primarily electrostatic, labile ion complexes are formed. These include complexes of Na^+, K^+, Rb^+, Cs^+, Be^{2+}, Sr^{2+}, Ba^{2+}, Ca^{2+}, and some other ions. But if the electrostatic interaction involves filling of the vacant orbitals of the central atom by the electrons of the donor N atoms of the ligand, stable porphyrin complexes of the covalent or predominantly covalent type are formed. In this case we have complexes of Fe^{2+}, Fe^{3+}, Co^{2+}, Ni^{2+}, Cu^{2+}, Zn^{2+}, Mn^{3+}, Cr^{3+}, Al^{3+}, Ga^{3+}, Si^{4+}, Ge^{4+}, Sc^{3+}, Ti^{4+}, VO^{2+}, Pt^{4+}, and other cations.

Another salient feature of porphyrins is their structural diversity, which can be seen from Fig 1.1. Porphyrins differ in the nature of the bridging groups

occupying meso positions in the porphyrin molecule. The bridging groups may only be –C=, –(X)C=, –N=, or their combinations. The structural diversity is further enhanced by the presence of various pyrrole substituents (R_1-R_8) which may be H, CH_3, C_2H_5, $CH{=}CH_2$, $CH(OH)CH_3$, C(O)H, COOH, CH_2COOH, and CH_2CH_2COOH. Moreover, if one or more pyrrole double bonds are hydrogenated, then the diversity of molecular structures of porphyrins, chlorins, azaporphyrins, phthalocyanines, phorbins, and so on becomes more evident. Some of the basic skeletons of modified porphyrin ring are shown in Fig. 1.3.

The specific features of metalloporphyrins as intercomplex compounds are due not only to the polydentate (tetradentate) nature of the ligand but also to its rigidity. Because of its high rigidity the porphyrin ligand imposes specific requirement on the geometric parameters of the metal ion, whereby they form two clearly defined groups of stable or labile complexes. Characteristically, the metal ion that has entered into coordination with a porphyrin is in fact a partner of the conjugated porphyrin system and may either stabilize or destabilize it. Owing to this direct contact with the atoms of the conjugated system it influences all, even the most remote parts, of the large molecule and alters the oxidation-reduction, acid-base, electron-optical, and all other properties of the porphyrin.

Finally, an important and unique feature of porphyrins and their metal derivatives is their electronic absorption and emission spectra. The diversity of metalloporphyrins corresponding to the great variety of porphyrins, the typical arrangement of spectral bands, the sensitivity to certain effects on the molecule and their complexity, make them not only a most reliable means for identifying porphyrins but also a rich source of information on the structure of porphyrins, the

type of coordination, the interaction between substituents and ionizing media, and the intramolecular energies.

The absorption spectra of all metalloporphyrins have some features in common.[36] They all exhibit a very intense band between 380 nm and 420 nm, called Soret or B or γ band; a much weaker band between 500 and 600 nm, called Q(0,0) or α band along with an associated vibronic side band called Q(0,1) or β band on the lower wavelength side of the α band. To the blue of the Soret band, metalloporphyrins generally show a weaker N band around 325 nm and an M band around 215 nm. Between these they often show a weaker L band. A typical absorption spectrum of NiOEP is shown in Fig. 1.4. In general, the electronic spectra of the nearly planar metalloporphyrins may be ascribed to the transition of the delocalized π-electrons which have their maximum density above and below the plane of the molecule. The σ-electrons are considered to be strongly localized and do not take part in the electronic transitions in the visible region of the spectrum. In addition to the normal $\pi \rightarrow \pi^*$ transitions, the absorption spectra of certain metalloporphyrins, for example involving Mn(III) and Fe(III) porphyrins, contain extra bands which may arise due to metal d→d transitions, configuration interaction between the porphyrin excited triplet and singlet states or the charge transfer transitions.[37]

Studies on the optical absorption and emission data of the "Periodic Table of the Porphyrins" allows a classification of metalloporphyrins into two broad classes called regular and irregular porphyrins.[36] The regular metalloporphyrins contain metal with closed electronic shells (e.g. Zn, Cd), while the irregular

metalloporphyrins contain metal (e.g. Fe, Co, etc.) with partly filled shells. For regular porphyrins the optical and emission spectra are determined essentially by the π-electrons of the porphyrin ring, with only minor perturbation from the electrons of the central metal. In the case of irregular porphyrins, the metal orbital have much stronger effects on the absorption and emission characteristics, either through stronger mixing with the ring orbitals or through the introduction of new low energy optical transitions. The regular porphyrins generally show normal absorption and emission spectra while irregular porphyrins differ from the regular ones in emission properties and most cases in absorption also. The unusual absorption types of irregular porphyrins can be further divided into hypso and hyper types. Absorption spectra for hypsoporphyrins are like normal absorption spectra but are blue shifted. Such spectra are shown by transition metal porphyrins of Groups VIII and IB with metal configuration d^m, m = 6 to 9, that have their e_g (d_π) orbitals filled. Metal-porphyrins with hyper absorption spectra show prominent extra absorption bands in addition to the usual Q, B and N bands in the region λ>320 nm. Changes in the oxidation state of the central metal ion and π-cation and anion radical formation also cause large changes in the absorption spectra of porphyrins. All the atomic groups known to form complexes with porphyrins are listed in Table 1.1, which also shows regular or irregular valences. The Table also displays the distribution of hypso and hyper porphyrin absorption types.

The absorption spectra of porphyrins can be perturbed to a greater or lesser extent by various chemical modifications or substitutions to the basic structure. Electrophilic side-chains such as vinyl or formyl groups found in some naturally occurring porphyrins and hemes, cause shift of the visible and Soret bands to longer

wavelength. Similarly, absorption bands in the tetraphenylporphyrin (TPP) complexes are red shifted compared to the octaethylporphyrins (OEP). The latter, in turn, are somewhat red shifted from complexes of porphin (H_2P). A change in the solvent often causes a spectral shift of a few nanometers depending upon the nature and physical properties of the solvent. The stable porphyrin chelating with metals such as Ni(II), Co(II) and Cu(II) show the order of intensities $\alpha>\beta$ while for the less stable chelates such as those with Mg(II), Zn(II), Cd(II), etc, this ratio is decreased or reversed.[38] On further coordination of metalloporphyrins at the axial positions, there is, in general, red shift of absorption bands depending on whether one or two extra ligands are added. The theoretical details of the absorption spectra of metalloporphyrins will be discussed in Chapter 2.

Beside the electronic absorption and emission studies, other numerous experimental techniques have been employed to study the various intrinsic physical and chemical properties of model porphyrin complexes that have direct bearing on their biophysical and biochemical functions. These include, X-ray studies,[39-43] electron spin resonance (ESR),[44-49] nuclear magnetic resonance (NMR),[49-52] cyclic voltammetry,[53] Mössbauer,[54,55] infrared (IR),[56] Raman spectroscopy,[57-61] magnetic susceptibility measurements,[62] magnetic circular dichronism (MCD),[63] etc. At the same time, many theoretical approaches including quantum mechanical calculations have been attempted which have helped to rationalize many experimental results.[64 65]

The extreme sensitivity of the vibrational frequencies of these macromolecules to the geometric and bonding arrangements of the localized groups in the molecule lends itself for studies of the intermolecular interactions of these systems in a continued effort for an understanding of the mode of functioning of

biosystems. The appearance of the laser as a convenient source of monochromatic radiation has facilitated Raman studies that attempt to correlate vibrational information with molecular structure. Although infrared spectroscopy yields intensities and energies of active modes, its utility in the study of porphyrins to date has been secondary to electronic absorption spectroscopy. A major obstacle in extracting structural information is the wealth of infrared-active modes in the porphyrin skeleton and problems related to interpret subtle changes in the spectra. Additionally, great interest resides in alterations of the porphyrin when it serves as a prosthetic group. But extraction of vibrations unique to the porphyrin in the presence of protein matrix is a formidable problem with IR spectroscopy.

The necessity of a technique that selectively exhibits porphyrin vibrations now exists with advances in Laser Raman spectroscopy.[66-68] The advent of lasers and innovations in pulse counting detection techniques have caused a renaissance in the use of Raman spectroscopy as a powerful tool in Physics, Chemistry and biosciences during the last three decades or so.

Raman scattering arises as a result of interaction of electromagnetic radiation with matter resulting in the change of frequency of the scattered radiation. Non-resonance or normal Raman spectroscopy consists of irradiating a molecule in a spectral region far removed from its electronic transitions. The scattered radiation is weak and high concentrations of the species are required under study.[69] In contrast, when a compound is excited with incident light whose frequency is within an electronic absorption band, the intensity of some Raman spectral lines is greatly and selectively enhanced. The effect is called resonance Raman (RR) scattering, and is due to coupling of electronic and vibrational transitions. By tuning the excitation

frequency through the optically allowed transitions of the system, i.e., under resonance, the intensity enhancement of vibrations coupled to electronic transitions may be 10^3 to 10^6 times higher than the intensity observed during normal Raman scattering. The significant increase in intensity allows one to work at much lower sample concentration. The peak position of vibrational modes in the resonance Raman spectra is a property of the ground electronic state, while the peak intensity of a particular mode is strongly dependent on the properties of the excited electronic states. The theoretical details of resonance Raman scattering will be dealt in Chapter 2.

In the past few decades, there has been an exponential increase in the use of resonance Raman (RR) spectroscopy for the study of structure-function relationships in biological compounds.[70-73] Normally the site of biological activity is close to the positions of biological chromophores, and there are many biological compounds containing chromophore groups that give rise to resonance Raman spectra. Under resonance conditions, the lines due to the vibrational modes of the chromophore or adjacent group of atoms are selectively enhanced, and the number of Raman bands under resonance conditions are less than the number of lines in the non-resonance Raman spectrum. In this way detailed selective information about the chromophore can be obtained. Obtaining more-detailed information by an increase in selectivity using resonance Raman spectroscopy outweighs the lost information. In other words, in most cases, the gain in selectivity surpasses the loss of broad information. Therefore, the resonance enhancement permits examination of the vibrational modes of the chromophore in a sample unobscured by the vibrational modes of the molecular matrix. It provides a means of selecting out specific chemical groups by

tuning the laser to their electronic transitions. This allows one to obtain the RR vibrational spectra of certain substrates even when they are inside the protein active site for studying zero-order questions in biological systems. That is, many questions related to biological problems can be answered by locating the region of a given change during the biological process, or by determining whether or not there has been any change in some active site. On the other hand, RR spectroscopy can be used for more detailed study involving analysis of the changes at the active site. Simple proteins normally give no resonance Raman spectra by excitation by laser light in the visible region; however, certain modes become resonance Raman active after conjugation with chromophores.

Porphyrins are attractive targets for resonance Raman spectroscopy because of their intense absorption bands in the visible and near ultraviolet regions. Biochemical interest has inspired much of the work on metalloporphyrin RR spectroscopy. Indeed, the first metalloporphyrin spectra were obtained for heme proteins.[74-77] These studies revealed novel spectroscopic phenomena which were of considerable theoretical interest. Structured excitation profiles were discovered and some RR bands were found to have anomalous polarization,[77] a phenomena that Placzek had predicted[78] some 60 years earlier in a footnote to his well-known monograph on Raman scattering theory. This prediction had been overlooked, however, and the appearance of Raman bands with stronger intensity in perpendicular than parallel polarization, which contravened the polarization rules in all textbooks, came as genuine surprise to spectroscopists.

In addition to these novel characteristics which reflect the nature of the porphyrin excited states, the early heme protein studies revealed ground state

vibrational frequency shifts associated with the ligation chemistry of the heme group.[79-82] Subsequent work has uncovered useful structure-spectra correlations, including sensitivities of specific vibrational modes to the porphyrin core size, and to ligation, oxidation, and spin-state of the central metal ion.[83-86]

Most of the RR bands have been assigned to metalloporphyrin normal modes on the basis of extensive isotope substitution studies and normal-coordinate analyses.[87-92] A valence force field has been developed that gives a good account of frequencies and isotope shifts for nickel porphyrins with different peripheral substituents.[93] These advances make it possible to apply RR spectroscopy in a discriminating way to interesting aspects of metalloporphyrin structural dynamics.

Vibrational analyses, utilizing ^{2}H and ^{15}N isotope substitution, have led to a fairly detailed description of the various in-plane vibrational modes of porphyrins with different classes of peripheral substituents: porphine,[89,91,94] tetraphenylporphyrin,[95,96] octaethylporphyrin,[92,93] protoporphyrin IX,[97] and porphyrin-A[98]. Metal and ligand isotope substitution has been used to identify bands due to the axial ligands and their bonds to the central metal atom.[99] These bands are especially useful in monitoring the interactions of the heme group with its protein environment. A beginning has been made in analyzing the porphyrin out-of-plane modes, which are believed to be responsible for a number of low-frequency RR bands seen for heme proteins.[92,100-102] These appear to be quite variable among different proteins and may give important information about the effect of the globin pocket on the heme when they have been properly assigned. In addition, out-of-plane force field is an important determinant of dynamic processes in heme proteins which are currently under intensive investigations.

Since the RR scattering from metalloporphyrins depends upon the π electronic structure of the conjugated system responsible for the absorption in the visible region, this technique can also be used to explore the effect of conjugating substituents with the macrocycle. If the delocalization of the π electron cloud extends over the side chain substituents like formyl, vinyl, phenyl groups, etc., the RR spectra should reflect changes in intensity of some of the vibrational modes and in some cases, extra bands due to the vibrational modes related to the substituents may also be observed. The study of the effect of the substituent groups on the RR spectra of porphyrins can sometimes bring conceptual simplicity in the understanding of many biological systems and their functions.

The dependence of Raman intensity and depolarization ratio as a function of exciting frequency has been used to account for many subtle effects and important aspects of these systems. The plot of the variation of Raman intensity of a particular mode with the excitation frequency gives Raman excitation profile (REP) and it resembles an absorption spectrum for the mode being monitored. The REPs can, therefore, be used for the study of electronically excited states. Since each observable Raman mode produces a separate REP, an enormous resolution over ordinary absorption spectroscopy is achieved. On the other hand, dispersion of depolarization ratio with excitation frequency can provide information of the structure of the molecule in solution.[103] The observations of Raman bands with inverse polarization in heme proteins and metalloporphyrins constituted the first experimental confirmation of anti-symmetric vibrational scattering, although the phenomenon was predicted theoretically by Placzek in 1934.[78]

Owing to the extreme sensitivity of RR bands to important aspects of porphyrin geometry and electronic structure, RR spectroscopy provides a promising tool for studying the redox properties of these systems. The oxidation-reduction reactions are among the most important reactions involving porphyrins and their complexes. This importance stems from the conditions under which metalloporphyrins perform their functions in biological systems, such as functions of energy storage, oxygen transport, oxidation, decomposition of H_2O_2, etc. The use of metalloporphyrins in commercial catalysis of many oxidation and reduction reactions is another factor making studies on the oxidation-reduction properties and transformations imperative. Therefore having a good knowledge of the role of charge transfer in these molecular complexes is of paramount importance. In fact, extensive experimental work has been focussed on the study of electron transfer in native heme proteins[104-106] as well as in various model compounds[107].

In the redox reactions of metalloporphyrins, either electron is removed from or added to the system. The addition or removal of an electron from metalloporphyrins could involve both the porphyrin π system and the central metal ion in the porphyrin core.[108,109] It is generally observed that for porphyrins containing metals like Zn, Cu, and Cd the first electron addition or removal involves the porphyrin π system.[36,110,111] On the other hand, with porphyrins containing metals like Co, Fe, and Mn the metal ion also participates in the redox chemistry.[112-114] Because of the unusual electronic properties and the novel reactivities of these oxidized/reduced species and their involvement in many biological processes as intermediates, there is great interest in preparation and characterization of these

species. In particular, oxidation of the parent porphyrin to give the oxidized species has been the subject of many studies.[109,115-118]

A number of experimental evidences have conclusively shown that the oxidized metalloporphyrins and related compounds play crucial roles in the electron transport and redox processes in living organisms. For example, in the catalytic reaction of peroxidases and catalases, an enzyme intermediate referred to as Compound I is produced, which possesses two oxidizing equivalents above the resting ferric state.[119] Compound I has been assigned to a ferryl porphyrin π-cation radical in which one oxidizing equivalent is stored in the form of a tetravalent iron stabilized by oxygen (Fe^{IV}=O) and the second equivalent resides in a porphyrin π-cation.[17,18] The porphyrin type π-cation radical species has also been implicated in the chlorophyll photochemical reaction for the primary products generated by the photooxidation of chlorins in the photosystems I and II[120] and, possibly, in the intermediate of cytochrome-P_{450} reaction cycle.[121,122] Moreover, oxidized forms of porphyrins, especially the π-cation radical, have been reported as extremely reactive intermediates,[123] and in most cases only their oxidation potentials are reported. Their transient formation has been proposed as the initial step in the formation of meso or β-substituted or other modified forms of porphyrin's core, such as isoporphyrins, chlorins, bilitrienes, etc.[124-127] The reactivity of the π-cation radical has been taken advantage of recently for the electrochemical substitution of porphyrin rings and more especially the electrochemical generation of covalently linked porphyrin dimers.[126,127]

In addition to these biological implications, the porphyrin π-cation radical has been subjected to a great deal of physicochemical study in recent past.[8,44] Mauzerall first reported generation of a stable porphyrin π-cation radical of magnesium(II) octaethylporphyrin ($Mg^{II}OEP$) by chemical oxidation.[128] Dolphin and his co-workers were able to oxidize several synthetic metalloporphyrins to a stable π-cation radical state.[8,44,129] Depending on the particular combination of solvents, porphyrins, central metals, and counter ions, there are two types (A_{1u} and A_{2u}) of porphyrin π-cation radicals having characteristic UV-vis spectra.[129] ESR spectra and molecular orbital calculations suggest that the highest filled π-orbitals, a_{1u} or a_{2u}, of porphyrin are comparable in energy and that oxidation removes an electron from either one of them, depending on the conditions.[130,131] The remarkable difference of these two types of porphyrin π-cation radicals are the electron spin distribution on the porphyrin ring; for the A_{2u} radical large spin density is placed at the meso carbons and the pyrrole nitrogens, while the A_{1u} radicals experience small spin density at the meso positions.[130]

Oxidation of metalloporphyrins has been carried out by chemical,[117,132] electrochemical,[115,132] or photochemical[109,118] methods to give either the central metal and/or the porphyrin ring centered oxidation products. The site of oxidation is influenced by many factors such as the electronegativity and oxidation state of the central metal, peripheral substituents at the porphyrin ring, axial ligands, solvents, temperature and electronic interactions which govern the overlap of electron clouds of the donor and acceptor molecules. Most of the chemically or electrochemically prepared π-cations of metal-porphyrins have been characterized and investigated

mainly by optical absorption,[109,116,117] emission,[133,134] ESR,[44-46,132,] magnetic circular dichronism (MCD),[109] NMR,[135] X-ray crystallography,[39] IR[136] and RR[115,117,118] spectroscopies.

Resonance Raman spectroscopy provides a promising tool for studying molecular and electronic structure in porphyrin radicals in solution with high sensitivity as the frequencies of RR bands are sensitive to changes in bonding and conformation, while their intensities are sensitive to the nature of resonant excited electronic state(s). Several RR studies have also appeared on the π-cation radicals of metallotetraphenylporphyrins (MTPP) and metallooctaethylporphyrins (MOEP).[115,117] Results on these systems were interpreted in terms of changes in the core size of porphyrin due to electron removal. Removal of electron does not significantly change the porphyrin normal mode compositions but changes in force constant lead to appreciable frequency shifts for some modes. These shifts are understood on the basis of the electron removal from the nearly degenerate HOMO a_{1u} and a_{2u} orbitals.[115] Due to near degeneracy of the a_{1u} and a_{2u} orbitals, the ground and first excited states of the radicals could be A_{1u} and A_{2u} or vice versa and are close in energy. They can mix vibronically producing a pseudo-Jahn-Teller (pJT) effect.[115] With few exceptions, it has been generally observed that octaethylporphyrin (OEP) radicals have predominantly A_{1u} character while meso-tetraphenylporphyrin (TPP) radicals have A_{2u} character.

Apart from usual chemical or electrochemical methods, photochemical synthesis of porphyrin radicals offers a potentially efficient and cleaner route to generate these species and build reasonably high concentration of the intermediate species by varying the concentration of electron acceptors and other parameters. This

method also avoids complication and interference from other chemicals used in chemical or electrochemical processes. Porphyrins generally lose an electron readily but not so readily gain one because of coulomb repulsion energy.[137] The low-lying excited electronic states of porphyrin are involved in electron transfer reactions from the porphyrin to an electron acceptor yielding charge-separated species. Some of the earlier reports of photooxidation involved the conversion of metalloporphyrins into metallochlorins. Calvin et al.[138,139] report photooxidation of Zn and Mg *meso*-tetraphenylchlorins by a series of quinones in benzene. Later, photooxidation of meso-tetraphenylporphin and its metal derivatives (Zn, Mg and Co) in organic solvents was observed by many research groups.[109,118] A clear case of photooxidation leading to disruption of the porphyrin macrocycle was also observed in Mg-octaethylporphyrin.[140] A final type of photooxidation reaction involves change in oxidation state of the central metal. Although, reports for such metal redox reactions are few compared to other types of photooxidations mentioned above, examples are provided by Co(II) *meso*-tetraphenylporphyrin[109a] and related Mn(II) phthalocyanines.[141]

Besides providing an alternative and a more advantageous method for preparing oxidized or reduced species, the photochemistry and photophysics of porphyrins and its metal derivatives are of continuing interest due to their biomimetic functions as chlorophylls in photosynthesis and their possibilities as photosensitizers for solar energy conversion. Photosynthesis involving either plants or bacteria is well known to be one of the most important energy-conversion mechanisms carried out by living systems. Hence a detailed understanding of the primary process that govern photosynthetic energy conversion is of great important,

both to an understanding of biological processes and to the development of systems capable of photochemical conversion and storage of solar energy. Since, ubiquinone (in bacterial systems) and plastoquinone (in photosystem II of green-plant systems) are involved as electron acceptors in photosynthesis, there has been considerable interest in the study of photochemical electron transfer from chloropylls or synthetic porphyrins to quinones. But much of this research has involved porphyrins covalently linked to electron acceptors.[133] For example, a carotene-porphyrin-porphyrin-benzoquinone tetrad has been characterized in an effort to mimic both the energy-transfer and electron-transfer process in bacterial photosynthetic reaction centers.[142] Joran et al. have used quinones appended to octaalkylporphyrins through phenyl-bicyclooctane spacers to examine the effect of distance on charge separation rates.[143] Porphyrin-quinone systems have also been used to examine the orientation dependence, bridge dependence, and solvent dependence of electron-transfer rates.[144-146]

. However, in spite of these many efforts, little definitive evidence is available about the mechanistic details of electron transfer reaction from the porphyrin to electron acceptors and, surprisingly only few studies[109b,118,147] have been devoted to examine electron transfer from excited porphyrins to quinones without covalent linkages. We, therefore, undertook systematic resonance Raman studies on the photooxidation of free-base octaethylporphyrin (H_2OEP) and Co(II) tetraphenylporphyrin ($Co^{II}TPP$) initiated by selective laser irradiation within the electronic absorption regions of these systems in the presence of p-benzoquinone (p-BQ) as electron acceptor. In RR spectroscopic study of photochemical reactions of porphyrins, irradiation of the sample to induce reaction and recording of the

spectrum is done at the same time. This is one of the advantages of using RR spectroscopy for investigating photochemical reactions. In these investigations of the photooxidation of H_2OEP and $Co^{II}TPP$, the reaction products are characterized by comparing with the optical absorption and RR spectra of the chemically oxidized products. Since steady-state resonance Raman and optical absorption sepctroscopies can not directly reveal excited state(s) reactions, the reaction mechanisms proposed in these studies are done from the dependence of the photochemical reactions on the experimental conditions.

Another aspect of the studies described in this thesis is concerned with the photoreduction of cytochrome-c. Photoreduction is the process whereby a molecule gains electron from an electron donor, initiated by photoexcitation of either the electron donor or the electron acceptor. As in the case of photooxidation, photoreduction of metalloporphyrin can take place at the metal center or at the porphyrin ring. Reduction at the porphyrin ring system results in the formation of π-anion radical where the unpaired electron is delocalized over the π-system of the tetrapyrrole ligand.[132] The π-radical anion undergoes a second reduction process yielding chlorin or phlorin depending on the pH of the reaction medium and the central metal. The π-radical anions and phlorin are important in the photochemical water splitting reactions as they reduce water to hydrogen on the surface of catalysts.[148,149]

Photoreduction of the metal oxidation state, but not of the macrocyle, is more common than porphyrin ring reduction, and has been reported for various metalloporphyrins[150-152] and heme proteins.[153-155] Study of the redox properties of metalloporphyrins and heme proteins is important mainly from the point view of use

of these compounds as catalysts for several chemical reactions involving organic molecules[156-159] and as electron mediator in the photochemical generation of hydrogen from hydrogenase.[160] In particular, many studies have been devoted to iron-porphyrins because of their possible use as photocatalysts in the oxidation of hydrocarbons with various oxidants[157-159] as well as in the reduction of haloalkanes.[156] Besides their importance in chemical catalysis, these processes, mimicking the behavior *in vivo* of cytochrome-P_{450}, allow one to better understanding of the detailed mechanism of this ubiquitous enzyme in biological systems. From the previous studies of this process in iron-porphyrins using different techniques and under various conditions, it was demonstrated, among other things, that (i) electron transfer from axially coordinated ligands to iron center cleaved in the excited electronic state by photoexcitation is the primary step in photoreduction;[150,152,161,162] (ii) primary alcohols are indispensable for photoreduction in various solvents and ligand systems, but no photoreduction occurs on excitation within the alcohol → iron charge-transfer (CT) band around 585 nm;[150,161,162] (iii) a ligand free, intermediate spin complex is the transient intermediate species involved in the process.[150,152,161,162]

As far as heme proteins are concerned, the situation is still far from clear due to complications from the protein moiety. Many of the previous studies have utilized external electron donors or sensitizers.[163-165] But photoreduction of heme proteins, such as cytochrome-c,[154b,166] has been reported in the absence of foreign donors. Resonance Raman spectroscopy has also been used in studies of heme protein photoreduction, both in solution[153,155b,162] and in single crystals,[154a] by monitoring the changes in the oxidation state maker band, ν_4.

In spite of these efforts, a detailed mechanism for heme photoreduction remains elusive. One of the main puzzles is the identification of the electron donor. In the study of electron transfer process in heme proteins, cytochrome-c becomes the choice of many workers because of its structural simplicity compared to other heme proteins, and availability of its X-ray molecular structural data. Recently Gu et al,[154b] have reported detailed studies of photoreduction in many heme proteins including cytochrome-c by illumination at discrete wavelengths and characterized the photoreduced products using optical absorption and resonance Raman spectroscopies. They also measured photoreduction cross-section as a function of excitation wavelengths and suggested that heme axial ligands play important, although not exclusive, role in determining the photoreduction cross-section, and may also involve multiple electron donors. On the other hand, earlier studies suggested the methionine axial ligand (Met-80) to play a crucial in the redox process,[166,167] while according to other views, electron might tunnel to the heme through some aromatic residues,[167,168] or through the exposed front portion of heme edge.[169,170] A mixing of the iron t_{2g} orbitals with the porphyrin π orbitals may extend the effective metal redox orbital density to the heme edge which may facilitate electron transfer to the metal, but the situation is still far from clear.

Therefore having good knowledge of the photophysical and photochemical properties of porphyrins are important from the point of view of their uses as photocatalyst, sensitizer and electron mediator in the photochemical conversion and storage of solar energy as well as for understanding the mechanistic details of many biological reaction processes such as photosynthetic reaction of chlorophylls in plants and electron transfer process of cytochromes in mitochondrial respiratory

chain. Accordingly we initiate these studies with the aim of having better insight into the basic mechanism of photoredox reaction of porphyrins in model systems and in hemeproteins. The work comprises of photooxidation of free base octaethylporphyrin and cobalt(II) *meso*-tetraphenylporphyrin in the presence of electron acceptors, and photoreduction of cytochrome-c without external electron donor.

In the photooxidation of H_2OEP by p-BQ in CH_2Cl_2 under aerobic or anaerobic conditions, the $(H_4OEP)^+$ diacid derivative is found to be the final stable product of the reaction. In this reaction, the solvent is suggested to act as proton source since changing the solvent to CS_2, CCl_4, C_6H_6 completely inhibited the reaction. No $H_2OEP^{+\bullet}$ π-cation RR signal was detected. But its transient formation and crucial role in the abstraction of proton form the solvents is suggested based on earlier reports. In CCl_4, simultaneous presence of p-BQ and alcohols (MeOH or EtOH) is essential for photochemical formation of diacid. On the other hand, in CH_2Cl_2, presence of alcohol results in the formation of monoacid derivative of H_2OEP, while the diacid formation is greatly inhibited. From wavenumber shift pattern of the ν_{11} mode in the RR spectra of the acid derivatives, the electronic ground states of H_3OEP^+ and $(H_4OEP)^{2+}$ are inferred to have a_{1u} character.

Unlike free-base OEP, the photooxidation of $Co^{II}TPP$ with 441.6 nm laser excitation in the presence of p-BQ in CH_2Cl_2 is very sensitive to the presence or absence of oxygen in the system. Under anaerobic conditions, photooxidation of $Co^{II}TPP$ takes place at the metal center to give $Co^{III}TPP$ complex. In the presence of molecular oxygen, electron removal occurs from the metal center as well as from the porphyrin ring π-system to give the two-electron oxidation product, $[Co^{III}TPP]^{2+\bullet}$

radical species of a_{2u} radical character. Alkylchloride peroxy radicals are believed to be the oxidant in the electron removal from the porphyrin ring. The reaction is also found to be very sensitive to the nature of the solvents. No photooxidation was observed in CCl_4, $CHCl_3$ and CS_2, while clean photooxidation was observed in solvents like CH_2Cl_2, $C_2H_4Cl_2$ and CH_2Cl_4.

As cytochrome-c undergoes a series of reversible conformational transitions involving replacement of axial ligands with change of pH, it is expected that pH dependent studies of photoreduction may help in clarifying the role of axial ligands and other amino acids in the photoreduction process. Therefore, in order to gain information about an access route of electron to the redox center either within or from the surrounding of the protein, we undertook the study of photoreduction of cytochrome-c as a function of pH, excitation wavelength, laser power, salt and buffer concentration.

During the course of our resonance Raman (RR) studies we had noticed that purified monomeric cytochrome-c (cyt-c) at neutral pH exhibits extensive photoreduction under anaerobic condition upon laser irradiation in the 400-440 nm region. However, only partial photoreduction occurred at pH 10.1 where the sixth axial methionine ligand is replaced probably by lysine, and no photoreduction took place after the transitions with pK_α = 12.76 and 2.5 where the fifth axial histidine ligand is replaced by other residue. Observation of photoreduction of cyt-c only when it retains its folded conformation suggests that either the histidine ligand or the non-bonding aromatic amino acids, viz Phe-82 or Tyr-67 could be the electron donor in the photoreduction process. Since ionization potential of such aromatic residues is much higher than the energy of the light at 400-440 nm, special mechanism

involving a hole-induced electron transfer is proposed. The photoreduction of cyt-c was completely inhibited in the presence of oxygen suggesting active participation of a triplet state in this process. The inhibitory effect of oxygen mostly results from excited state energy transfer rather than electron transfer to molecular oxygen. Presence of chloride or phosphate ion also produces inhibitory action to the process of photoreduction. The dependence of photoreduction on the nature of anion is expected to be a consequence of the binding of the anion to some specific cationic amino acids like lysines on the surface and in the proximal part of the protein thereby exerting their inhibitory effect *via* interaction with the charge separated complex formed during photoreduction or by weakening the overlap of electron clouds between the acceptor and donor orbitals. Apart from these, detailed experiments were also conducted on the photoreduction as a function of excitation wavelength with constant photon flux. We find that the relative quantum yield for photoreduction of pure cyt-c at neutral pH as a function of excitation wavelengths shows a weak maximum centered around 410 nm while it increases almost exponentially when the excitation wavelength is moved from 390 to 300 nm. This type of behavior is a manifestation of different mechanisms of photoreduction: direct participation of non-bonding aromatic amino acid residue of the protein in the excitation region below 360 nm and active participation of the heme excited states in the 400-440 nm region. During the process of photoreduction, there always exists photo-oxidation process, which competes strongly with the photoreduction even under anaerobic condition.

References

1. Milgrom, L.R. in *The Colours of Life: An Introduction to the Chemistry of Porphyrins and Related Compounds*; Oxford University Press: Oxford, 1997.
2. James, B.R. In *The Porphyrins*; Dolphin, D., Ed.; Academic Press: New York, 1978; Vol. 5, p. 205.
3. Mathis, P.; Paillotin, G. In *Photosynthesis*; Hatch, M.D.; Boarddman, N.K., Eds.; Academic Press: New York, 1981.
4. Clayton, R.K. *Photosynthesis: Physical Mechanics and Chemical Patterns*; Cambridge Press: Cambridge (UK), 1980.
5. The Chlorophylls; Vernon, L.P.; Seely, G.R., Eds.; Academic Press: New York, 1966.
6. Shlyk, A.A. In *Current Problems of Photosynthesis*; Moscow University Press: Moscow, 1973, p. 85.
7. Kutyurin, V.M.; Yu, I.; Artamkina; Melinkov, N.P.; Anisomov, I.N. In *Chlorophyll*; Nauka i tekhnika: Minsk, 1974, p. 85.
8. Lever, A.B.P.; Gray, H.B., Eds.; *Iron Porphyrin*; Addison-Wesley Publishing Company: Amsterdam, 1983; Part I & II.
9. James, B.R. In *The Porphyrins*; Dolphin, D., Ed.; Academic Press: New York, 1978; Vol. V, pp. 206-301.
10. Proniewicz, L.M.; Bajdor, K.; Nakamoto, K. *J. Phys. Chem.* 1986, 90, 1760.
11. (a) Hori, H.; Kitagawa, T. *J. Am. Chem. Soc.* 1980, 102, 3608. Nagai, K.; Kitagawa, T. *Proc. Natl. Acad. Sci. USA*. 1980, 77, 2033.

12. (a) Antonini, E.; Brunori, M. In *Hemoglobin and Myoglobin in their Reaction with Ligands*; North-Holand: Amsterdam, 1971. (b) Hewson, W.D.; Hager, L.P. In *The Porphyrin*; Dolphin, D., Ed.; Academic Press: New York, 1979; Vol. 7, pp. 295-332.

13. (a) Davies, H.S.; Forman, A.; Fajer, J. *Proc. Natl. Acad. Sci. U.S.A.* 1979, 76, 1476. (b) Harbury, H.A.; Marks, R.H.L. In *Inorganic Biochemistry*; Eichhorn, G., Ed.; Elsevier: Amsterdam, 1973; Vol. 2, Chapter 1. (c) *The Porphyrins*; Dolphin, D., Ed.; Academic Press: New York, 1976; Vol. 13, pp 363.

14. Schonbaun, G.R.; Chance, B. In *The Enzymes*; Boyer, P.D., Ed.; Academic Press: New York, 1976; Vol. 13, pp 363.

15. Sato, R.; Omura, T., Eds.; *Cytochrome-P_{450}*; Academic Press: New York, 1978.

16. Dunford, H.B.; Stillman, J.S. *Coord. Chem. Rev.* 1976, 19, 187.

17. La Mar, G.N.; deRopp, J.S.; Latos-Grazynski, L.; Balch, A.L.; Johnson, R.B.; Smith, K.M.; Parish, D.W.; Cheng, R.-J. *J. Am, Chem. Soc.* 1983, 105, 782.

18. Fujita, I.; Hanson, L.K.; Walker, F.A.; Fajer, J. *J. Am. Chem. Soc.* 1983. 105, 3296.

19. Goldberg, A.; Rimington, C. In *Diseases of Porphyrin Metabolism*; Thomas: Springfield, 1962.

20. Jori, G. In *Laser in Photomedicine and Photobiology*; Pratesi, R.; Sacchi, C.A., Eds.; Springer: New York, 1980; pp. 58.

21. Lacey, J.A.; Phillips, D.; Milgrom, L.R.; Yahioglu, G.; Rees, R.D. *Photochem. Photobiol.* 1998, 67, 97.

22. Varani, G.; Maldotti, A.; Bartocci, C. *New. J. Chem.* 1992, 16, 827.

23. Wolf, M. *Electronics* 1963, 36, 35.

24. Haak, F.; Nolta, J. *J. Chem. Phys.* 1967, *38*, 2648.

25. Adler, A.D. *J. Polym. Sci. Part C* 1970, 39, 73.

26. Alt, H.; Binder, H.; Sandstede, G. *J. Catalysis* 1973, 28, 8.

27. Berezin, B.D. In *Coordination Compounds of Porphyrins and Phthalocyanines*; John Wiley: New York, 1981, Chapter 1.

28. Kane, A.R.; Sullivan, J.F.; Kenny, M.E. *Inorg. Chem.* 1970, 9, 1445 and refs. therein.

29. Wasielewski, M.R. *Chem. Rev.* 1992, 92, 435.

30. Collman, J.P.; McDevitt, J.T.; Leidner, C.R.; Yee, G.T.; Torrance, J.B.; Little, W.A. *J. Am. Chem. Soc.* 1987, 109, 4606.

31. Simon, J.; Sirlin, C. *Pure Appl. Chem.* 1989, 61, 1625.

32. Bruce, D.W.; Dunmur, D.A.; Sauta, L.S.; Wali, M.A. *J. Mater. Chem.* 1992, 2, 363.

33. Loutfy, R.O.; Sharp, J.H. *J. Chem. Phys.* 1979, 71, 1211.

34. Wheeler, B.L.; Nagasubramanian, Bard, A.J.; Schechtman, L.A.; Dininny, D.R.; Kenny, M.E. *J. Am. Chem. Soc.* 1984, 106, 7404.

35. Kivits, P.; deBont, R.; van der Veen, J. *Appl. Phys.* 1981, A26, 101.

36. Gouterman, M. In *The Porphyrins*; Dolphin, D., Ed.; Academic Press: New York, 1978; Vol. 3, pp. 1-156.

37. Kobayashi, H.; Yanaga, Y.; Osada, H. *Bull. Chem. Soc. Jpn.* 1973, 1471.

38. Falk, J.E. In *Porphyrins and Metalloporphyrins*; Elsevier: Amsterdam, 1964; Chapter 6.

39. Gans, P.; Buisson, G.; Duee, E.; Marchon, J.-C.; Erler, B.S.; Scholz, W.F.; Reed, C.A. *J. Am. Chem. Soc.* 1986, 108, 1223.

40. Boldt, N.J.; Donohoe, R.J.; Birge, R.R.; Bocian, D.F. *J. Am. Chem. Soc.* 1987, 109, 2284.

41. Scheidt, W.R.; Lee, Y.J.; Hatano, K. *J. Am. Chem. Soc.* 1984, 106, 3191.

42. Li, N.; Coppens, P.; Landrum, J. *Inorg. Chem.* 1988, 27, 482.

43. Lecomte, C.; Rohmer, M.-M.; Benard, M. In *The Porphyrin Handbook*; Kadish, K.M.; Smith, K.M.; Guilard, R., Eds.; Academic Press: New York, 1999; Vol. 7, Chapter 48.

44. Fajer, J.; Davis, M.S. In *The Porphyrins*; Dolphin, D.; Ed.; Academic Press: New York, 1979; Vol. 4, pp 197-256.

45. Subramanian, J. In *Porphyrins and Metalloporphyrins*; Smith, K.M., Ed.; Elsevier: Amsterdam, 1975; pp. 555-589.

46. Sandusky, P.O.; Oertling, W.A.; Chang, C.K.; Babcock, G.T. *J. Phys. Chem.* 1991, 95, 4300.

47. Van der Waals, J.H.; van Dorp, W.G.; Schaafsma, T.J. In *The Porphyrins*; Dolphin, D.; Ed.; Academic Press: New York, 1979; Vol. 4, pp 257-312.

48. Palmer, G. In *The Porphyrins*; Dolphin, D.; Ed.; Academic Press: New York, 1979; Vol. 4, pp 313-353.

49. Walker, F.A. In *The Porphyrin Handbook*; Kadish, K.M.; Smith, K.M.; Guilard, R., Eds.; Academic Press: New York, 1999; Vol. 5, Chapter 36.

50. Scheer, H.; Katz, J.J. In *Porphyrins and Metalloporphyrins*; Smith, K.M., Ed.; Elsevier: Amsterdam, 1975; pp. 399-524.

51. Janson, T.R.; Katz, J.J. In *The Porphyrins*; Dolphin, D.; Ed.; Academic Press: New York, 1979; Vol. 4, pp 1-59.

52. La Mar, G.N.; Satterlee, J.D.; De Ropp, J.S. In *The Porphyrin Handbook*; Kadish, K.M.; Smith, K.M.; Guilard, R., Eds.; Academic Press: New York, 1999; Vol. 5, Chapter 37.

53. Fuhrhop, J.-H. In *Porphyrins and Metalloporphyrins*; Smith, K.M., Ed.; Elsevier: Amsterdam, 1975; pp. 593-614.

54. Hambright, P.; Bearden, A.J. In *Porphyrins and Metalloporphyrins*; Smith, K.M., Ed.; Elsevier: Amsterdam, 1975; pp. 539-553.

55. Sams, J.R.; Tsin, T.B. In *The Porphyrins*; Dolphin, D.; Ed.; Academic Press: New York, 1979; Vol. 4, pp 425-478.

56. Alben, J.O. In *The Porphyrins*; Dolphin, D.; Ed.; Academic Press: New York, 1979; Vol. 3, pp 323-345.

57. Johnson, B.B.; Peticolas, W.L. *Annu. Rev. Phys. Chem.* 1976, 27, 465.

58. Verma, A.L. *Indian J. Phys.* 1980, 54B, 54.

59. Spiro, T.G. In *Iron Porphyrins*; Lever, A.B.P.; Gray, H.B., Eds.; Addison-Wesley: Reading MA, 1983; Part 2, pp 89-159.

60. Spiro, T.G.; Li, X.-Y. In *Biological Applications of Raman Spectroscopy*; Spiro, T.G., Ed.; Wiley-Interscience: New York, 1988; Vol. 3, Chapter 1.

61. Spiro, T.G.; Czernuszewicz, R.S.; Li, X.-Y. *Coord. Chem. Rev.* 1990, 100, 541-571.

62. Mitra, S. In *Iron Porphyrins*; Lever, A.B.P.; Gray, H.B., Eds.; Addison-Wesley: Reading MA, 1983; Part 2, pp 1-42.

63. Holmquist, B. In *The Porphyrins*; Dolphin, D.; Ed.; Academic Press: New York, 1979; Vol. 3, pp 249-269.

64. Chantrell, S.J.; McAuliffe, C.A.; Munn, R.W.; Pratt, A.C. *Coord. Chem. Rev.* 1975, 16, 259.

65. Antipas, A.; Gouterman, M. *J. Am. Chem Soc.* 1983, 105, 4896.

66. Spiro, T.G. *Accounts Chem. Res.* 1974, 7, 339.

67. Spiro, T.G. In *Chemical and Biochemical Applications of Lasers*; Moore, C.B., Ed.; Academic Press: New York, 1974; Chapter 2.

68. Warshel, A. *Ann. Rev. Biophys. Bioeng.* 1977, 6, 273.

69. Yu, N.-Y. In CRC Critical Reviews in Biochemistry; Fasman, G., Ed.; The Chemical Rubber Co.: Ohio, 1977; Vol. 4, p. 229.

70. Tang, J.; Albrecht, A.C. In *Raman Spectroscopy*; Szymanski, H.A., Ed.; Plenum: New York, 1970; Vol. 2, pp. 33-38.

71. Behringer, J. In *Molecular Spectroscopy*; Barrow, R.F.; Long, D.A.; Millen, D.J., Eds.; The Chemical Society: London, 1974; Vol. 2, pp. 100-172.

72. Spiro, T.G. *Biochim, Biophys. Acta* 1975, 416, 169.

73. Lewis, A.; Spoonhower, J. In Spectroscopy in Chemistry and Biophysics; Chen, S.; Yip, S., Eds.; Academic Press: New York, 1974; pp. 347-375.

74. Strekas, T.C.; Spiro, T.G. *Biophys. Biochim. Acta* 1972, 263, 830.

75. Strekas, T.C.; Spiro, T.G. *Biophys. Biochim. Acta* 1972, 278, 188.

76. Brunner, H.; Mayer, A.; Sussner, H. *J. Mol. Biol.* 1972, 70, 153.

77. Spiro, T.G.; Strekas, T.C. *Proc. Natl. Acad. Sc. USA* 1972, 69, 2622.

78. Placzek, G. In *Handbuch der Radiologie*; Marx, E., Ed.; Akademische Verlagsgesellschaft 6: Leipzig, 1934; Vo.2, pp. 209-374.

79. Yamamoto, Y.; Palmer, G.; Gill, D.; Salmeen, I.T.; Rimai, L. *J. Biol. Chem.* 1973, 248, 5211.

80. (a) Spiro, T.G.; Strekas, T.C. *J. Am. Chem. Soc.* 1974, 96, 338. (b) Verma, A.L.; Bernstein, H.J. *J. Raman Spectrosc.* 1974, 2, 163.

81. Spiro, T.G.; Burke, J.M. *J. Am. Chem. Soc.* 1976, 98, 5482.

82. Spaulding, L.D.; Cheng, C.C.; Yu, N.-Y.; Felton, R.H. *J. Am. Chem. Soc.* 1975, 97, 2517.

83. Spiro, T.G.; Stong, J.D.; Stein, P. *J. Am. Chem. Soc.* 1979, 101, 2648.

84. Choi, S.; Spiro, T.G.; Langry, K.C.; Smith, K.M.; Budd, L.D.; Lamar, G.N. *J. Am. Chem. Soc.* 1982, 104, 4345.

85. Parthasarathi, N.; Hansen, C.; Yamaguchi, S.; Spiro, T.G.; *J. Am. Chem. Soc.* 1987, 109, 3865.

86. Spiro, T.G *Adv. Protein Chem.* 1985, 37, 11.

87. Stein, P.; Burke, J.M.; Spiro, T.G. *J. Am. Chem. Soc.* 1975, 97, 2304.

88. Ogoshi, H.; Saito, Y.; Nakamoto, K. *J. Chem. Phys.* 1972, 57, 4194.

89. Sunder, S.; Bernstein, H. *J. Raman Spectros.* 1976, 5, 351.

90. Susi, H.; Ard, J.S. *Spectrochim. Acta, Part A*, 1977, 33, 561.

91. (a) Verma, A.L.; Assetin, M.; Sunder, S.; Bernstein, H.J. *J. Raman Spectrosc.* 1976, 4, 295. (b) Mendelsohn, R.; Sunder, S.; Verma, A.L.;Bernstein, H.J. *J. Chem. Phys.* 1975, 62, 37. (c) Gladkov, L.L.; Solovyov, K.N. *Spectrochim. Acta, Part A*, 1985, 41, 1437, 1443.

92. Kitagawa, T.; Abe, M.; Ogoshi, H. *J. Chem. Phys.* 1978, 69, 4516.

93. Li, X.-Y.; Czernuszewicz, R.S.; Kincaid, J.R.; Stein, P.; Spiro, T.G. *J. Chem. Phys.* 1990, 94, 47.

94. Li, X.-Y.; Zgierski, M.Z. *J. Chem. Phys.* 1991, 95, 4268.

95. Stein, P.; Ulman, A.; Spiro, T.G. *J. Phys. Chem.* 1984, 88, 369.

96. Li, X.-Y.; Czernuszewicz, R.S.; Kincaid, J.R.; Su, Y.O.; Spiro, T.G. *J. Chem. Phys.* 1990, 94, 31.

97. Choi, S.; Spiro, T.G.; Langry, K.C.; Smith, K.M.; *J. Am. Chem. Soc.* 1982, 104, 4337.

98. Choi, S.; Lee, J.J.; Wei, Y.H.; Spiro, T.G. *J. Am. Chem. Soc.* 1983, 105, 3707.

99. *Biological Applications of Raman Spectroscopy*; Spiro, T.G., Ed.; Wiley-Interscience: New York, 1988; Vol. 3, Chapter 2 and 3.

100. Besbois, A.; Lutz, M.; Banerjee, R. *Biochim, Biophys. Acta*, 1981, 671, 168.

101. Choi, S.; Spiro, T.G. *J. Am. Chem. Soc.* 1983, 105, 3683.

102. Czernuszewicz, R.S.; Li, X.-Y.; Spiro, T.G. *J. Am. Chem. Soc.* 1989, 111, 7024.

103. (a) Verma, A.L.; Bernstein, H.J. *J. Chem. Phys.* 1974, 61, 2560. (b) Verma, A.L.; Mendelsohn, R.; Bernstein, H.J. *J. Chem. Phys.* 1974, 61, 383.

104. Nocek, J.M.; Liang, N.; Wallin, S.A.; Mauk, A.G.; Hoffman, B.M. *J. Am. Chem. Soc.* 1990, 112, 1623.

105. Natan, M.J.; Hoffaman, B.M. *J. Am. Chem. Soc.* 1989, 111, 6468.

106. Meade, T.J.; Gray, H.B.; Winkler, J.R. . *J. Am. Chem. Soc.* 1989, 111, 4353.

107. Fukuzumi, S. In *The Porphyrin Handbook*; Kadish, K.M.; Smith, K.M.; Guilard, R., Eds.; Academic Press: New York, 1999; Vol. 8, Chapter 56.

108. Hambright, P.; Neta, P.; Richoux, M.-C.; Gamra, Z.A.; Harriman, A. *J. Photochem.* 1987, 36, 255.

109. (a) Gasyna, Z.; Browett, W.R.; Stillman, M.J. *Inorg. Chem.* 1984, 23, 382. (b) Gasyna, Z.; Browett, W.R.; Stillman, M.J. *Inorg. Chem.* 1985, 24, 2440

110. Lin, X.Q.; Cocolios, B.B.; Kadish, K.M. *Inorg. Chem.* 1986, 25, 3242.

111. Neta, P.; Grebel, V.; Levanon, H. *J. Phys. Chem.* 1981, 85, 2117.

112. Mu, X.H.; Kadish, K.M. *Inorg. Chem.* 1989, 28, 3743.

113. Swistak, C.; Kadish, K.M. *Inorg. Chem.* 1987, 26, 405.

114. Kelley, S.L.; Kadish, *Inorg. Chem.* 1982, 21, 3631.

115. Czernuszewicz, R.S.; Macor, K.A.; Li, X.-Y.; Kincaid, J.R.; Spiro, T.G. *J. Am. Chem. Soc.* 1989, 111, 3860.

116. Reddy, D.; Reddy, N.S.; Chandrashekar, T.K.; van Willigen, H. *J. Chem. Soc. Dalton Trans.* 1991, 2097.

117. Oertling, W.A.; Salehi, A.; Chung, Y.C.; Leroi, G.E.; Chang, C.K.; Babcock, G.T. *J. Phys. Chem.* 1987, 91, 5887.

118. (a) Saini, G.S.S.; Chaudhury, N.K.; Verma, A.L.; *J. Chem. Soc. Farad. Trans.* 1992, 88, 2853. (b) Saini, G.S.S.; Chaudhury, N.K.; Verma, A.L.; *Photochem. Photobiol.* 1992, 55, 815.

119. Palcic, M.M.; Rutter, R.; Araiso, T.; Hager, L.P; Dunford, H.B. *Biochem. Biophys. Res. Comm.* 1980, 94, 1123.

120. Barett, J. *Nature (London)* 1967, 215, 733.

121. Chang, C.K.; Dolphin, D. In *Bioorganic Chemistry*; van Tamalen, E.E., Ed.; Academic Press: New York, 1978; Vol. 4, pp. 37-80.

122. Groves, J.T.; Kruper, W.J.; Nemo, T.E.; Myers, R.S. *J. Mol. Catal.* 1980, 7, 167.

123. Inisan, C.; Saillard, J.-Y.; Guilard, R.; Tabard, A.; Mest, Y.L. *New J. Chem.* 1998, 22, 823.

124. Dolphin, D.; Felton, R.H. *Acc. Chem. Res.* 1974, 7, 26.

125. Barkigia, K.M.; Renner, M.W.; Xie, H.; Smith, K.M.; Fajer, J. *J. Am. Chem. Soc.* 1993, 115, 7894.

126. Giraudeau, A.; Ruhlmann, L.; El Kahef, L.; Gross, M. *J. Am. Chem. Soc.* 1996, 118, 2969.

127. El Kahef, L.; Gross, M.; Giraudeau, A. *J. Chem. Soc. Commun.* 1989, 963.

128. Fuhrhop, J.-H.; Mauzerall, D. *J. Am. Chem. Soc.* 1968, 90, 3875.

129. Dolphin, D.; Forman, A.; Borg, D.C.; Fajer, J.; Felton, R.H. *Proc. Natl. Acad. Sci. U.S.A.* 1971, 68, 614.

130. Fajer, J.; Borg, D.C.; Forman, A.; Dolphin, D.; Felton, R.H. *J. Am. Chem. Soc.* 1970, 92, 3451.

131. Maggiora, G.M. *J. Am. Chem. Soc.* 1973, 95, 6555.

132. Felton, R.H. In The porphyrins; Dolphin, D., Ed.; Academic Press: New York, 1978; Vol. 5, pp 53-125.

133. McIntosh, A.R.; Siemiarczuk, A.; Bolton, J.R.; Stillman, M.J.; Ho, T.-F.; Weedon, A.C. *J. Am. Chem. Soc.* 1983, 105, 7215.

134. Gerdorff, J.V.; Huber, M.; Schubert, H.; Niethammer, D.; Kirste, B.; Plato, M.; Mobius, K.; Kurreck, H.; Eichberger, R.; Kietzmann, R.; Willig, F. *Angew. Chem. (Int. Ed. Eng.)* 1990, 29, 670.

135. Morishima, I.; Takamuki, Y.; Shiro, Y. *J. Am. Chem. Soc.* 1984, 106, 7666.

136. Itoh, K.; Nakahasi, K.; Toeda, H. *J. Phys. Chem.* 1988, 92, 1464.

137. Mauzerall, D. In *The Porphyrins*; Dolphin, D., Ed.; Academic Press: New York, 1978; Vol. 5, pp. 29-52.

138. Calvin, M.; Dorough, G.D. *J. Am. Chem. Soc.* 1948, 70, 699.

139. Huennekens, F.M.; Calvin, M. *J. Am. Chem. Soc.* 1949, 71, 4024.

140. (a) Fuhrhop, J.-H.; Mauzarell, D. *Photochem. Photobiol.* 1971, 13, 453. (b) Wasser, P.K.-W.; Fuhrhop, J.-H. *Ann. N.Y. Acad. Sci.* 1973, 206, 533.

141. Hopf, F.R.; Whitten, D.G. In *Porphyrins and Metalloporphyrins*; Smith, K.M., Ed.; Elsevier: Amsterdam, 1975; p. 691.

142. Gust, D.; Moore, T.A.; Moore, A.L.; Makings, L.R.; Seely, G.R.; Ma, X.; Trier, T.T.; Gao, F. *J. Am. Chem. Soc.* 1988, 110, 7567.

143. Joran, A.D.; Leland, B.A.; Geller, G.G.; Hopfield, J.J.; Dervan, P.B. *J. Am. Chem. Soc.* 1984, 106, 6090.

144. Sessler, J.L.; Johnson, M.R.; Lin, T.-Y.; Creager, S.E. *J. Am. Chem. Soc.* 1988, 110, 3659.

145. Skata, Y.; Nakashima, S.; Goto, Y.; Tatemitsu, H.; Misumi, S.; Asahi, T.; Hagihara, M.; Nishikawa, S.; Okada, T.; Mataga, N. *J. Am. Chem. Soc.* 1989, 111, 8979.

146. Liu, J.-Y.; Schmodt, J.A.; Bolton, J.R. *J. Phys. Chem.* 1991, 95, 6924.

147. Seki, H.; Hoshino, M.; Shizuka, H. *J. Phys. Chem.* 1989, 93, 3630.

148. (a) Harriman, A.; Porter, G.; Richoux, M.-C. *J. Chem. Soc. Farad. Trans.* 1981, 77, 2. (b) Harriman, A.; Porter, G.; Richoux, M.-C. *J. Chem. Soc. Farad. Trans.* 1981, 77, 1939.

149. Kalyanasundaram, K.; Gratzel, M. *Helv. Chim. Acta* 1980, 87, 478.

150. (a) Bartocci, C.; Scandola, F.; Ferri, A.; Carassiti, V. *J. Am. Chem. Soc.* 1980, 102, 7067. (b) Bartocci, C.; Maldotti, A.; Varani, G.; Battioni, P.; Carassiti, V.; Mansuy, D. *Inorg. Chem.* 1991, 30, 1255.

151. Kalyanasundaram, K. *J. Photochem. Photobiol.* 1988, 42, 87.

152. Hendrickson, D.N.; Kinnaird, M.G.; Suslick, K.S. *J. Am. Chem. Soc.* 1987, 109, 1243.

153. Adar, F.; Yonetani, T. *Biochim. Biophys. Acta* 1978, 502, 80.

154. (a) Sage, J.T.; Morikis, D.; Champion, P.M. *J. Phys. Chem.* 1989, 75, 1543. (b) Gu, Y.; Li, P.; Sage, T.; Champion, P.M. *J. Am. Chem. Soc.* 1993, 115, 4993.

155. (a) Kitagawa, T.; Nagai, K. Nature (London) 1979, 281, 503. (b) Kitagawa, T.; Chihara, S.; Fushitani, K.; Morimoto, H. *J. Am. Chem. Soc.* 1984, 106, 1860. (c) Ogura, T.; Sone, N.; Tagawa, K.; Kitagawa, T. *Biochemistry* 1984, 23, 2826.

156. Brault, D. *Environmen. Health Perspect.* 1985, 64, 53.

157. Meunier, B. *Bull. Soc. Chim. Fr.* 1986, 578.

158. McMurry, T.J.; Groves, J.T. In *Cytochrome-P_{450}, Structure, Mechanism and Biochemistry*; Ortiz de Montellano, P.R., Ed.; Plenum Press: New York, 1986.

159. Mansuy, D. *Pure Appl. Chem.* 1987, 59, 759.

160. Eng, L.H.; Lewin, M.B.-M.; Neujahr, H.Y. *Photochem. Photobiol.* 1993, 58, 594.

161. Fidler, V.; Ogura,T.; Sato, S.; Aoyagi, K.; Kitagawa, T. *Bull. Chem. Soc. Jpn.* 1991, 64, 2315.

162. Verma, A.L.; Chaudhury, N.K. *J. Raman Spectrosc.* 1991, 22, 427.

163. Marinov, B.S. *Photochem. Photobiol.* 1986, 44, 665.

164. Goda, K.; Hisaoka, M.; Ueda, T. *Biochemistry Intnl.* 1987, 15, 635.

165. Ferri, A.; Patt, D.; Chiozzi, P.; Cattozzo, M.; Bartocci, C.; Maldotti, A. *J. Photochem. Photobiol. B* 1988, 2, 341.

166. Bartocci, C.; Maldotti, A.; Carassiti, V.; Traverso, O. *Inorg. Chim. Acta* 1985, 107, 5.

167. (a) *Structure and Bonding: Long Range Electron Transfer in Biology*; Palmer, G., Ed.; Springer-Verlag: Berlin, 1991; Vol. 75. (b) Lanir, A.; Aviram, I. *Arch. Biochem. Biophys.* 1975, 166, 439. (c) Dickerson, R.E.; Timkovich, R. In *The Enzymes*; Boyer, P.D., Ed.; Academic Press: New York, 1975.

168. Isied, S.S.; Vassilian, A. *J. Am. Chem. Soc.* 1984, 106, 1726.

169. Wilson, M.T.; Greenwood, C. *In Cytochrome-c: A Multidisciplinary Approach*; Scott, R.A.; Mauk, A.G., Eds.; University Science Book: Mill Valley, CA, 1996.

170. Armstrong, F.A.; Hill, H.A.O.; Walton, N.J. *Quart. Rev. Biophysics.* 1986, 1, 261.

Table 1.1. Valence for Regular and Irregular Metalloporphyrins

Main group	IA	IIA	IIIA	IVA	VA			
Regular valence	I	II	III	IV	V			
Irregular valence	[p^2]	—	I*	II*	III*			
Transitional metals IIB	IIIB	IVB	VB	VIB	VIIB	VIII	IB	
Regular valence	III	IV	V	V*	V*	VI*	III†	II
Irregular valence	[d^n, $1 \leq n \leq 9$]		IV	IV III* II	IV* III* II I*	IV* III(*†) II(*†) I*	II† I(?)	
Lanthanide and actinide								
Regular valence	[f^0 or f^{14}, d^0 or d^{10}], e.g., Lu(III), Th(IV), U(VI)							
Irregular valence	[f^n, $1 \leq n \leq 13$], e.g., Eu(III), Gd(III), Yb(III), etc.							

(*) Hyper in all (some) cases.
† (†) Hypso in all (some) cases.

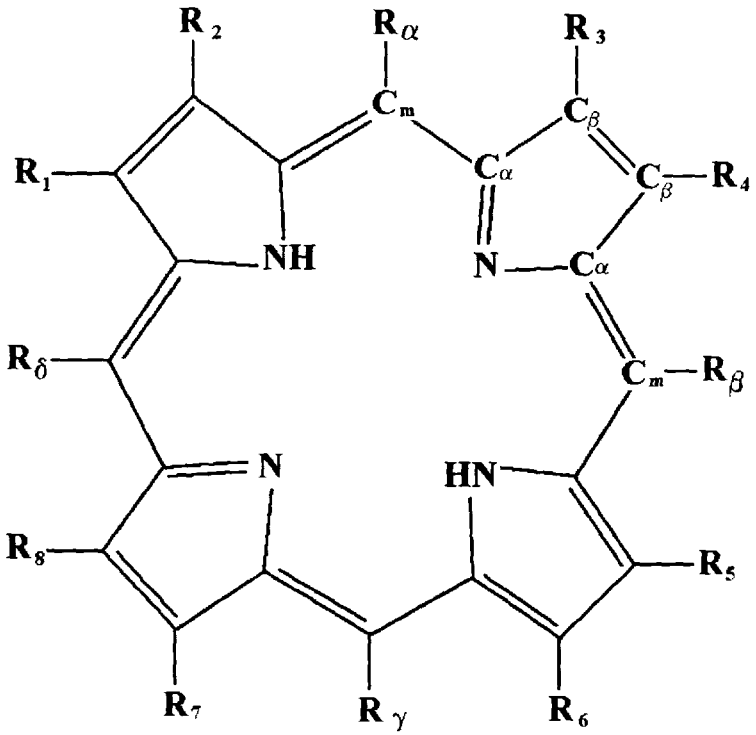

Porphyrin	Abbrev	R_1	R_2	R_3	R_4	R_5	R_6	R_7	R_8	α	β	γ	δ
Octamethylporphyrin	OMP	M	M	M	M	M	M	M	M	H	H	H	H
Octaethylporphyrin	OEP	E	E	E	E	E	E	E	E	H	H	H	H
Tetraphenylporphyrin	TPP	H	H	H	H	H	H	H	H	Ph	Ph	Ph	Ph
Protoporphyrin-IX	PP	M	V	M	V	M	P	P	M	H	H	H	H
Deuteroporphyrin-IX	DP	M	H	M	H	M	P	P	M	H	H	H	H
Mesoporphyrin-IX	MP	M	E	M	E	M	P	P	M	H	H	H	H

M = $-CH_3$; E = $-CH_2CH_3$; V = $-CH{-}CH_2$; Ph = $-C_6H_5$; P = $-CH_2CH_2COOH$

Fig. 1.1 Structure and nomenclature of porphyrin molecule.

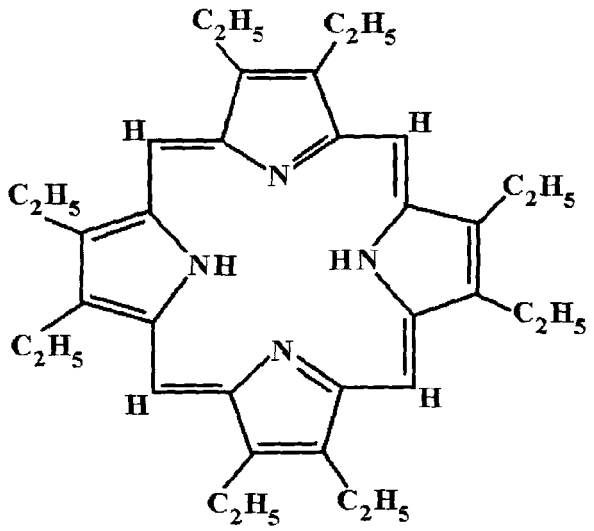

(A)

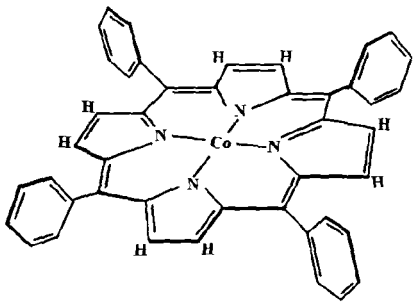

(B)

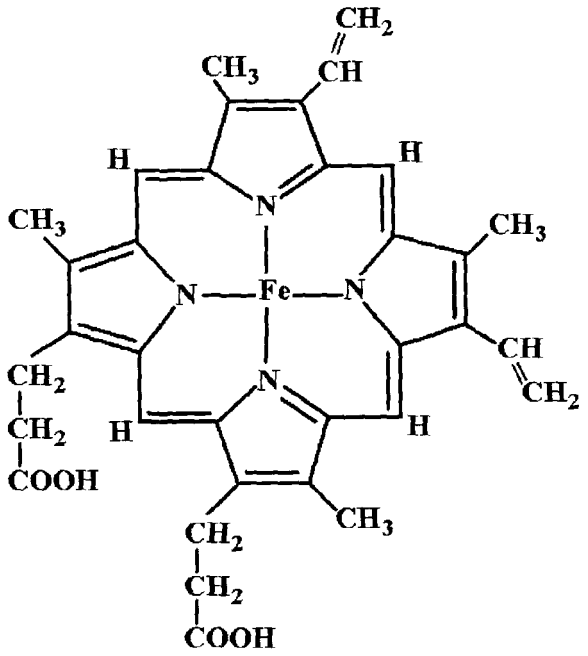

(C)

Fig. 1.2 Molecular structure of (A) Free base octaethylporphyrin;
(B) Cobalt meso-tetraphenylporphyrin;
(C)Iron protoporphyrin-IX.

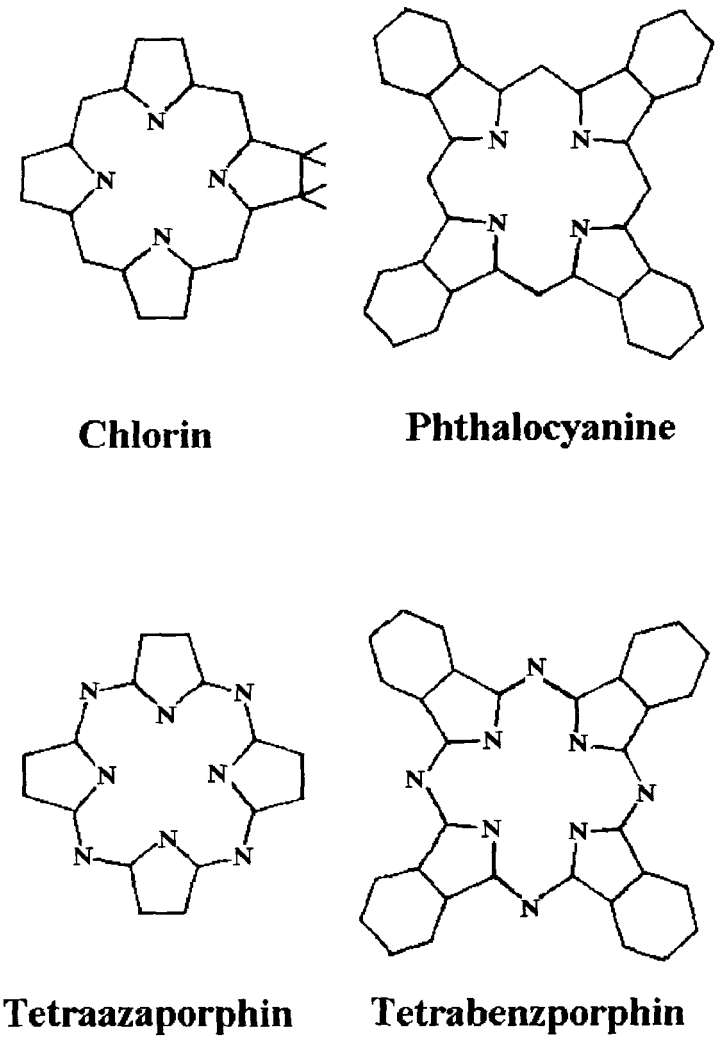

Fig. 1.3 Basic carbon and nitrogen skeletons for porphyrin related molecules.

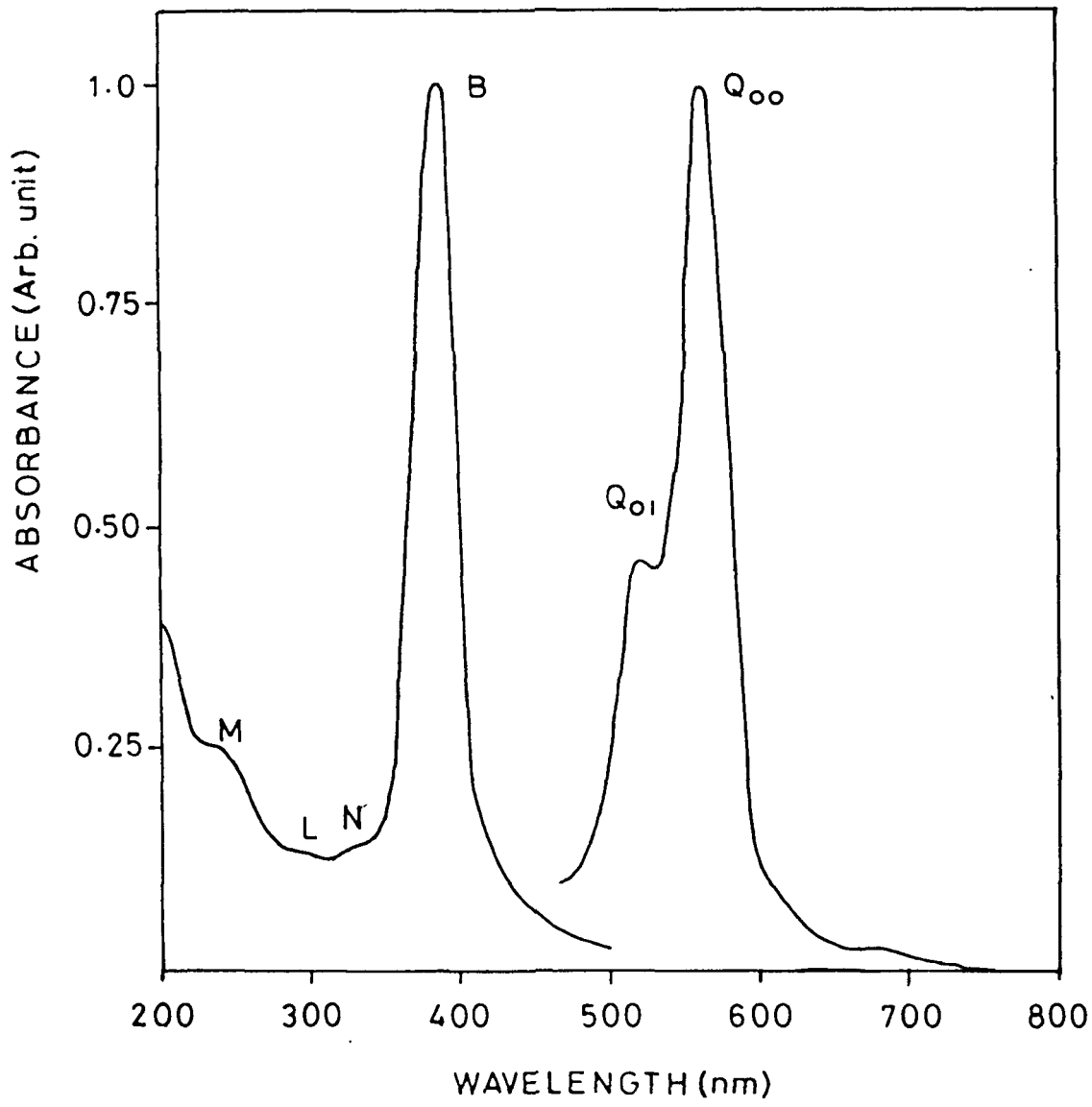

Fig. 1.4 Electronic absorption spectra of Ni (II) octaethylporphyrin [Ref. no. 36].

CHAPTER 2

THEORY

This chapter describes briefly the theoretical aspects of photophysical processes, absorption spectra of porphyrins and their metal derivatives as well as theory of resonance Raman effect.

2.1 Basic Aspects of Photophysical Processes

2.1.1 Photochemical Energy

Generally speaking a certain amount of energy called *activation energy,* has to be supplied to molecules so as to bring about chemical reaction. In some reactions activation energy requirements have been so low that molecules undergo spontaneous transformations even at room temperature. But in most of the cases, additional energy has to be supplied to the molecules before they are able to undergo a chemical change. Very commonly, energy has been supplied by increasing the reaction temperature which yields an energy distribution in such a way that most molecules present in the system acquire the same amount of energy. This method involves molecules in their ground electronic state, and it is not possible to activate one specific component of a mixture by thermal methods.

Photochemical method provides an alternative way to add activation energy to the system. In photochemistry, energy is provided through absorption of electromagnetic radiation in the visible or ultraviolet region by the chromophore of molecules in the system. Unlike thermal activation, the absorption of light is able to excite an individual molecule to an excited electronic state without immediately

effecting the surrounding molecules. This selective excitation of individual molecules has been a unique feature of photochemical reactions. The importance of this alternative method is the capability of directing reactions in rather specific ways.

As radiation in the infrared region of the spectrum corresponds to 1-10 kcal/mole of energy, it is capable of producing vibrationally or rotationally excited molecules. However, light in the visible and ultraviolet region possesses sufficient energy to encompass the range of chemical bond energies and is often able to induce chemical changes by exciting molecules to higher electronic states. The energy associated with visible light vary from 38 kcal/mole (750 nm) to 71 kcal/mole (400 nm), whereas ultraviolet light provides energy upto 143 kcal/mole (200 nm).

2.1.2 Absorption of light

Beer and Lambert proposed laws of light absorption, which form the working principle of spectrophotometer. The laws state that the fraction of the incident light absorbed is proportional to the number of molecules in the path. Mathematically the law is expressed as follows:

$$\text{Absorbance (A)} = \log_{10}(I_o/I) = \epsilon.b.c \qquad 2.1$$

where, I_o represents the intensity of incident light, I represents intensity of transmitted light, b is the optical path length, c represents concentration of the sample in moles/litre, and ϵ is the molar extinction coefficient. The significance of ϵ values lies in the fact that these are directly related to the probability of transitions taking place. Electronic transitions may be allowed (high probability) or forbidden (low probability) and the selection rules govern these probabilities.

2.1.3 Excitation of Electrons

Electrons in ground-state of organic molecules are assigned to orbitals labelled sigma (σ), pi (π), or non-bonding (n). When a photon is absorbed by a molecule one of the electrons in a bonding or non-bonding orbital is excited to an unoccupied orbital of higher energy, which is generally *antibonding orbital*. The excited state orbitals corresponding to σ and π bonds are referred to as the σ^* and π^*, respectively. There are five types of electronic transitions which are observed in the visible and ultraviolet region: $\sigma \rightarrow \sigma^*$; $\sigma \rightarrow \pi^*$; $n \rightarrow \sigma^*$; $n \rightarrow \pi^*$; and $\pi \rightarrow \pi^*$. The energies needed for $\sigma \rightarrow \sigma^*$ and $n \rightarrow \sigma^*$ transitions are usually very high, needing a wavelength of far less than 200 nm. Although photochemical excitation could be carried out using such light, only two of the possible transitions, $n \rightarrow \pi^*$ and $\pi \rightarrow \pi^*$, are of interest in organic photochemistry. These transitions need lower energy and take place at longer excitation wavelengths.

2.1.4 Excitation Pathways

A molecule in which all the electrons are paired is said to be in *singlet state* (S). When two electrons are unpaired the molecule is said to be in a *triplet state* (T). A schematic representation of these electronic configurations for $\pi \rightarrow \pi^*$ transition is given in Fig. 2.1. The first step in a photochemical reaction is excitation of a molecule through absorption of light to a higher electronic state, say from S_o to S_1. The initially excited molecules may be in any of the allowed vibrational levels of the S_1 state but it rapidly decays to the lowest vibrational level of this electronic singlet

state via process called *vibrational relaxation*. S_1 may further undergo one of the following energy-degradation processes.

(i) It may drop to S_0 by emitting the energy in the form of photon. This process generally takes place within 10^{-9} to 10^{-6}s. This process is known as *fluorescence*.

(ii) It may return to S_0 state by non-radiative process in which the excited state looses its energy to vibrational modes.

(iii) It may involve chemical reaction.

(iv) It may decay to a triplet state (T_1) through a process called *intersystem crossing* which is radiationless process.

The singlet and triplet states have considerable excess energy and are thus quite labile. But the conversion of S_1 to T_1 has been energetically a slow process in accordance with the spectroscopic rule that change in multiplicity is a forbidden process. However, if the singlet state is sufficiently long-lived, the intersystem crossing can take place with a high degree of efficiency. For every singlet state there exists a corresponding triplet state, and the average lifetime of the latter is 10^{-5} to 10^{-3} s. The majority of photochemical reactions occur from the triplet state because of its long lifetime. The triplet state is also paramagnetic because of its two parallel unpaired electrons whereas the singlet state is diamagnetic. Photochemical reactions involving triplet states are thus susceptible to quenching by paramagnetic salts and by free radical scavengers like oxygen, iodine, nitric oxide, etc. If no chemical reaction takes place from the excited triplet state, the molecule can loose energy and return to the ground state by emitting photon, a process called phosphorescence, or by radiationless process.

2.1.5 Photo-Induced Electron Transfer

An electronically excited state is obtained when a molecule absorbs a photon of suitable energy [Eqn. 2.2],

$$A + h\nu \rightarrow A^{*} \qquad 2.2$$

Each electronically excited state is virtually a new chemical species with its own chemical and physical properties. In dealing with electronically excited state the following features have to be taken into consideration: (i) the excited molecules are transient species whose lifetimes may range from 10^{-12} to 10^{-3} s. in fluid solution; (ii) an excited state has always a higher electronic affinity and a lower ionization potential compared to the ground- state molecule, and thus it is both a better oxidant and a better reductant than the ground state; (iii) the equilibrium nuclear geometry of the molecule in the excited state may be different from that of the ground state; and (iv) formation of an excited state usually involves population of high-energy, expanded molecular orbitals.

In fluid solution, an excited state which has a lifetime long enough to encounter other species can be deactivated (" *quenched*") in a bimolecular process. The intimate mechanism of the quenching process is often difficult to elucidate, but the final result [Fig. 2.1] is either (i) the electronic energy transfer from the excited state to the quencher, (ii) a chemical reaction between the excited state and the quencher or (iii) the deactivation of the excited state by some catalytic action of the quencher. The quenching of an excited state of a transition metal complex by chemical reaction can occur, in principle, by means of any of the intermolecular reactions which transition metal complexes are able to undergo. Intermolecular excited state reactions, however, can only occur if they are fast enough to compete

with the intramolecular deactivation modes of the excited state and with the other quenching process.

The most important classes of bimolecular reactions of transition metal complexes are ligand substitutions, reactions of the coordinated ligands and inner and outer sphere oxidation-reduction reactions.[1] Ligand substitution reactions are unlikely to be able to compete with the excited state decay unless the entering ligand is the solvent or a counter ion. Some intermolecular reactions involving the coordinated ligands may be fast enough to compete with the excited state decay.

Inner sphere oxidation-reduction reactions, which cannot be faster than ligand substitution reactions, are also unlikely to occur within the excited state lifetime. On the contrary, outer-sphere electron-transfer reactions, which only involve the transfer of one electron without any bond making or bond breaking processes, can be very fast (even diffusion controlled) and can certainly occur within the excited state lifetime of many transition metal complexes. In agreement with these expectations, no example of inner sphere excited state electron-transfer reaction has yet been reported, where as a great number of outer-sphere excited state electron-transfer reactions have been reported.

In dealing with neutral organic molecules in fluid solutions, it has been found that the formation of the electron transfer products in the excited state quenching process may be the result of a very complicated series of events. In particular, the encounter complex may give rise to an excited state complex (*exciplex*), i.e., a situation in which the excited state and the quencher are linked by some kind of interaction,[2,3-5] as illustrated below.

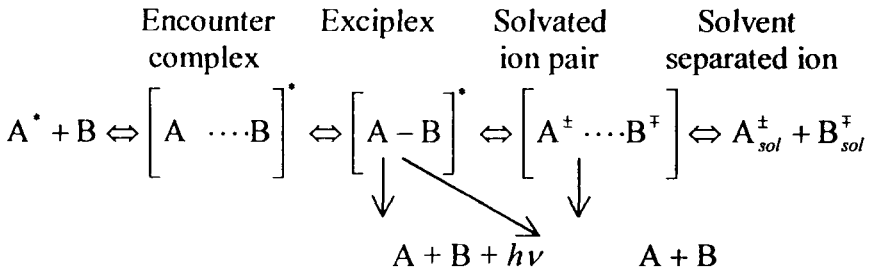

Depending on its own properties and on the experimental conditions, the exciplex can deactivate by luminescence, radiationless transitions or chemical reaction. It is now generally accepted that the exciplex is an intermediate in many bimolecular photochemical transformations of organic molecules. In literature, there are many evidences of exciplex formation between excited state porphyrins and a number of electron acceptors and donors.[6-9] Absorption spectra of exciplexes are slightly red shifted compared to the respective porphyrins as observed for Zn-etioporphyrin[6] and chloroindium(III) TPP[7]. Since the lifetime of the exciplex is generally very short, these complexes can be detected only if a sufficient population is built up by irradiating with intense light source.

When the chemical reaction is electron transfer, a solvated ion pair is formed first, which then dissociates into solvent-separated ions. The encounter rate is determined by diffusion rate constant, which for the usual solvents is of the order of 10^{10} $M^{-1}s^{-1}$. Simple kinetic considerations show that even when high quencher concentrations are used, only those excited states that have lifetimes longer that 10^{-10}-10^{-9} s can be involved in encounters with the quencher. This usually precludes the participation in bimolecular processes to all the excited states except the lowest one of any multiplicity, i.e., S_1 or T_1. An important consequence of this kinetic constraint is that the excited states involved in electron-transfer processes in fluid

solution are thermally equilibrated species, so that their reactions can be dealt with using thermodynamic and kinetic arguments as in the case of any other chemical reactions.[10]

2.2 Absorption Spectra

The porphyrin molecule is highly colored and possesses a number of absorption bands in the optical region, a qualitative description of which is given below.

The free base porphyrin shows a four-banded structure in the visible region numbered as I to IV and intense band between 380 and 420 nm called Soret or B or γ band. In some cases another weak band is observed between the band I and II. The normal metalloporphyrin absorption spectra contain a Soret band and two visible bands called α or Q(0,0) and β or Q(0,1) bands, where α band is considered to be related to the bands I and III and β with bands II and IV respectively of free base porphyrins. In addition to this, some metalloporphyrins such as Mn-porphyrins show distinct additional features, which may arise due to charge transfer transitions, metal d→d transitions or some other types of transitions. These bands arise for those metal-porphyrins for which there is a strong interaction between the metal electrons and those of the porphyrin ring. Fig. 2.2 gives the absorption spectra of free base octaethylporphyrin (H_2OEP) and Co(II) *meso*-tetraphenylporphyrin ($Co^{II}TPP$). The H_2OEP spectrum consists of four bands in the visible region of the spectrum along with strong Soret band. On going to $Co^{II}TPP$, the four-banded visible spectrum reduces to the normal metalloporphyrin absorption spectrum.

The electronic absorption spectra of porphyrins and metalloporphyrins vary with the nature of the chromophoric system and with the peripheral substituents which modify the basic structure. For example, electrophilic side chains such as vinyl and formyl groups, etc. cause a shift of the absorption bands to higher wavelengths due to increase in the π electron density at the periphery of the porphyrin nucleus, i.e., with the decrease of the porphyrin basicity. The correlation between the nature of the side chains and optical absorption spectra were first described by Stern et al.,[11] and later by other workers.[12-14] The ratio of the intensities of the visible bands vary with the nature and distribution of the substituents and accordingly visible spectra can be classified as aetio, phyllo, rhodo and oxorhodo type, as shown in Fig. 2.3.

2.2.1 Theoretical Aspects of Absorption Spectra

Considering the inner 16 membered ring with 18 π electrons (each of the 16 atoms of the inner ring contributes one π electron while the imine nitrogens contribute two electron each), as the delocalization pathway for the electrons, Simpson[15] proposed the first theoretical treatment to explain the optical spectra of the porphyrins. Fig. 2.4 shows the π-electron system for free-base porphyrin. In his free electron model, Simpson predicted that the lower energy transitions would be forbidden whereas the higher energy transition would be allowed. In analogy with benzene, the electrons were placed in orbitals of increasing angular momentum, two in the lowest level ($l_z = 0$) and four each in the $l_z = 1, 2, 3, 4$ levels. The lowest excited states are formed by promoting one of the four electrons of the highest filled orbital with angular momentum $l_z = \pm 4$ to the empty orbital with angular momentum $l_z = \pm 5$. The change

in the orbital angular momentum (Δl_z) will then be either ± 1 or ± 9 and the pairs of the transitions would be allowed or forbidden, respectively. Hund's rules predict that the lower energy state will correspond to $\Delta l_z = \pm 9$. This predicts, as observed, that the longer wavelength transitions are much weaker than the UV-transitions. Simpson also suggested that the two sets of visible bands observed in the metal free porphyrins were due to two forms of tautomers of the free base. However, the extra spectral features of the free base porphyrins are due to the large distortion from square-planar symmetry of the porphyrin skeleton as the free base porphyrin has protons on opposite nitrogen atoms. Replacement of the imine protons by a metal results in four-fold axial symmetry. Platt[13] was the first to realize that the four visible bands of free base porphyrins collapse to two bands in the metal complexes.

In spite of early success, Simpson's model was unable to explain many quantitative features, as the porphyrin was assumed to have cylindrical symmetry $D_{\infty h}$, instead of the actual D_{4h} or D_{2h} symmetry for these molecules. In the subsequent theoretical work on the electron systems, the molecular orbitals were expressed as linear combination of atomic orbitals (LCAO) and the orbital coefficients were determined by a variational procedure. Later on, Longuet-Higgins et al[16] made the first Huckel LCAO treatment and showed that the $3a_{2u}(\pi)$ and $1a_{1u}(\pi)$ were the top filled orbitals and lowest empty degenerate orbital was $4e_g(\pi^*)$. The orbital coefficients for these orbitals are shown in Fig. 2.5. According to this model, the transition $3a_{2u} \rightarrow 4e_g$ at lower energy was identified with the Q(0,0) band and the transition $1a_{1u} \rightarrow 4e_g$ at higher energy as Soret band. This model predicts equal absorption intensities for both the transitions which is, however, not the case.

In order to account for the observed electronic absorption spectra, Gouterman[17,18] developed the "four orbital model", which is a combination of the free electron model[15] and the LCAO-MO[16] description. In this model, Gouterman considered only the two lowest empty and the two highest filled orbitals of porphyrin in the ground state. Because of the four-fold symmetry, the two empty orbitals are degenerate and carry the e_g label of the D_{4h} symmetry. The two highest occupied molecular orbitals are designated as a_{1u} and a_{2u}. Fig. 2.5 shows these four orbitals, depicting the electronic wave function amplitude on the molecular frame. The top filled orbitals are not symmetry degenerate but are assumed to be accidentally degenerate. The a_{1u}, a_{2u} and e_g orbitals are analogous to the free-electron orbitals with $l_z = \pm 4$ and ± 5 respectively in the Simpson's model.[19] The one-electron transitions arise due to excitation of electron from either a_{1u} or a_{2u} to the e_g orbital. These excited states or configuration are denoted by (a_{1u}, e_g) and (a_{2u}, e_g). As they have the same symmetry, their overlap due to Coulomb repulsion energy is finite and the states mix together via configuration interaction. Thus the singly excited configurations are not adequate descriptions of the excited states. If H_{eff} be the Hamiltonian of the pure configurations and if their interaction via Coulomb repulsion between electrons be represented by $H' = e^2/r_{ij}$, then the total Hamiltonian of the system can be written as

$$H = H_{eff} + H' \qquad 2.3$$

The coefficients for the mixed states can be calculated by defining the parameters as follows:

$$A'_{1g} = \frac{1}{2}\left[E(a_{1u}e_{gx}) + E(a_{2u}e_{gy}\right] \quad 2.4$$

$$A'_{1g} = \frac{1}{2}\left[E(a_{2u}e_{gy}) - E(a_{1u}e_{gx}\right] \quad 2.5$$

$$A''_{1g} = \int (a_{2u}e_{gx})H(a_{1u}e_{gy})dv \quad 2.6$$

$$R_{1y} = \int (a_{1u}e_{gx})y\psi_o dv \quad 2.7$$

$$R_{2y} = \int (a_{2u}e_{gx})y\psi_o dv \quad 2.8$$

Since $R_1 \approx R_2$, we have

$$R = \frac{1}{\sqrt{2}}(R_1 \pm R_2) \quad 2.9$$

where A'_{1g} is the center of gravity of the two configurations before their interaction, A_{1g} is the splitting between them, A''_{1g} is configurational interaction and R's are the transition dipole moments. Because of X-Y degeneracy, the matrix describing only the Y-polarized mixed states is given in Table 2.1. The rows of the table represent approximate mixtures for the case in which the configurational interaction is much larger than the splitting between the pure states. This case predicts weak Q band and a minimum in the energy difference E(Soret) – E(Q) which is observed in the absorption spectra of metalloporphyrins. Moreover, it is expected that,

$$E_B - E_Q \approx 2A'_{1g} = Constant \quad 2.10$$

and

$$q_B^2 \approx R^2 = Constant \quad 2.11$$

where the oscillator strength f_B of the Soret band is related to q_B by an expression

$$f_B \approx E_B q_B^2 f_B \qquad 2.12$$

The major conclusion of this calculation is removal of the degeneracy of the Soret and Q states by configuration interaction.

The lower energy transition α, borrows back some intensity of the higher energy transition (Soret) (about 10%) through vibronic coupling with the formation of a vibronic side band called β or Q(0,1) band on the higher energy side of the α-band, such that

$$\nu_\beta \max = \nu_\alpha \max + \nu_{vib} \qquad 2.13$$

where ν_{vib} is the frequency of vibrational modes in the excited electronic state which are responsible for the vibronic coupling.

It is necessary to apply degenerate perturbation theory to linear combinations of the degenerate components as the electronic states of the metalloporphyrins are degenerate. Since only those vibrations contained in the cross product of the symmetries of the two excited states would be active and as both Q and B states originate from configurations of E_u symmetry, vibronic coupling between the two states can occur through vibrations having symmetry species given by:

$$\Gamma_{vib} \subset Eu \times Eu = A_{1g} + A_{2g} + B_{1g} + B_{2g} \qquad 2.14$$

It is argued that A_{1g} modes will not be vibronically active if the cyclic polyene model is strictly applicable to metalloporphyrins.[20] Thus in D_{4h} point group, the only modes vibronically active are those belonging to B_{1g}, B_{2g} and A_{2g} symmetry species.

The vibrational structure that can be resolved in the Soret band region of the porphyrin can be assigned to the Franck-Condon activity of the symmetric vibrations while the vibrational transitions in the Q(0,1) or the β-band region have been

attributed to the vibronic borrowing from the Soret band.[19-21] Experimental evidence of the correctness of this model came from Resonance Raman experiments,[22,23] where it was shown that under Q band resonance excitation of porphyrin complexes, the A_{2g}, B_{1g} and B_{2g} vibrational modes are strongly enhanced, identified by their depolarization ratios. The theoretical section on RR scattering in this chapter will cover further details on the vibronic coupling, Herzberg-Teller activity and the Raman activity of the non-totally symmetric vibrations based on group theoretical and other considerations.

In the case of free base porphyrins (H_2Ps), the symmetry of the molecule is lowered from D_{4h} to D_{2h}. The molecular orbitals (MOs) a_{1u} and a_{2u} become a_u and b_{1u} and degenerate pair of e_g MOs spit into a b_{2g} and a b_{3g} MO in D_{2h} symmetry as shown in Fig. 2.5. Under the changed situation, strong configuration interaction (CI) still exists between the electronic configurations of like symmetry, B_{2u} and B_{3u}, and again a strong Soret band and a weak Q-band arise. But because of the lowering of symmetry, the degeneracy of both the S_1 ($\Delta l_z = \pm 9$) and S_2 ($\Delta l_z = \pm 1$) states, which occurs in metal-porphyrin, is removed. The transition to lower state gives rise to the Q_x band and the higher energy one produces Q_y band.

2.3 Raman Scattering

The interaction of the electric field of electromagnetic radiation with the charge distribution of an atom or a molecule induces an oscillating dipole in the latter. The induced dipole becomes a source of secondary radiations, emitting at the frequency of incident primary radiation. The interference of these primary and secondary radiations is responsible for the phenomena of reflection, refraction and

scattering. Scattering refers to light deflected from the direction of incident-light propagation. The interaction of the electric vector of an electromagnetic wave with the electrons of a compound results in the scattering of the incident light. Such interaction induces periodic vibrations in the electrons of the compound, thereby producing oscillating electric moments. Such oscillating electrons become new sources for emitting radiation, that is, the scattered light. There are two basic types of scattering- elastic and inelastic scattering. Elastic scattering results in scattered radiation of the same frequency (wavelength) as the incident light. This phenomenon is called Rayleigh scattering. On the other hand, inelastic scattering produces radiations with frequencies lower and higher than that of incident light. The effect is called Raman scattering. If the scattered light has lower energy (lower frequency) than that of the incident light, the effect is called Stokes Raman scattering. On the other hand, if the scattered light has higher energy (higher frequency) than that of the incident light, the effect is called anti-Stokes Raman scattering.

In order for a molecule to exhibit the Raman effect, the incident light must induce a dipole-moment change or a change in molecular polarizability. The change in polarizability can be visualized as a change in the shape of the electron cloud of a molecule. The induced dipole moment couples with certain vibrational motion of the molecule through changes in the polarizability of the molecule and lead to scattered photons with altered frequency. The scattered light contains a small portion of light due to Raman scattering (different frequency than that of incident light), in addition to that due to normal Rayleigh scattering (same frequency as the incident light). The Raman scattering contains both Stokes and anti-Stokes lines; their frequencies correspond to the sum and difference of the frequency of the incident light and the

allowed molecular vibrational frequencies. When photons interact with a molecule, part of their energy can be converted into various modes of vibrations of the molecule. Stokes Raman effect is obtained when the scattered light loses energy equivalent to the energy given to molecular vibrations. If the energy is transferred to incident light from a molecule, the scattered light has more energy than the original incident light (anti-Stokes Raman effect). Observation of anti-Stokes Raman scattering requires that the scattering molecule must already be in an excited vibrational state of the electronic ground state.

The fraction of incident photons scattered during Raman process is always very small, and thereby Raman peaks are of extremely weak intensity – only about 10^{-8} fraction of the incident light appears as Raman scattered signal. Intense monochromatic laser, therefore, is used as excitation source to obtain good quality Raman spectra. In the case of normal Raman scattering, the excitation frequency of radiation is far away from the stationary energy states of the system. That is, the intermediate state is not associated with any particular molecular eigen state as such and is considered to be a statistical superposition/summation of a large number of excited electronic states of the system. When the incident light approaches an electronic absorption band, the intermediate state becomes more important and the summation term is dominated by this electronic state. Thus one obtains pre-resonance and resonance Raman scattering conditions by tuning the exciting frequency through the electronic absorption band (Fig. 2.6). In resonance Raman scattering, a few vibronic levels in the vicinity of the incident light energy dominate the intermediate state. Finally, the resonance fluorescence limit is reached when the incident light coincides with a single sharp level of the electronic state. Though both

resonance fluorescence and resonance Raman involve excitation and emission in the electronic absorption band, there is a very precise difference between these two processes. The resonant scattering processes depend not only on the energy difference between the molecule and the photon states, but also on the line shapes associated with them. In the case of resonance fluorescence, the molecular state is much sharper than the photon state and is thus completely in resonance with the incident beam. The scattering may then be described as a rapid population of the excited state followed by a slow decay characterized by the lifetime of this state. In the resonance Raman limit, the photon state is much sharper than the molecular state and thus is in resonance with only a small part of it. In this case two emission processes are involved; a fast one with the lifetime of the incident photon state and a slower one with the excited molecular state lifetime. The former part represents the resonant scattering, while the later represents the non-resonant part of the scattering. Thus the re-emission lifetime is characteristic of either the excited state or of the incident radiation, whichever has the narrower line-width. The resonance fluorescence is attributed to the later situation and resonance Raman scattering to the former.[24] The physical process, however, remains the same in spite of this distinction between the two phenomenon.

2.3.1 Theory of Resonance Raman Scattering

The charge distribution of a molecule is perturbed periodically by electric field of the exciting electromagnetic wave. The induced alternating dipole moment resulting from the interaction acts as a source of secondary radiation and forms a basis of light scattering phenomena. This treatment fairly demonstrates how

polarizability fluctuations give rise to frequency shifts in the scattered radiation. This simple classical treatment, however, offers no clues to the inherent nature of the interaction of radiation with matter, nor it explains important phenomena like resonance and stimulated Raman scattering. Therefore, a fully quantum mechanical electrodynamical approach in which both the radiation and matter are quantized was first applied by Jacon[25] for understanding the RR scattering. However, the correct results for RR scattering may also be obtained by using semi-classical treatment of Kramers and Heisenberg[26] that correlates the scattering tensors to the wave functions and the energy levels of the scatterer. The radiation is treated classically and is regarded as a source of perturbation to the energy levels of the scattering system while quantum mechanical techniques are used to investigate transitions between the quantized levels of the perturbed system. Many workers in the later studies have extended this approach.[27-31]

Consider a non-rotating molecule at the origin of a space-fixed coordinate system interacting with an incident plane wave of light with electric vector represented as

$$\bar{E}_\sigma = \bar{E}^o_\sigma \exp i(\bar{k}.r - \omega) \qquad 2.15$$

Propagating along $\bar{k}$ with angular frequency ω, the oscillating electric dipole moment induced in the molecule is given by

$$(\bar{\mu}_\sigma)_{mn} = (\tilde{\alpha}_{\rho\sigma})_{mn} \bar{E}_\sigma \qquad 2.16$$

where $(\bar{\mu}_\sigma)_{mn} = \langle \psi_m | \bar{e}_\sigma | \psi_n \rangle$ is the amplitude of the transition moment and ψ_m and ψ_n are the time dependent wavefunctions of the initial and final states respectively,

$(\tilde{\alpha}_{\rho\sigma})_{mn}$ is the polarizability tensor for the transitions from m to n and $\bar{\rho}$ and $\bar{\sigma}$ are molecular cartesian axes of the scattering tensor $(\tilde{\alpha}_{\rho\sigma})_{mn}$.

Let us consider a molecule, initially in a vibronic state $|m\rangle$, which is perturbed by plane polarized incident light of frequency ν_o and intensity I_o causing a transition to a vibronic state $|n\rangle$ giving rise to the scattered light of frequency $(\nu_o \pm \nu_{mn})$. The scattered light intensity I_{mn} in terms of photons per molecule per second in the 4π solid angle, after averaging over all orientations of the molecule, is given by[32]

$$I_{mn} = \frac{128\pi^5}{9c^4}(\nu_o \pm \nu_{mn})^4 I_o \sum_{\rho,\sigma} \left|(\alpha_{\rho\sigma})_{mn}\right|^2 \qquad 2.17$$

where c is the velocity of light and the sum goes over $\rho, \sigma = x, y, z$.

From equation 2.17, it is clear that the intensity of the scattered radiation depends upon the frequency of the incident radiation, and more critically it depends on $\left|(\alpha_{\rho\sigma})_{mn}\right|^2$ when the exciting radiation approaches an electronic absorption band in the resonance Raman effect. Consequently, the main effort in the development of Raman theory is to provide a theoretical framework for calculating $(\alpha_{\rho\sigma})_{mn}$ in terms of molecular parameters.

In order to determine the polarizability, the distortion of the wave functions due to periodic perturbations by the incident electromagnetic wave has to be known or calculated and then to evaluate the electric dipole transition moment with the new wave functions using time dependent perturbation theory. The molecular wave functions are obtained from time dependent Schrodinger equation

$$i\hbar\frac{\partial}{\partial t}|\psi\rangle = (H_o + V)|\psi\rangle \qquad 2.18$$

where H_o is the unperturbed hamiltonian and

$$|\psi\rangle = \sum_k a_k(t)|\psi_k^o(t)\rangle \qquad 2.19$$

where

$$|\psi_k^o(t)\rangle = |\psi_k^o\rangle \exp(^{-iH_o t}/_{\hbar}) \qquad 2.20$$

is the solution for V=0

$$V = -\frac{1}{2}\left[\bar{\mu}_\rho\left\{\bar{E}_\rho^o \exp(-i\omega t) + \bar{E}_\rho^o \exp(i\omega t)\right\}\right] \qquad 2.21$$

describes the major part of the interaction of the molecule with electromagnetic radiation.

The $(\rho\sigma)^{th}$ component of the matrix element of the polarizability tensor for the transition from vibronic state $|m\rangle$ to a vibronic state $|n\rangle$ is given by the second order perturbation theory as described by Kramers-Heisenberg-Dirac.[26]

$$(\alpha_{\rho\sigma})_{mn} = \frac{1}{h}\sum_e\left[\frac{\langle n|\mu_\sigma|e\rangle\langle e|\mu_\rho|m\rangle}{\nu_{em} - \nu_o + i\Gamma_e} + \frac{\langle n|\mu_\rho|e\rangle\langle e|\mu_\sigma|m\rangle}{\nu_{en} + \nu_o + i\Gamma_e}\right] \qquad 2.22$$

where μ_σ and μ_ρ are the dipole moment operators and the sum goes over the excited vibronic states $|e\rangle$ of the molecule.

When $\langle e|\mu|m\rangle$ is finite for a real state $|e\rangle$, the transition from $|m\rangle$ to $|e\rangle$ is accompanied by light absorption with center frequency ν_{em} and full-width at half maximum of $2\Gamma_e$, and the absorption intensity would be proportional to $|\langle e|\mu|m\rangle|^2$. If the photon energy $(h\nu_o)$ of Raman excitation were close to the energy of the

electronic transition, the first term of $(\alpha_{\rho\sigma})_{mn}$ and thus I_{mn} would be remarkably large. This is called resonance Raman scattering. The vibrational modes which gain resonance enhancement in intensity are limited to the vibrations associated with the chromophore responsible for the absorption band.

The Eq. 2.22 can be made more meaningful by incorporating Born-Oppenheimer adiabatic approximation[33] for all wave functions involved and then expanding the electronic wave functions in a Taylor's series around the ground state equilibrium configuration of the nuclei. Thus a given vibronic state must now be identified according to electronic and vibrational levels, as $|m\rangle = |g,i\rangle$, $|n\rangle = |g,j\rangle$ and $|e\rangle = |r,v\rangle$ which depends on both the nuclear and electronic wave functions for the ground and excited states, respectively; $|i\rangle$, $|j\rangle$ and $|v\rangle$ are the vibrational wave functions with the quantum numbers *i*, *j* and *v*, respectively. In this formulation it is also postulated that the vibrational wave functions in the electronic excited states are the same as those in the electronic ground state except for the origin of the coordinates, i.e., the equilibrium structure of the molecule, which differs between the two states. The change of the electronic wave function due to the origin shift is incorporated with Herzberg-Teller expansion. Then the main terms contributing to the polarizability tensor of Eq. 2.22 under resonance with a particular electronic state, $|r\rangle$, are the following two terms

$$(\alpha_{\rho\sigma})_{ij}^{r} = (A_{\rho\sigma})_{ij}^{r} + (B_{\rho\sigma})_{ij}^{r} \qquad 2.23$$

where

$$(A_{\rho\sigma})_{ij}^{r} = \frac{M_{\sigma}^{gr} M_{\rho}^{gr}}{h} \sum_{v} \frac{\langle j|v\rangle\langle v|i\rangle}{\nu_{rg} + (v-i)\Delta\nu_{a} - \nu_{0} + i\Gamma_{r}} \qquad 2.24$$

and

$$(\mathrm{B}_{\rho\sigma})_{ij}^{r} = \frac{\mathrm{M}_{\sigma}^{gr} h_{a}^{rs} \mathrm{M}_{\rho}^{sg}}{h^{2}(\nu_{r}-\nu_{s})} \sum_{v} \frac{\langle j|v\rangle\langle v|i\rangle}{\nu_{rg}+(v-i)\Delta\nu_{a}-\nu_{o}+i\Gamma_{r}} +$$

$$\frac{\mathrm{M}_{\sigma}^{gs} h_{a}^{sr} \mathrm{M}_{\rho}^{rg}}{h^{2}(\nu_{r}-\nu_{s})} \sum_{v} \frac{\langle j|v\rangle\langle v|Q_{a}|i\rangle}{\nu_{rg}+(v-i)\Delta\nu_{a}-\nu_{o}+i\Gamma_{r}} \qquad 2.25$$

where $\mathrm{M}_{\sigma}^{gr} = \langle g^{o}|\mu_{\sigma}|r^{o}\rangle$, $h\nu_{rg}$ is the energy separation between the $|r\rangle$ and $|g\rangle$ states, $\Delta\nu_{a}$ is the frequency of the normal mode with coordinates Q_a and $h_{a}^{rs} = \langle r|\frac{\partial H}{\partial Q_{a}}|s\rangle$ is the vibronic coupling operator that mixes the two electronic states via a given normal mode Q_a

The above results can be summarized as follows: when Raman spectra are obtained with excitation in the region of an electronic absorption band, the vibrational modes which are expected to show enhancement are the one which contribute intensity to the electronic spectrum, i.e., they are vibronically active modes, which are of two types: (i) modes which connect the ground state to the excited state involved in resonance through the Frank-Condon overlap (A-term); (ii) modes which mix the resonant electronic state to another one of higher energy state (B-term). The potential energy curve of the excited electronic state is shifted in the Frank-Condon effect so that the vibrational wave functions are non-orthogonal. Raman scattering from modes due to Frank-Condon effect can arise only when the orthogonality is removed between a ground state and an excited state vibrational wave function. Since A-term is the leading term, it is generally the dominant contribution to RR intensity. A-term enhancement varies directly with the strength of the electronic transition and inversely with its bandwidth and it also depends on the

magnitude of the product $\langle j|v\rangle\langle v|i\rangle$. This increases with increase in displacement of the excited state potential well along the normal coordinate, i.e., A-term modes gain intensity via origin shift. Hence, the extent of excited state distortion determines the degree of enhancement of a given mode. As for non-totally symmetric modes, there is no origin shift, the Frank-Condon product $\langle j|v\rangle\langle v|i\rangle$ is zero and thereby no enhancement of these modes via the Frank-Condon term.

However, non-totally symmetric modes can gain intensity via the B-term because of the Q-dependent vibrational integrals. The contributions of $\langle 1|Q|0\rangle\langle 0|0\rangle$ and $\langle 1|1\rangle\langle 1|Q|0\rangle$ terms are significant to the B-term for vibrational modes differing by one quantum. Therefore, the B-term becomes important in situations where a forbidden or weakly allowed transition gains intensity from vibronic mixing with a strongly allowed transition. The mixing modes are then prominent in the RR spectrum when excited at the weak transition. The enhancement depends on the magnitude of the mixing integral and on the proximity of the electronic states. A limiting case is the Jahn-Teller effect, in which the mixing states are degenerate. In this case, the mixing vibrations (Jahn-Teller active modes) are strongly enhanced.

2.4 Normal Modes of Vibration

In diatomic molecules, the vibration of the nuclei occurs only along the line connecting two nuclei. In polyatomic molecules, however, the situation is much more complicated because all the nuclei perform their own harmonic oscillations. It can be shown, however, that any of these extremely complicated vibrations of the

molecule may be represented as a superposition of a number of independent vibrations called *normal modes of vibration*. In each normal vibration, the individual nuclei carry out a simple harmonic motion, and all the nuclei have the same frequency of oscillation and are moving in the same phase. Although the motion of many atoms is involved in each of the normal modes, a simplification of the expressions for many properties of the molecule results. For example, the total vibrational energy of the molecule is then just the sum of the vibrational energy from each normal mode. For general N-atom molecule, the number of normal vibrations is 3N-6 (or, if linear, 3N-5 normal vibrations). Thus the general form of the molecular vibration is a superposition of the 3N-6 (or 3N-5) normal vibrations. For any given molecule, however, only vibrations that are permitted by the selection rule for the molecule appear in the infrared and Raman spectra. According to the selection rule for harmonic oscillator, any transitions corresponding to $\Delta v = \pm 1$ are allowed. Under ordinary conditions, however, only the normal modes that originate in the transition from $v = 0$ to $v = 1$ in the electronic ground state can be observed because of the Maxwell-Boltzmann distribution law. In addition to the selection rule for the harmonic oscillator, another restriction results from the symmetry of the molecule. Thus the number of allowed transitions in polyatomic molecules is greatly reduced. The overtones and combination bands of these normal vibrations are forbidden by the selection rule of the harmonic oscillator. However, they are weakly observed in the same spectrum because of anharmonicity of the vibration.

If a molecule has a number of symmetry elements, the (3N-6 or 3N-5) normal vibrations are classified as various species according to the number and the kind of symmetry elements preserved during the vibration. The number of normal vibrations

in each species can be found using group theory. For the 38 atoms free base porphyrin (assuming side chain to be point masses), there are 108 normal modes of vibration, which classify as

$$\Gamma_{\text{in-plane}} = 19\,A_g + 18\,B_{1g} + 18\,B_{2u} + 18B_{3u} \qquad 2.26$$

$$\Gamma_{\text{out-of-plane}} = 8\,A_u + 10\,B_{1u} + 8\,B_{2g} + 9B_{3g} \qquad 2.27$$

vibrations for D_{2h} symmetry point group of free-base porphyrin. Similarly, assuming all the peripheral substituents as point mass in metalloporphyrin, the 37-atom D_{4h} model will have 105 normal modes of vibration which classify as

$$\Gamma_{\text{in-plane}} = 9A_1g + 8A_{2g} + 9B_{1g} + 9B_{2g} + 18E_u \qquad 2.28$$

$$\Gamma_{\text{out-of-plane}} = 3A_{1u} + 6A_{2u} + 5B_{1u} + 4B_{2u} + 8E_g \qquad 2.29$$

2.5 The Polarizability Tensor and Depolarization Ratios

As mentioned earlier, when electromagnetic radiation interacts with the charge distribution of a molecule, the polarization of the charge cloud induced by the electric field of the incident radiation results in an induced dipole moment. The dipole moment so induced is proportional to the electric field and the polarizability α for small electric field strength is given by:

$$\bar{\mu} = \alpha\bar{E} \qquad 2.30$$

For an isotropically polarizable molecule, the induced dipole moment vector $\bar{\mu}$ is in the same direction as that of the electric field vector $\bar{E}$. However, for an anisotropic molecule, the induced dipole moment in any direction is given by

$$\mu_{ij} = \sum \alpha_{ij}\bar{E}_j \qquad 2.31$$

where $i,j = x, y, z$. The polarizability tensor α_{ij} can be expressed as

$$\alpha_{ij} = \begin{bmatrix} \alpha_{xx} & \alpha_{xy} & \alpha_{xz} \\ \alpha_{yx} & \alpha_{yy} & \alpha_{yz} \\ \alpha_{zx} & \alpha_{zy} & \alpha_{zz} \end{bmatrix} \qquad 2.32$$

Because of symmetry there are only six polarizability tensor components. The elements of α_{ij} generally depend on the frequency of the incident radiation, apart from the wave functions and electronic properties of the molecular systems. However, certain combinations of the polarizability tensor elements remain invariant with respect to change of coordinate system and are given by

$$(\bar{\alpha})^2 = \frac{1}{9}\left[\alpha_{xx} + \alpha_{yy} + \alpha_{zz}\right]^2 \qquad 2.33$$

$$\gamma_s^2 = \frac{1}{2}\left[(\alpha_{xx} - \alpha_{yy})^2 + (\alpha_{yy} - \alpha_{zz})^2 + (\alpha_{zz} - \alpha_{xx})^2\right]$$

$$+ \frac{3}{2}\left[(\alpha_{xy} + \alpha_{yx})^2 + (\alpha_{yz} + \alpha_{zy})^2 + (\alpha_{zx} + \alpha_{xz})^2\right] \qquad 2.34$$

$$\gamma_{as}^2 = \frac{3}{4}\left[(\alpha_{xy} - \alpha_{yx})^2 + (\alpha_{yz} - \alpha_{zy})^2 + (\alpha_{zx} - \alpha_{xz})^2\right] \qquad 2.35$$

where $\bar{\alpha}$, γ_s and γ_{as} represent the isotropic, symmetric isotropic and the antisymmetric anisotropic tensor invariants.

The scattering geometry for incident light propagating along the Y-axis is shown in Fig. 2.7. The scattered radiation is detected along the Z-axis. For this geometry, the depolarization ratio for randomly oriented molecules in fluid state in 90° scattering geometry is defined as follows:

$$\rho_l(\theta = 90^o) = \frac{I_\perp}{I_\parallel} \qquad 2.36$$

The subscript on ρ_l indicates that it is defined for linearly polarized radiation. In terms of polarizability components,

$$\rho_l = \frac{3\gamma_s^2 + 5\gamma_{as}^2}{45(\bar{\alpha})^2 + 4\gamma_s^2} \qquad 2.37$$

For normal Raman effect, the tensor is symmetric and $\alpha_{ij} = \alpha_{ji}$. Hence $\gamma_{as}^2 = 0$ and ρ_l has its well known form for non-resonant Raman scattering given by

$$\rho_l = \frac{3\gamma_s^2}{45(\bar{\alpha})^2 + 4\gamma_s^2} \qquad 2.38$$

and reduces Eq. 2.34 to

$$\gamma_s^2 = \frac{1}{2}\left[(\alpha_{xx} - \alpha_{yy})^2 + (\alpha_{yy} - \alpha_{zz})^2 + (\alpha_{zz} - \alpha_{xx})^2\right] + 3\left[\alpha_{xy}^2 + \alpha_{xz}^2 + \alpha_{yz}^2\right] \qquad 2.39$$

For Raman scattering from non-totally symmetric modes, $(\bar{\alpha})^2 = 0$ and $\rho_l = \frac{3}{4} + \frac{5\gamma_{as}^2}{4\gamma_s^2}$.

If $\gamma_{as}^2 = 0$, we have normal polarization with $\rho_l = 3/4$.

Under resonance Raman scattering the tensor need not remain symmetric, i.e., $\alpha_{ij} \neq \alpha_{ji}$.

If $\gamma_{as}^2 \neq 0$, then $\rho_l > 3/4$ and we have anomalous polarization provided $\gamma_s^2 \neq 0$; if $\gamma_s^2 = 0$, then $\rho_l = \infty$ (inverse polarization).

For totally symmetric modes, where $(\bar{\alpha})^2 \neq 0$ and $\gamma_{as}^2 = 0$;

$$\rho_l = \frac{3}{\{45(\bar{\alpha})^2 \quad \gamma_s^2\} + 4} \qquad 2.40$$

and so $0 \leq \rho_l < 3/4$ according as $\infty \geq \frac{45(\bar{\alpha})^2}{\gamma_s^2} > 0$

Group theoretical considerations can provide information about the invariants which are non-zero for particular vibrational modes in molecules of a given symmetry, and thus about the symmetry properties of the general polarizability tensor. McClain[34] has given the symmetries of the scattering tensor for different molecular point groups. This helps in evaluating the contributions from any of the invariants for a Raman process transforming under any irreducible representations of a point group pertinent to the molecule. Dispersion of ρ_l with exciting frequency often provides valuable structural information about the symmetry of the molecule.

Experimentally the evaluation of all the three tensor invariants requires three independent intensity measurements, The measurement of the total scattering at 90°, ($I_\perp + I_\parallel$), and the depolarization ratio ρ_l, may be supplemented by a measurement involving circularly polarized light. It is usual to measure the reversal coefficient I_{contra}/I_{co}, which is the ratio of the intensity of contra-rotating to that of co-rotating light for the back scattering of pure circularly polarized incident radiation. This is, however, not sufficient to determine the point group symmetry of the molecule having modes which show a dispersion of ρ_l. In addition to the measurement at a particular exciting frequency, one requires measurements at various values of ν_o and if $I_\perp$ and $I_\parallel$ are measured at various exciting frequencies.

2.5.1 Antisymmetric Tensor Contributions

The first experimental evidence of inverse polarization in resonance Raman studies of porphyrins and heme proteins was provided by Verma and Bersntein[35] and, Spiro and Strekas,[22] respectively. The modes, which are responsible for this effect, are of A_{2g} symmetry. Since A_{2g} modes are associated with antisymmetric scattering tensor i.e., $\alpha_{ij} = -\alpha_{ji}$ and they are inactive in normal Raman scattering. Warshel[36] has explicitly demonstrated the antisymmetry of the scattering tensor in D_{4h} symmetry, and has shown that such a situation can exist in the presence of a doubly degenerate electronic level and a rotational type vibrational mode, which leads to equal rotation of the two orthogonal transition moments. The A_{2g} vibrations have rotational symmetry about the four-fold axis. Inverse polarization may be observed with proper exciting line, i.e., the plane of polarization of the incident light is rotated through 90° on scattering and $\rho_l = \infty$. Some of the Raman bands in different systems have been observed with $\rho_l \neq \infty$ but $\rho_l > 3/4$, which are called anomalously polarized bands. There are two possible explanations for observation of anomalous polarization in resonance Raman spectra of porphyrins. The effective symmetry of the molecule may be less than D_{4h} in which case the A_{2g} mode may acquire symmetric as well as antisymmetric contributions from scattering tensors. Alternatively, there may be accidental degeneracies between A_{2g} modes and the modes of other symmetries, which are polarized (A_{1g}) or depolarized (B_{1g} or B_{2g}), giving an overall depolarization ratio less than ∞. From systematic RR studies and careful measurements of depolarization ratios of some selected Raman bands as a function of excitation wavelength on Cu-porphin and Cu-mesoporphyrin, Verma et

al,[37,38] had shown that the former has rigorous D_{4h} symmetry while the symmetry of the latter is reduced to C_s due to asymmetric placement of substituents.

References

1. Cotton, F.A.; Wilkinson, G. *Advance Inorganic Chemistry*; 3th edition.; Wiley: New York, 1972.
2. Balzani, V.; Moggi, L.; Manfrin, M.F.; Bolletta, F.; Laurence, G.S. *Coord. Chem. Rev.* 1975, 15, 321.
3. Grellmann, K.H.; Watkins, A.R.; Weller, A. *J. Phys. Chem.* 1972, 76, 469.
4. Labianca, D.A.; Taylor, G.N.; Hammond, G.S. *J. Am. Chem. Soc.* 1972, 94, 3679.
5. Hino, T.; Akazawa, H.; Masuhara, H.; Mataga, N. *J. Phy. Chem.* 1976, 80, 33.
6. (a) Whitten, D.G.; Lopp, I.G.; Wildes, P.D. *J. Am. Chem. Soc.* 1968, 90, 7196. (b) Roy, J.K.; Carroll, F.A.; Whitten, D.G. *J. Am. Chem. Soc.* 1974, 96, 6349.
7. Hoshino, M.; Seki, H.; Shizuka, H. *J. Phy. Chem.* 1985, 89, 470.
8. Turpin, P.-Y.; Chinsky, L.; Laigle, A.; Tsuboi, M.; Kincaid, J.R.; Nakamoto, K. *Photochem. Photobiol.* 1990, 51, 591.
9. Becker, H.G.O.; Lehmann, T.; Zieba, J. *J. Prakt. Chemie.* 1989, 331, 806.
10. Harriman, A. *J. Chem. Soc. Farad. Trans. 2* 1981, 77, 1281.
11. (a) Stern, A.; Wenderlein, H. *Z. Physik. Chem.* 1936, A177, 165. (b) Stern, A.; Molvig, H. *Z. Physik. Chem.* 1936, A177, 365. (c) Stern, A.; Wenderlein, H. *Z. Physik. Chem.* 1937, A178, 161. (d) Stern, A.; Prunckner, F. *Z. Physik. Chem.* 1937, A178, 420. (e) Stern, A.; Prunckner, F. *Z. Physik. Chem.* 1937, A179, 275.
12. Falk, J.E. In *Porphyrins and Metalloporphyrins*; Elsevier: Amsterdam, 1964.

13. Platt, J.R. In *Radiation Biology*; Hollaender, A., Ed.; McGraw-Hill: New York, 1956; Vol. 3, Chapter 2.

14. Gouterman, M. *J. Chem. Phys.* 1959, 30, 1139.

15. Simpson, W.T. *J. Chem. Phys.* 1949, 17, 1218.

16. Longuet-Higgins, H.C.; Rector, C.W.; Platt, J.R. *J. Chem. Phys.* 1950, 18, 1174.

17. Gouterman, M. In *Excited States of Matter*; Shoppee, C.W., Ed.; Graduate Studies Tech. Univ., 1973; Vol. 2, pp. 1.

18. Gouterman, M. *J. Mol. Spectrosc.* 1961, 6, 138.

19. Eaton, W.E.;. *J. Chem. Phys.* 1967, 46, 2533.

20. Perrin, W.E.; Gouterman, M.; Perrin, C.L. *J. Chem. Phys.* 1969, 50, 4137.

21. Solov'ev, K.N. *Opt. Spectrosc.* 1961, 10, 389.

22. Spiro, T.G.; Strekas, T.G. *Proc, Natl. Acad. Sci. USA*, 1972, 69, 2622.

23. (a) Friedman, J.M.; Hochstrasser, R.M. *J. Am. Chem. Soc.* 1976, 98, 4043. (b) Friedman, J.M.; Hochstrasser, R.M. *Chem. Phys.* 1973, 1, 457.

24. Friedman, J.M.; Hochstrasser, R.M. *Chem. Phys.* 1974, 6, 155.

25. Jacon, M. In *Advances in Raman Spectroscopy*; Mathein, J.P., Ed.; 1973, Vol. 1.

26. Kramers, H.A.; Heisenberg, W. *Z. Physik* 1925, 31, 681.

27. Dirac, P.A.M. *Proc. Roy. Soc. (London)* 1927, 114, 710.

28. Albrecht, A.C. *J. Chem. Phys.* 1961, 34, 1476.

29. Krushinskie, L.L.; Shorygin, P.P. *Opt. Spectrosc. USSR* 1965, 19, 312.

30. Savin, F.A. *Opt. Spectrosc.* 1965, 19, 308.

31. Verlan, E.M. *Opt. Spectrosc. USSR* 1966, 20, 341 and 447.

32. Tang, J.; Albrecht, A.C. In *Raman Spectroscopy*; Szymanski, H.A., Ed.; Plenum: New York, 1970; Vol. 2, pp. 33.

33. Herzberg, G. In *Electronic Spectra of Polyatomic Molecules*; van Nostrand Reinhold Co.: New York, 1960.

34. McClain, W.M. *J. Chem. Phys.* 1971, 5, 2789.

35. Verma, A.L.; Bernstein, H.J. *J. Raman Spectrosc.* 1974, 2, 163.

36. Warshel, A. *Chem. Phys. Lett.* 1976, 43, 273.

37. Verma, A.L.; Bernstein, H.J. *J. Chem. Phys.* 1974, 61, 2560.

38. Verma, A.L.; Mendelsohn, R.; Bernstein, H.J. *J. Chem. Phys.* 1974, 61, 383.

Table 2.1 Hamiltonian for y Polarized States

			Dipole Strength (q^2)
	$(a_{2u}e_{g1})$	$(a_{1u}e_{gx})$	
(a)			
$(a_{2u}e_{g1})$	$A'_{1g} + A_{1g}$	A''_{1g}	R_2^2
$(a_{1u}e_{gx})$	A''_{1g}	$A'_{1g} - A_{1g}$	R_1^2
	B_1^0	Q_1^0	
(a')			
$B_1^0 \equiv \frac{1}{\sqrt{2}}[(a_{2u}e_{g1}) + (a_{1u}e_{gx})]$	$A'_{1g} + A''_{1g}$	A_{1g}	$R^2 \equiv \frac{1}{2}(R_1 + R_2)^2$
$Q_1^0 \equiv \frac{1}{\sqrt{2}}[(a_{2u}e_{g1}) - (a_{1u}e_{gx})]$	A_{1g}	$A'_{1g} - A''_{1g}$	$r^2 \equiv \frac{1}{2}(R_1 - R_2)^2$
	B_1	Q_1	
$(b)\left[\tan 2v \equiv A_{1g}/A''_{1g}\right]$			
$B_1 \equiv \cos v B_1^0 + \sin v Q_1^0$	$A'_{1g} + A''_{1g}/\cos 2v$	0	$\frac{1}{2}(1+\cos 2v)R^2 + Rr\sin 2v + \frac{1}{2}(1-\cos 2v)r^2$
$Q_1 \equiv -\sin v B_1^0 + \cos v Q_1^0$	0	$A'_{1g} - A''_{1g}/\cos 2v$	$\frac{1}{2}(1-\cos 2v)R^2 - Rr\sin 2v + \frac{1}{2}(1+\cos 2v)r^2$
$(c)\left[2v = A_{1g}/A''_{1g} << 1\right]$			
$B_1 = B_1^0 + vQ_1^0$	$A'_{1g} + A''_{1g}(1+2v^2)$	0	$R^2 - v^2R^2 + 2vRr$
$Q_1 = Q_1^0 - vB_1^0$	0	$A'_{1g} - A''_{1g}(1+2v^2)$	$(vR - r)^2$

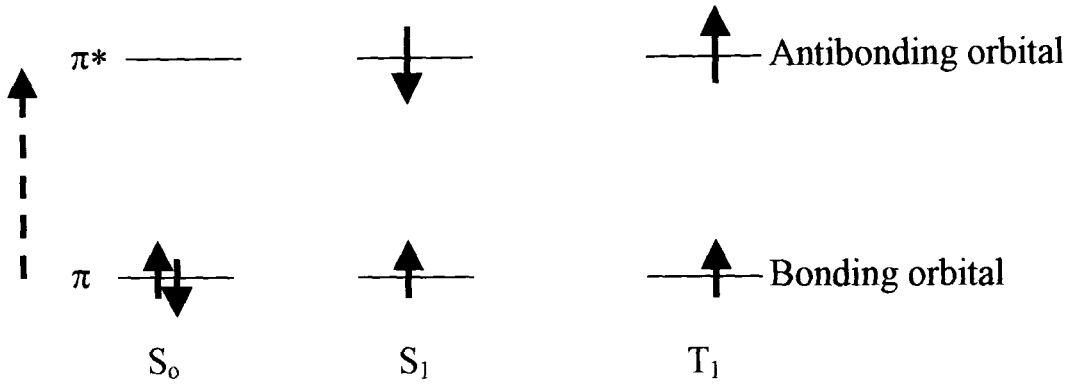

(A)

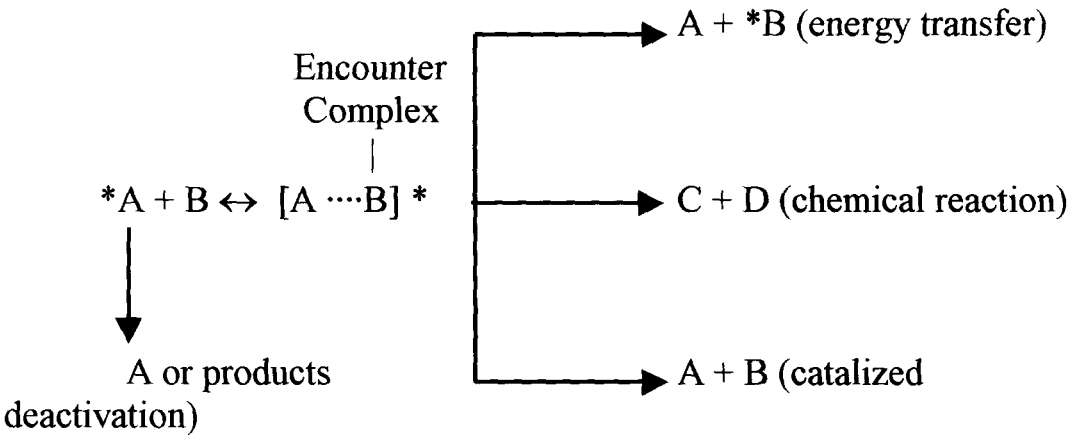

(B)

Fig. 2.1 (A) Electronic configuration of singlet (S) and triplet (T) states (B) Bimolecular quenching process for an excited-state molecule.

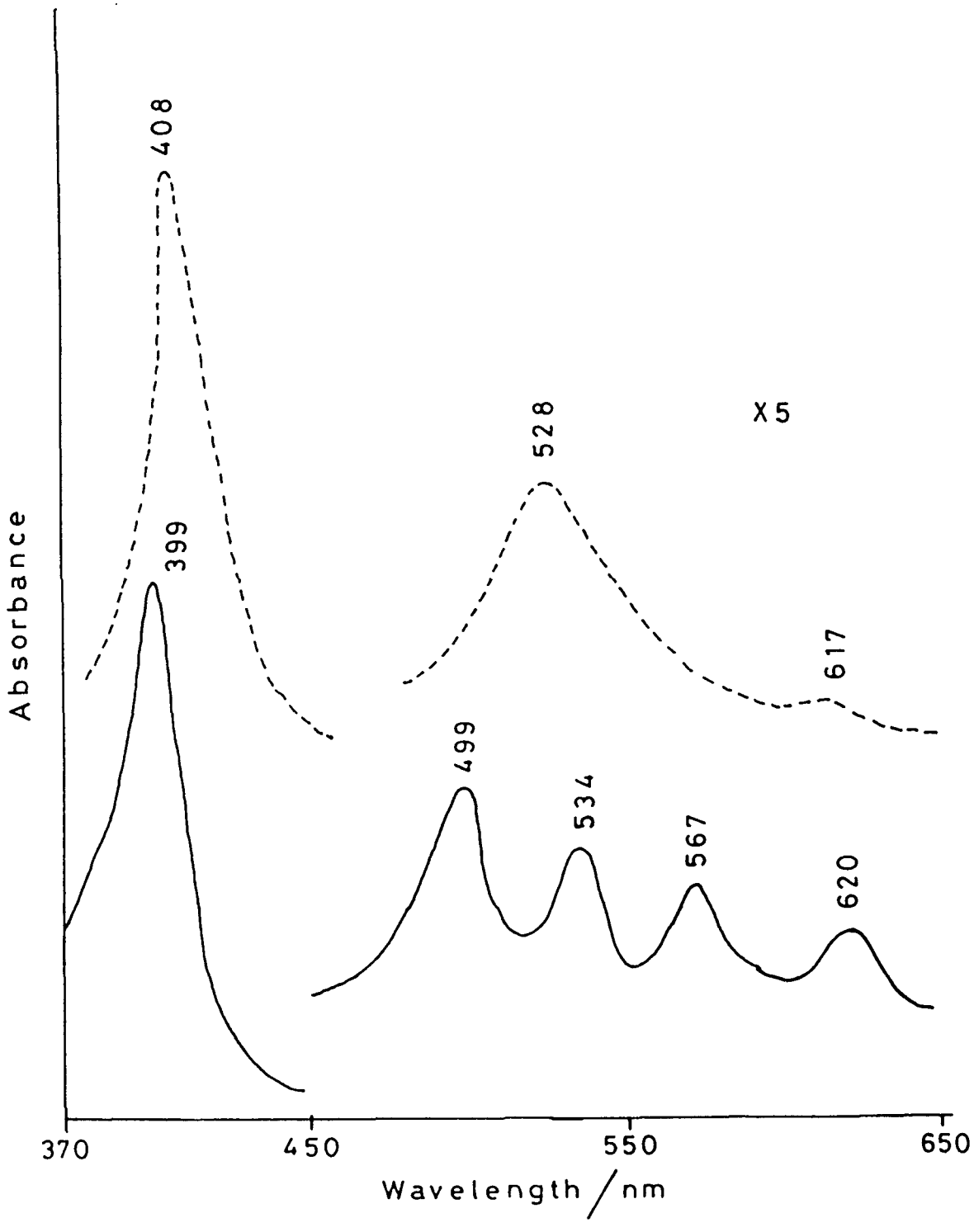

Fig. 2.2 Electronic absorption spectra of: (A) free base octaethylporphyrin (H_2OEP); (B) cobalt(II) *meso*-tetraphenylporphyrin ($Co^{II}TPP$) in CH_2Cl_2.

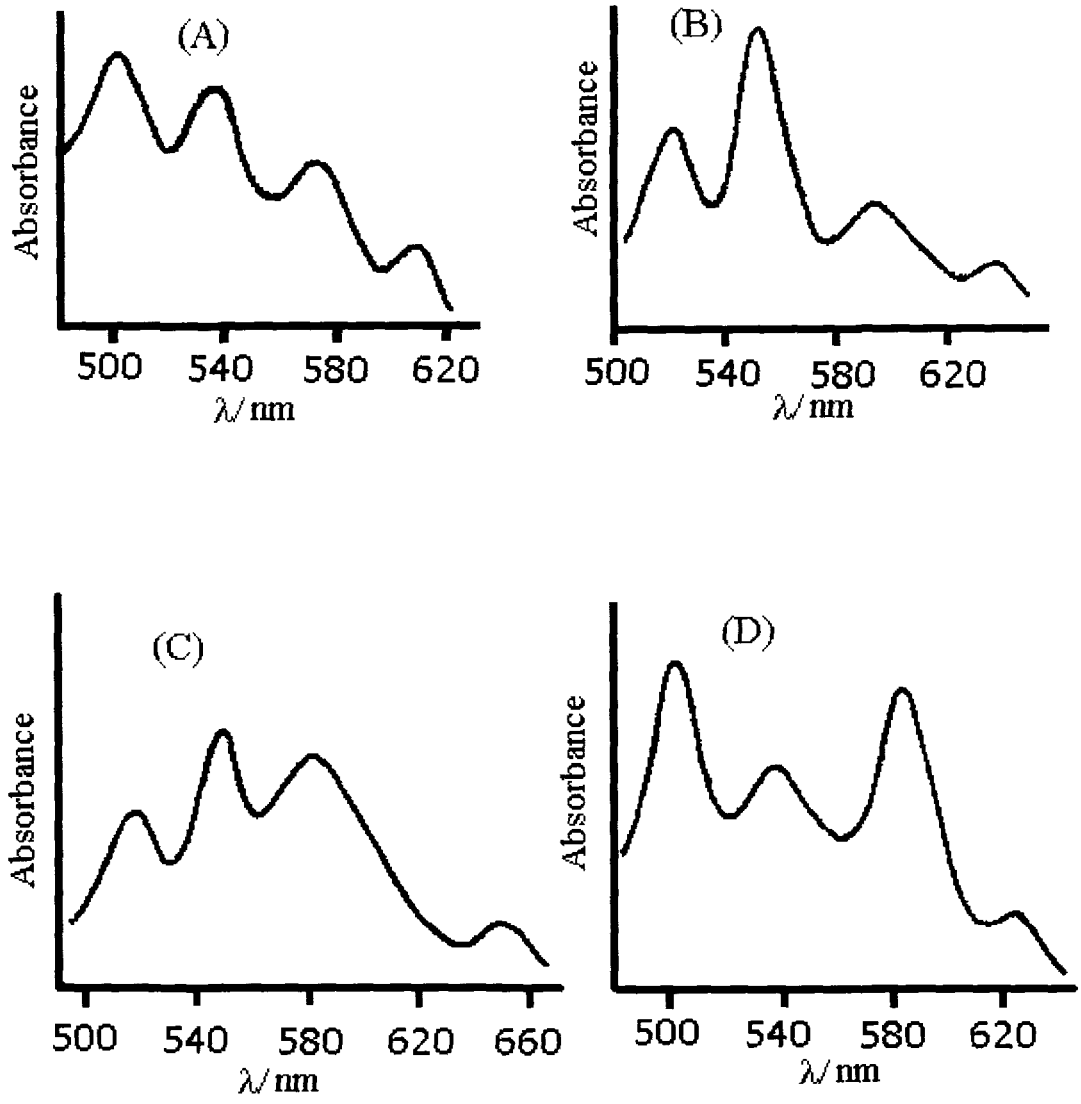

Fig. 2.3 Representative visible absorption spectra of typical porphyrins (A) aetio-; (B) rhodo-; (C) oxorhodo-; (D) phyllo- type

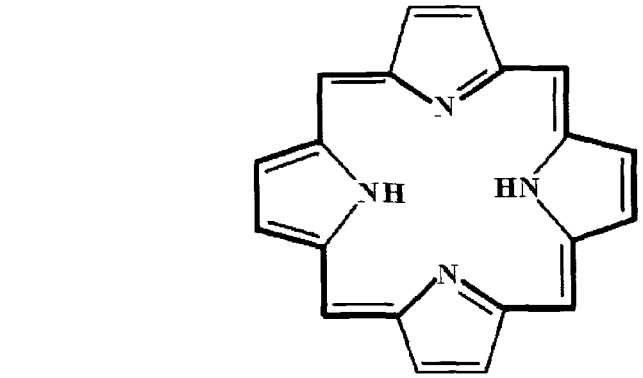

(A)

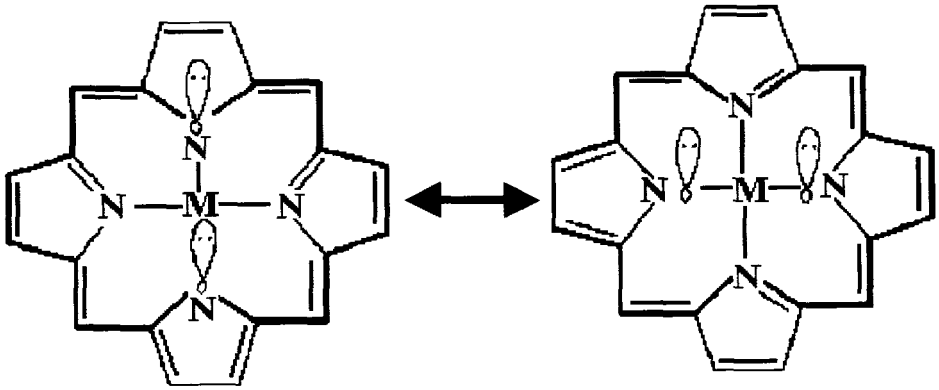

(B)

Fig. 2.4 (A) Resonance structure of free base porphyrin. The heavy bonds indicate the 18-membered cyclic polyene.
(B) Resonance structure for metalloporphyrin.

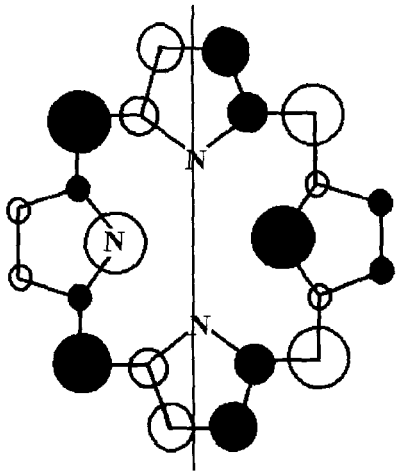

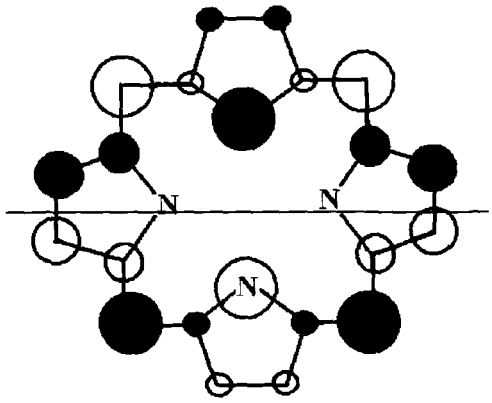

D_{4h} $e_g(\pi^*)$ $e_g(\pi^*)$

D_{2h} $b_{2g}(\pi^*)$ $b_{3g}(\pi^*)$

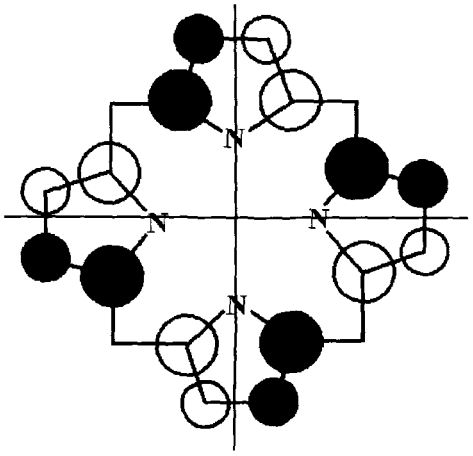

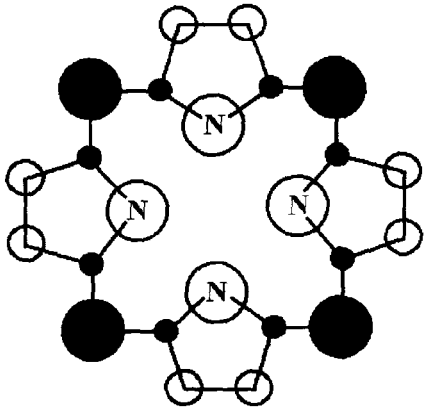

D_{4h} $a_{1u}(\pi)$ $a_{2u}(\pi)$

D_{2h} $a_u(\pi)$ $b_{1u}(\pi)$

Fig. 2.5 Atomic Orbital structure of porphyrin HOMO and LUMO orbitals in D_{4h} and D_{2h} symmetry point groups. The orbital coefficients are proportional to the size of the circles. Opened and filled circles indicate sign of the orbitals. Lines indicate the symmetry nodes.

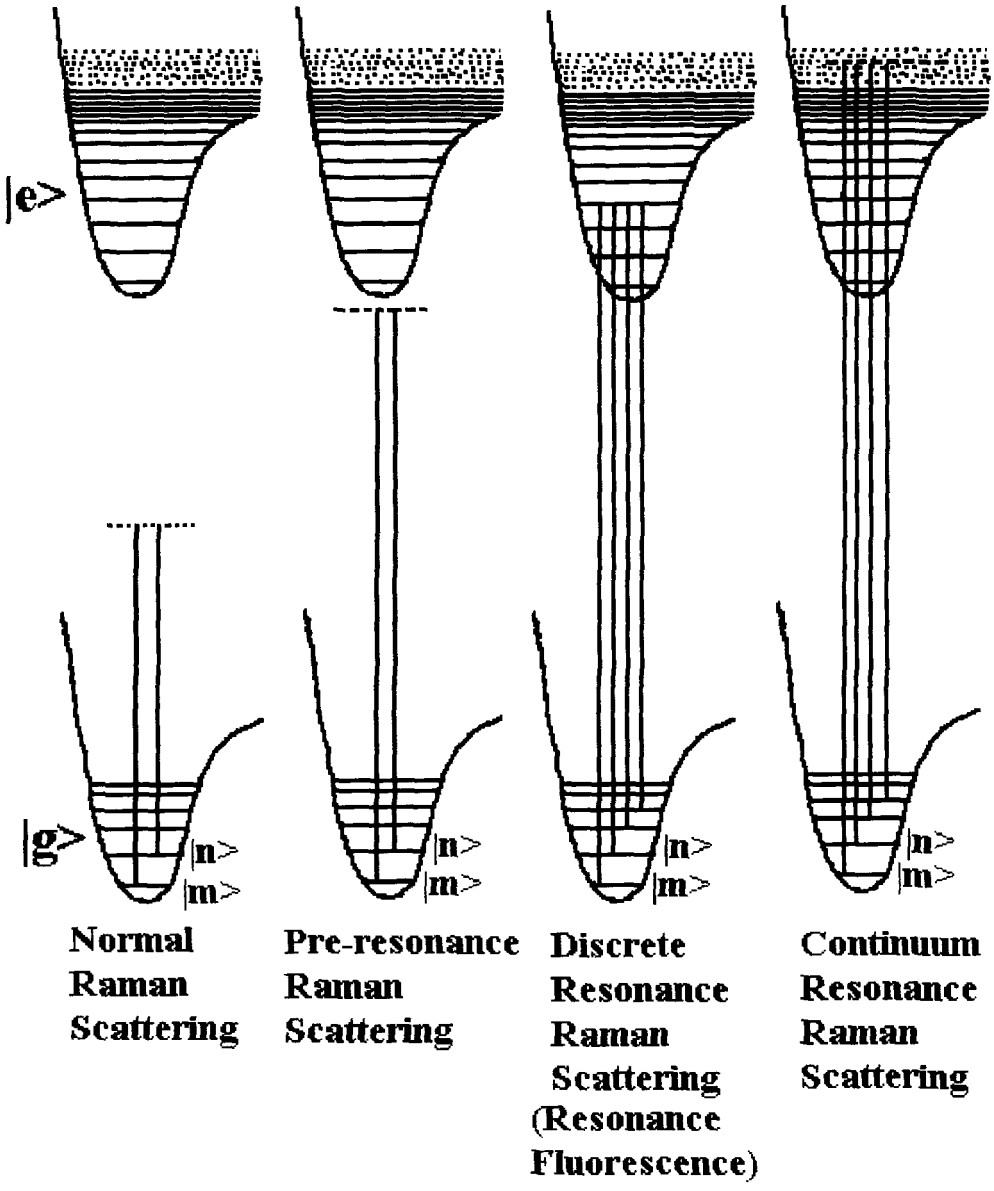

Fig. 2.6 Ilustration of various light scattering processes

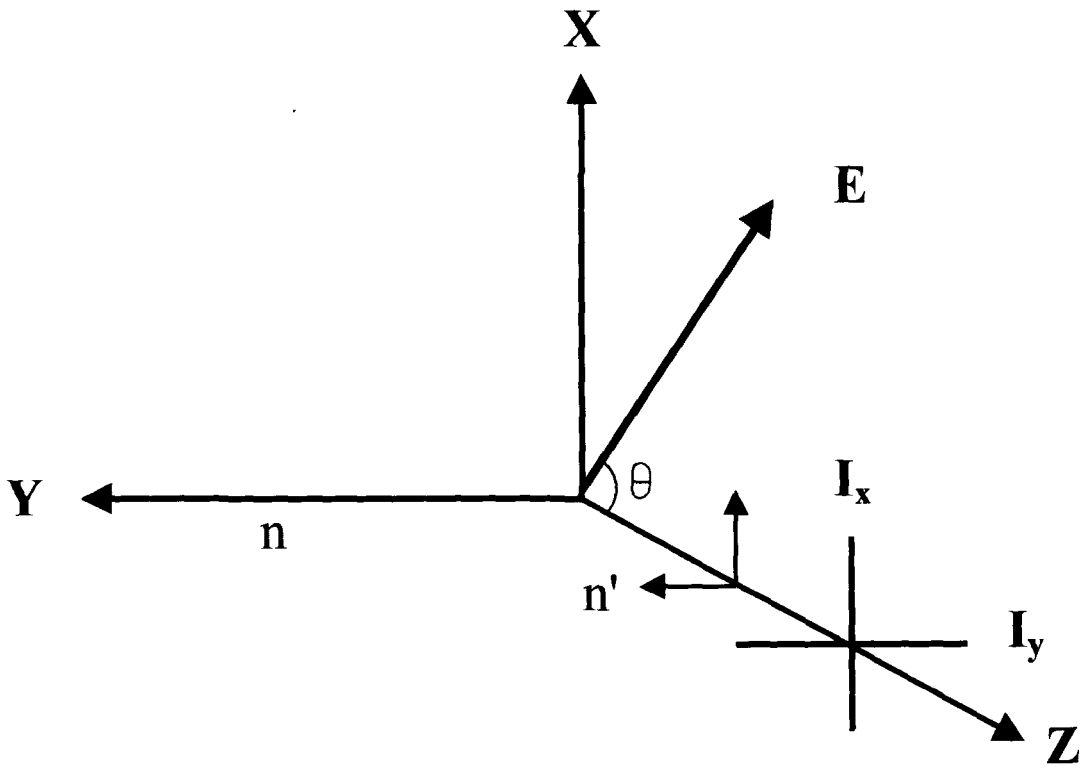

$$\rho_l = \frac{I_y}{I_x}$$

Fig. 2.7 Raman scattering geometry. An electric vector E lying in the XZ plane characterizes light propagating along the Y direction. Scattered radiation is detected along the Z direction. Conventional scattering experiment has $\theta = 90^{\circ}$.

CHAPTER 3

EXPERIMENTAL TECHNIQUES

A brief description of methods of sample preparation, experimental techniques and the instruments used to obtain the vibrational and electronic spectra are presented in this chapter.

3.1 Sample Preparation

Free base octaethylporphyrin (H_2OEP) , cobalt(II) *meso*-tetraphenylporphyrin ($Co^{II}TPP$) and horse heart cytochrome-c (cyt-c) were commercially purchased from Porphyrin Products Inc. (USA), Aldrich Chem. Co., and Sigma Chemical Co., respectively. Cytochrome-c (Sigma type VI) was further purified by column chromatography, while other porphyrins were directly used as received. The nitrogenous ligand 2-methylimidazole (2-MeIm) and electron acceptor p-benzoquinone (p-BQ) were obtained from Aldrich Chemical Co. The nitrogenous base was recrystallized from benzene before use. Dichloromethane, dichloroethane and tetrachloroethane were of reagent grade and purified by washing with concentrated H_2SO_4, 15% solution of potassium carbonate, large volume of water, dried over anhydrous calcium chloride, distilled and then stored over molecular shieves. Methanol and carbon disulphide were also reagent grade and purified by storing over anhydrous potassium carbonate and anhydrous calcium carbonate respectively for about 18 hrs, filtered and glass distilled. All other solvents used were of HPLC grade and used without further purification. Aqueous solutions of cyt-c were prepared with triple distilled, deionized water.

Chemical oxidation and reduction of porphyrin were performed by adding the appropriate oxidizing or reducing agents to the porphyrin solutions. The oxidizing agent used in this work is dilute solution of bromine and sodium dithionite is used as reducing agent. Diacid derivative of free base octaethylporphyrin diacid was prepared by addition of conc. HCl, dilute $HClO_4$ and dilute bromine to the solutions of the free base.

3.2 Degassing of Solutions

Free and dissolved air contained in the solution is removed using freeze-pump-thaw cycles. The solution for Raman studies is first transferred to a quartz cell fitted with accessories for evacuation and cooling. The sample is frozen by liquid nitrogen and the cell is evacuated with the help of a vacuum pump with fore pressure of 10^{-4} Torr. After sufficient evacuation, the cell is allowed to warm up to room temperature. The solution is purged with nitrogen gas for few minutes and the above cycle is repeated. The entire cycle is repeated at least three times to ensure proper degassing and removal of dissolved oxygen from the solution. After degassing, the solution is transferred to a Raman cell which is connected to the evacuating cell with vacuum tight joint. The unit is then mounted on a stand for laser excitation and Raman measurements under anaerobic conditions.

3.3 Measurement of Raman Spectra

Raman spectra of different porphyrins were recorded in a 90° scattering geometry with a Raman spectrometer (SPEX Ramalog 1403 and JOEL 400D)

equipped with a thermoelectrically cooled RCA 31034 photomultiplier and photon counting arrangement. The spectrometer control and data processing were achieved with the help of a microprocessor based SPEX " Datamate". Excitation lines were obtained from HeCd (Liconix, model 4240 and Kinmon Electronics, model CDR80MGE), Krypton Ion (Spectra-Physics, model 164) and Argon Ion lasers (Spectra-Physics, model 165-09 and NEC, model GLG3200).

The excitation wavelength dependence of photoreduction of cytochrome-c was measured using high photon flux from Okazaki large spectrograph (Japan).

3.3.1 Helium-Cadmium Laser (Liconix Model 4240)

This laser consists of two units: a laser head and a power supply. Three cables, one for control functions and other two for the high voltage supply to the laser tube connect the head and supply.

The optical section of laser head is formed by two mirrors mounted on adjustable plates and held at a precise separation by three invar rods that run along the length of the laser tube which is made of pyrex glass. The mirrors are adjusted to reflect the laser light down the bore of the pyrex glass laser tube and to allow the emission of a precise amount of light as an output laser beam. Functionally, the helium-cadmium laser is a helium filled plasma discharge tube containing cadmium metal within a reservoir and is terminated in a vertically polarized Brewster windows of the resonating cavity. The coherent laser emission occurs by a mechanism similar to that of the helium neon laser. The laser action takes place between the energy levels of Cd atoms while He gas helps in creating population inversion in Cd atoms.

This laser head is a air cooled system and requires no external cooling. The maximum output power at 441.6 nm is about 40 mW.

The power supply unit utilizes AC power from the primary source and converts it into different DC levels for maintaining constant output power by controlling gas pressure (both helium pressure and cadmium vapor pressure) and associated current regulations in different electronic circuits.

3.3.2 Argon Ion Laser (Spectra-Physics Model 165-09)

The Argon ion laser is a CW laser consisting of laser head and Exciter. The laser head is made up of a beryllium oxide (BeO) plasma tube closed at both ends by fused-silica Brewster's angle windows, a solenoid for providing necessary magnetic field and an optical resonator. The plasma tube is mounted in an optical cavity resonator formed by a spherical reflector at the output and a prism assisted by a flat mirror (to select wavelengths) at the high reflector end. The whole assembly of the resonator is held solidly against quartz rods with springs to minimize microphonic frequency shifts. The plasma tube is supported on a kinematically adjustable mount and is adjusted in such a way that the plasma tube is exactly centered. The external thumb wheel controls are provided for wavelength selection and for changing the intra-cavity aperture. The laser gives polarized light and by using the polarizer the plane of polarization can be changed to the desired plane for recording the polarized Raman spectra.

The Exciter is fully equipped with the necessary electronic circuits to create, sustain and regulate the ion discharge in the plasma tube and to control the output power from the laser by simultaneously regulating the solenoid current. An

arrangement is provided to have a desired constant output optical power. The Exciter is fed with a stabilized three phase 380 V (phase to phase) power line. This unit requires cooling of the transistor pass bank in the exciter, the solenoid and the BeO plasma tube which is achieved by circulating distilled and deionized water at 15° C.

3.3.3 Krypton Ion (Spectra-Physics, model 164)

The construction and basic unit of Krypton Ion laser is in general similar to that of Argon Ion laser. The main advantage of Krypton Ion laser lies in the availability of more number of lasing lines at reasonable output powers. But Krypton Ion lasers are not as stable in power output or discharge characteristics as Argon Ion lasers. The effect of gas pressure change during warmup is significant, especially if ouput is on lines higher than 647.1 nm. There is a tendency for the laser to operate closer to plasma instability points when output is at 568.2, 530.9, 350.7, or 356.4 nm. To minimize pressure change effects and avoid plasma instabilities during operation, specific steps have to be followed in the turn-on procedure.

3.3.4 Okazaki Large Spectrograph

Okazaki Large Spectrograph is a computer-operated, large-scale spectrograph recently built at the National Institute for Basic Biology at Okazaki, Japan. The design and performance of the spectrograph are described below.[1]

The spectrograph is composed principally of 5 parts: light sources, a monochromator, automatically-controlled boxes for sample irradiation, a carrier system for the boxes, and a microcomputer system for control. The spatial arrangement of these components is shown in Fig. 3.1.

Two Xe short arc lamps (30 and 6 kW) and a 450 W medium pressure Hg lamp form the light sources. A Monk-Gillieson mounting is adopted as the optical arrangement so that different biological specimens can be irradiated simultaneously with a continuos range of wavelengths from 250 to 1000 nm. The diffraction grating of the monochromator has 1200 grooves mm^{-1} and first order diffracted light is used. Seven kinds of bandpass or sharp-cut-off filters are used to remove higher-order diffracted light and other stray light. A stage is installed so that samples or boxes containing samples are exposed to light from the monochromator. Sample is placed in a computer-controlled 'sample box' having programmed parameters such as wavelength, photon fluence rate, photon fluence and timing. Through data communication between a host computer and the corresponding parts of the whole system of the spectrograph control over the following processes are done automatically: selection of the light source, opening and closing of the shutter, control of the entrance slit width, automatic transportation of the sample boxes to desired wavelength positions, irradiation conditions in terms of photon fluence rate, photon fluence and timing, etc. At present, up to 12 sample boxes can be placed at once. Photon fluence rates and the timing of irradiations in each boxes are controlled independently. Wavelength calibration is provided by a Hg lamp and an automatic sample box.

3.3.5 SPEX Model Ramalog 1403 Laser Raman Spectrometer

Fig. 3.2 shows the relevant optical diagram of the instrument. This spectrometer (SPEX 1403 double monochromator) is a f/7.8 instrument with spectral coverage from 31000 cm^{-1} to 11000 cm^{-1} with an accuracy of ± 1 cm^{-1} in the

10000 cm^{-1} range. The spectral repeatability of ± 0.2 cm^{-1} and resolution of 0.15 cm^{-1} at 5791 $\mathring{A}$ (Hg line, FWHM) can be achieved by this instrument. The gratings used in this instrument are of holographic type having rulings with 1800 grooves/mm and blazed at 5000 $\mathring{A}$. The gratings are mounted on a modified Czerny-Turner mount [Fig. 3.3] using the following fundamental grating equation:

$$m\lambda = d\,(\mathrm{Sin}\alpha + \mathrm{Sin}\beta) \qquad 3.1$$

where

m = spectral order

λ = wavelength

d = grating spacing

α = angle of incidence

β = angle of diffraction

For simplicity, let us put

$$\alpha = \theta + \phi$$

and $\beta = \theta - \phi$

where θ is the angle of grating rotation measured from zero as shown in Fig. 3.3, and is a constant angle, depending on the instrument's design. Therefore equation 3.1 can be rewritten as

$$m\lambda = 2d\,\mathrm{Sin}\theta\,\mathrm{Cos}\phi \qquad 3.2$$

The Raman peaks are measured in terms of wavenumber shift in cm^{-1} on a linear X-axis by utilizing a cosecant drive for grating rotation with a $\phi = 10^{o}$ and thus $\mathrm{Cos}\phi$ = 0.984 (manufacturer's supplied values).

To record the Raman spectra, the laser beam is deflected upward (90°) by a mirror and focused on to the sample to a spot of diameter 10 μm by fused silica condensing lens. Scattered radiation from the sample then passes through a polarization analyzer (optional), a device based on birefringence and total reflection or on dichroism. Use of polarization analyzer provides direct information about the state of polarization of the observed Raman bands. For powdered sample or for samples in KBr matrix (pellet), the use of polarization analyzer becomes redundant because of the random orientation of the constituent molecules or microcrystals of the sample. The scattered radiation is then collected by an elliptical mirror (f/1.4) and focused onto the entrance slit (S_3) [Fig. 3.2] of the spectrometer after deflecting from the mirror (M_7) and passing through a polarization scrambler. The polarization scrambler converts the plane-polarized scattered radiation to a circularly polarized radiation before it reaches the spectrometer and thus cancels variations in spectrometer response that result from polarization-dependent efficiencies. The polychromatic scattered radiation focused onto the entrance slit gets dispersed by the 1800 lines/mm holographic gratings (G_2 and G_3). Thus, finally a nearly monochromatic light signal of a particular wavenumber (cm^{-1}) selected by spectrometer control reaches the exit slit (S_7) of the double monochromator. This exit slit can be coupled to the third monochromator Model SPEX 1442V.

3.3.6 The Third Monochromator Model SPEX 1442V

This device is used for reducing stray light in Raman scattering where the weak spectral features are not clearly resolved in the vicinity of the intense Rayleigh line. This device functions as a variable band pass, variable frequency filter. The

third monochromator is a modified Czerny-Turner spectrograph attached to the exit slit of the double monochromator. The light entering the third monochromator is nearly monochromatic at the particular tuned frequency of the double monochromator with some stray light at the exciting frequency. This light is further dispersed and finally made to fall onto the exit slit of the third monochromator to which the photomultiplier tube is attached. This final dispersion and adjustment of the exit slit allows only the desired components of the incoming monochromatic light to pass between the slit blades of the exit slit of the third monochromator while the stray radiation at other frequencies are obstructed by the slit blades. The third monochromator can operate in the fixed mirror mode, in the scanning grating mode, or in the stationary grating mode. The fixed mirror mode essentially converts the system to a double monochromator and so maximizes the signal intensity. It is ideal getting high resolution for low intensity signal. The scanning grating mode is suggested for substances plagued by unwanted scattered light over the complete Raman spectrum. The stationary grating mode is especially valuable for identifying Raman lines close to the excitation frequency (Rayleigh line).

3.3.7 Spectrometer Control and Data Processing

The spectrometer control (frequency scanning) and data processing are achieved with a 8-bit dedicated micro-computer SPEX 'DATAMATE'. With the help of the in-built software, it is possible to manipulate the spectral data by back ground subtraction, integration, addition, division, frequency range and intensity range expansion/reduction, differentiation, etc., whenever necessary. The incoming spectral data as well as the manipulated data array can be stored in the 4K data point

storage in any of the eight variable length files. The stored data can be plotted on a stripchart recorder or transfer to external peripherals, e.g., floppy disc or to a PC through the standard RS 232 port for further manipulation. Applying the radiometric corrections from the in-built 1K EAROM it is possible to erase the unavoidable wavelength dependent distortions to the spectral data from the spectrometer optics. Using the programming option, the entire spectrometer control as well as data collection and manipulation could be completely automated. The data storing facility could be bypassed and real time spectra could be recorded directly on the stripchart recorder.

The raw data is obtained from the output of the pre-amplifier (PC Dam). The anode of the photomultiplier tube is the input of the PC Dam. The pre-amplifier gain is 400. The high voltage (-1750 volts) required for operating the photomultiplier tube is also supplied by the Datamate with a stability of ± 0.002% after half an hour warm up.

The photomultiplier tube Model RCA 31034 used with the instrument is a 2" diameter, head-on, 11-stage QUANTACON photomultiplier having a gallium arsenide chip as its photocathode, an ultraviolet transmitting glass window and in-line copper beryllium dynode structure. This tube is cooled to –30° C by a thermoelectric cooling device and has almost linear absolute response in the 3000 $\mathring{A}$ to 8500 $\mathring{A}$ wavelength range. It operates with a current gain of 10^6 with a maximum dark pulse summation of 12 CPS (count per second).

3.3.8 Scanning of Raman Spectra

There are a number of difficulties associated with recording the Raman spectra of colored samples under resonance conditions. The most prominent include: (a) the optimization of the concentration of the sample to minimize re-absorption of the scattered light by the sample and at the same time allowing the scattering to be maximum; (b) the local heating of the sample due to absorption of the exciting light which may give rise to thermal lens effect and also lead to thermal decomposition of the sample; and (c) the strong background due to fluorescence from impurities in the compound or in the solvent or intrinsic fluorescence from the sample itself.

The first point can be taken care by using samples of different concentrations until a good quality spectrum is obtained. To avoid local heating effect, Kiefer and Bernstein[2,3] had developed a technique which involves continuous rotation of the sample with respect to the laser beam. In this cases, as the sample rotates continuously, the small portion of the sample from which light scattering takes place remains in the laser beam only for a short period of time and thereby reducing the local heating and thermal decomposition. To reduce the fluorescence background, Raman spectra can be measured in the solid form in KBr pellet. In solution, purification of the compound and solvents by standard methods is an effective way of avoiding fluorescence coming from impurities.

To record the Raman spectra of liquid solution, 1-2 ml solution of respective porphyrin at an appropriate concentration is taken in a cylindrical quartz cell and positioned in a proper mount. The laser beam at selected wavelength is then made to strike the bottom of the cell very near to its perimeter. In this way, self-absorption of the scattered light is minimized. The spectra were routinely calibrated with known

CH_2Cl_2 lines in the lower (100-50 cm^{-1}) and with indene[4] in the higher frequency region (1200-1700 cm^{-1}) and some times with known Raman lines of solvents that are being used. Other spectral parameters such as laser power, integrating time, wavenumber increment, slit width, etc., are adjusted time to time in order to optimize signal to noise ratio.

3.4 Electronic Absorption Spectra

The electronic absorption spectra were recorded on a Varian Carey 2300 UV-VIS-NIR and on a Hitachi 124S spectrophotometers.

3.4.1 Varian Carey 2300 UV-VIS-NIR Spectrophotometer

This spectrophotometer is a double-beam recording instrument for measuring light intensity at specified wavelengths in a continuous manner. The model employs two lamp sources: a tungsten-halogen lamp for VIS-NIR wavelengths (3152-340 nm) and a deuterium source for UV wavelengths (185-340 nm). Light from the appropriate source is directed through a band pass or long wave pass filter to the single grating monochromator. The monochromatic beam is split into two components of equal intensity, one beam passing through the reference and the other through the sample. The intensity of light emerging from the reference/sample cells is detected by a photomultiplier tube for UV/VIS wavelengths and a lead sulphide detector for NIR wavelengths. The current pulses generated by light from the sample/reference cells are amplified and recorded in transmission or absorbance mode. In the absorbance mode the amplified signal is analyzed by a log converter

which transforms the light transmission current values to optical density and absorbance is equal to log 1/T (T = transmission). The resolution of the spectrophotometer is 0.07 nm with a wavelength repeatability of ± 0.05 nm and a wavelength accuracy of ± 0.2 nm in the UV-VIS region.

References

1. Watanabe, M.; Furuya, M.; Miyoshi, Y.; Inoue, Y.; Iwahashi, I.; Matsumoto, K. *Photochem. Photobiol.* 1982, 36, 491.

2. Kiefer, W.; Bernstein, H.J. *Appl. Spectrosc.* 1871, 25, 500.

3. Kiefer, W.; Bernstein, H.J. *Appl. Spectrosc.* 1871, 25, 609.

4. Hendra, P.J.; Loader, E.J. *Chem. Ind. (London)* 1968, 7, 18.

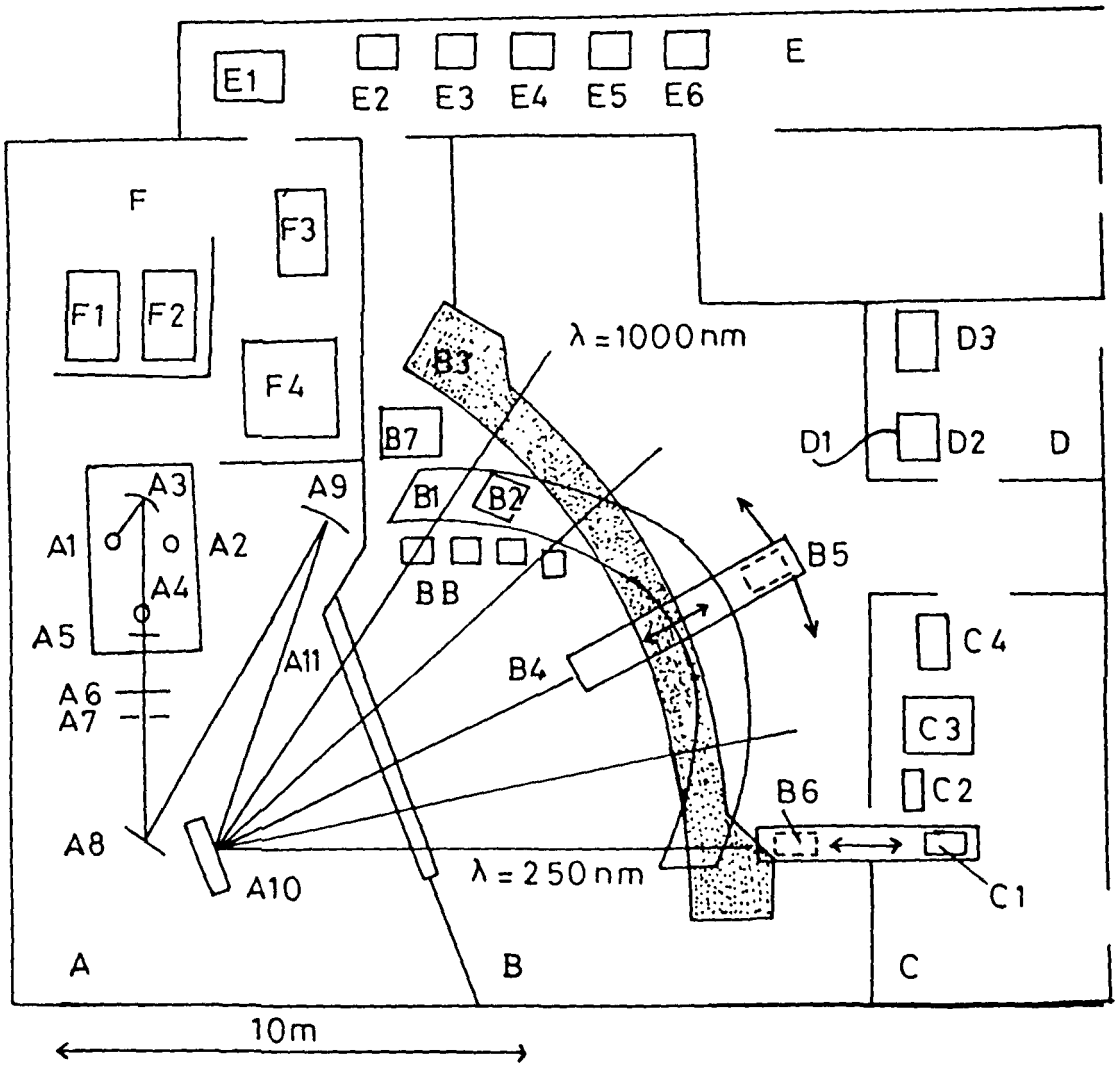

Fig. 3.1 Spatial arrangement of the Okazaki large spectrograph. A, monochromator room; B, irradiation room; C, sample box preparation room; D, optical fiber room; E, microcomputer room; F, power supply room. A1, 30 kW Xe short arc lamp; A2, 6 kW Xe short arc lamp; A3, rotable condensing mirror; A4, medium pressure Hg lamp; A5, shutter; A6, heat-absorbing filter; A7, entrance slit; A8, plane mirror; A9, condensing mirror; A10, double-blazed plane grating; A11, window. B1, focal curve stage; B2, sample box; B3, x-axis frame; B4, y-axis frame; B5, arm, hanging under and moving along the y-axis frame; B6, origin of the automatic carrier system; B7, interface for entrance slit control and mirror cover drive; B8, interface for connector drive. C1, trolley; C2, control panel; C3, CRT terminal; C4, printer. D1, optical fiber bundle; D2, optical fiber outlet unit; D3, panel for monitoring the fluence rate data from the photodiode to the host computer. E1, host computer; E2, data typewriter; E3, CRT terminal; E4, printer; E5, NC; E6, NC interface. F1, arc cooling unit for lamps; F2, power supply for lamps; F3, control panel for lamps; F4, water cooling unit for lamps.

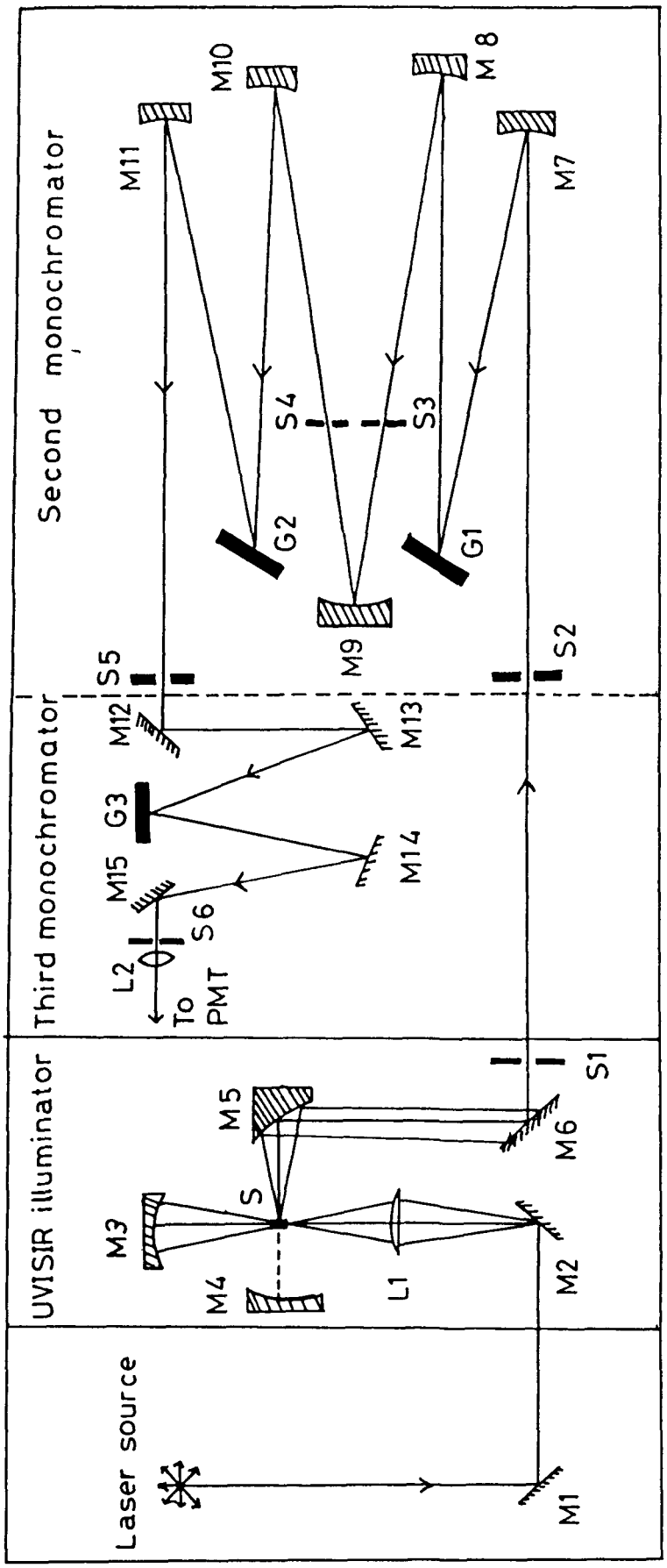

Fig. 3.2 Optical diagram of a Spec Model Ramalog spectrometer, including the UVISIR illuminator and the third monochromator. M1, M2, M6, M12, M13, M14, M15, plane mirrors; M3, M4, M7, M8, M9, M10, M11, concave mirrors; M5, elliptical mirror; S1 – S6, slits; L1, fused silica condenser lens; L2, field lens; S, sample; G1, G2, G3, gratings; PMT, photomultiplier tube.

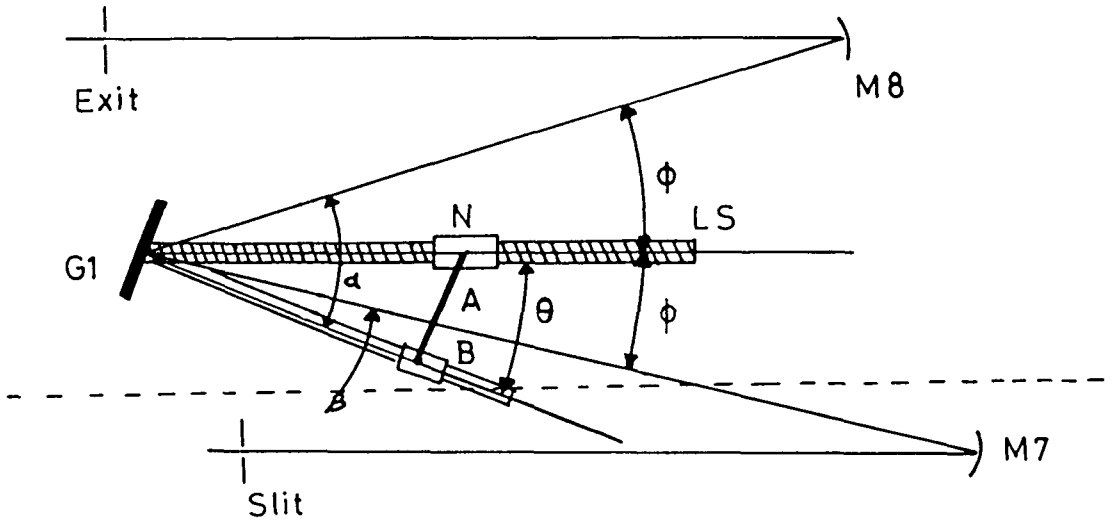

Fig. 3.3 Mechanical cosecant drive mechanism for the Czerny-Turner mount of gratings for the Spex Model 1403 Ramalog spectrometer. The nut N moves along lead screw LS while the slide B moves along a bar held at right angles to the gratings G1. The grating rotates as the arm A moves along the bar. M7 and M8 are mirrors.

CHAPTER 4

Photo-Induced Diacid Products of Octaethylporphyrin Probed by Resonance Raman and Absorption Techniques

---

This chapter describes the photochemical formation of di- and monoacid derivatives of free base octaethylporphyrin (H_2OEP) in CH_2Cl_2 or CCl_4/alcohol mixtures in the presence of p-benzoquinone (p-BQ) studied by resonance Raman and optical absorption techniques. The results indicate that the solvent or co-solvent acts as the proton source in the reaction. Simultaneous presence of p-BQ and methanol is found to be essential for diacid formation in CCl_4, while methanol greatly inhibits the process in CH_2Cl_2 solvent. However, in the presence of excess methanol in CH_2Cl_2 and p-BQ, porphyrin monoacid is formed. A chain mechanism is proposed for the photon-induced formation of octaethylporphyrin diacid product.

4.1 Introduction

Porphyrins and their metal derivatives can be oxidized chemically[1], electrochemically[2] or photochemically[3,4] to form either metal- or porphyrin-ring-centered oxidized products. Study of the photochemical formation of these oxidized products has gained much importance due to their involvement in many biological processes such as in the primary photoagent in bacterial and plant photosynthesis[5] and in compound I of the peroxidase enzymes in which two-electron oxidation of Fe^{III}-heme takes place[6]. Accordingly, photooxidation of the parent metalloporphyrins by an electron acceptor to give π-cation radical species has been the subject of many studies.[3a,4,7] However, compared to metalloporphyrins, understanding of the metal-free macrocycles, the so-called free base, has remained elusive.[2,7,8]

From EPR studies,[9-11] the π-cation radicals of free base porphyrins are known to be short lived and highly reactive. A recent investigation[12] has shown that free base π-cation radicals (H_2OEP, H_2TPP, H_2CdiE) electrogenerated in strictly anhydrous solvents are not stable and give rise to a follow-up reaction in which the free bases are protonated. The transient formation of the free base π-cation radical has also been proposed as the initial step in the photochemical formation of H_2TPP diacid.[13,14] Thus, study of the photochemical formation and characterization of diacid is as important as the π-cation radicals themselves because of the high tendency of the latter to decay into the corresponding acid derivatives.

In the present work, we report results of resonance Raman (RR) and optical absorption studies on the catalytic formation of OEP acid derivatives by irradiating

free base octaethylporphyrin within the Soret absorption band in the presence of p-benzoquinone (p-BQ) as electron acceptor in different solvents.

4.2 Experimental Techniques

Free base octaethylporphyrin (H_2OEP) was commercially purchased from Porphyrin Products Inc., USA, and used without further purification. Methanol and ethanol were dried over anhydrous potassium carbonate and distilled. Carbontetrachloride (CCl_4) was of spectroscopic grade and used as received from SISCO, India. Dichloromethane (CH_2Cl_2) was purified by washing with concentrated H_2SO_4, a 15% solution of potassium carbonate, and a large volume of water, then dried over anhydrous calcium chloride, distilled and stored over molecular shieves. p-Benzoquinone (p-BQ) was used as received from Aldrich Co., USA.

The octaethylporphyrin diacid was prepared with concentrated HCl according to the method given in the literature[15] or by addition of dilute Br_2 to the solution of H_2OEP in CH_2Cl_2. The diacid has a characteristic violet color in solution. The monoacid derivative was prepared by dropwise addition of a (MeOH + 5% H_2O) mixture to the solution of diacid in CH_2Cl_2 until the solution color changed from violet to orange red.

Raman spectra were recorded with a SPEX Ramalog 1403 double monochromator equipped with a water-cooled RCA 31034 photomultiplier. A Liconix 4240 HeCd laser provided the excitation line at 441.6 nm. A microprocessor-based SPEX Datamate was used for spectrometer control, data acquisition and processing facilities. The typical laser power at the sample was ~ 35-40 mW and most of the Raman spectra were measured at a spectral resolution of

4 to 5 cm^{-1}. The position of the Raman peaks was calibrated with indene or the known bands of the solvents used. A minimum of three freeze-pump-thaw cycles was employed whenever anaerobic conditions of the solutions were required.

Electronic absorption spectra were recorded on a Carey 2300 UV-VIS spectrometer using 10 mm path length quartz cuvettes.

4.3 Results

The UV-VIS absorption spectra of H_2OEP and its diacid $(H_4OEP)^{2+}2Cl^-$ in CH_2Cl_2 are shown in Fig. 4.1 (A,C). Neutral H_2OEP displays a Soret band at 399 nm and four bands in the visible region at 499, 534, 567 and 620 nm, similar to the reported ones.[12] In the diprotonated form, as is well-documented, [12,15] the visible spectral region is dominated by two major bands at 554 and 600 nm with a weaker band at 582 nm, which appears as a shoulder to the main peak at 554 nm. The spectral simplification from H_2OEP to the diacid $(H_4OEP)^{2+}$ is a result of the approach towards square symmetry (i.e., D_{4h}) in the diacid when protons are added to the pyrrole nitrogen atoms. A similar type of change was observed when dilute Br_2 was added to the solution of H_2OEP in CH_2Cl_2 [Fig. 4.1(B)]. Titrative addition of MeOH containing 5% H_2O to the solution of $(H_4OEP)^{2+}2Cl^-$ gives the familiar optical spectra [12,15,16] of the monoacid $(H_3OEP)^+$ derivative showing three main visible bands at 524, 558, and 600 nm, and the Soret band at 395 nm [Fig. 4.1(D)]. It is interesting to note that addition of dry methanol alone to the diacid solution did not result in appreciable formation of monoacid, while water alone gives the neutral form of OEP. It is believed that although water is slightly more acidic than MeOH, it assists in dissociation of the chloride counter ion from the diacid either by H-bonding

or due to its high polarity, thereby setting up favorable conditions for monoacid formation in the presence of MeOH.

The corresponding RR spectra of H_2OEP and the chemically prepared acid derivatives are shown in Fig. 4.2. Table 4.1 gives the mode numbering and assignment based on results[17,18] obtained from isotopic substitution and depolarization ratio measurements. According to the assignment, the RR spectrum of H_2OEP in CH_2Cl_2 shows the ν_4, ν_{11} and ν_{10} modes at 1369, 1546 and 1615 cm^{-1} respectively [Fig 4.2(A)]. In the $(H_4OEP)^{2+}2Cl^-$ diacid product, these modes are shifted to 1388, 1561 and 1603 cm^{-1}, respectively, along with a change in the relative intensities of the bands at 1210 and 1133 cm^{-1} [Fig. 4.2(C)]. The RR spectrum of the monoacid derivative is slightly different from that of the diacid, and is mainly characterized by observation of the ν_4 and ν_{11} modes, respectively at 1385 and 1554 cm^{-1} and appearance of a band at 1515 cm^{-1} [Fig. 4.2(D)]. The bromide adduct of OEP diacid [Fig. 4.2(B)] shows some of the RR bands at slightly different wavenumbers compared to that of the chloride adduct.

Fig. 4.3 shows the resonance Raman spectra of H_2OEP (ca. 1 mM) in CH_2Cl_2 obtained with 441.6 nm excitation in the presence of p-BQ. Under aerobic conditions, addition of p-BQ (ca. 8 mM) results in spectral changes as shown in Fig. 4.3(A,B). The ν_4, ν_{11} and ν_{10} modes shift to 1388, 1561 and 1603 cm^{-1}, respectively, and there is a change in the relative intensities of the bands at 1210 and 1133 cm^{-1}, same as in Fig. 4.2(C). Similar result was also obtained under anaerobic condition [Fig. 4.3(C)]. The RR spectra of OEP obtained under these conditions is identical to that of the chemically prepared $(H_4OEP)^{2+}2Cl^-$ [Fig. 4.2(C)], but different from that of the monoacid $(H_3OEP)^+Cl^-$ [Fig. 4.2(D)] for which the ν_4 and

ν_{11} modes are observed at 1385 and 1554 cm^{-1}, respectively, with a broad band feature in the ν_{10} mode region. Therefore, it appears that laser excitation of a dichloromethane solution of H_2OEP in the presence of p-BQ results in the formation of the diacid derivative. Similar photochemical changes were also observed with 406.7 nm in the presence of p-BQ or chloranil [Fig. 4.4(A-C)] and with 488 and 514.5 nm laser excitations.[19] But no photochemical reaction occurs in neat CCl_4 at 406.7 nm excitation [Fig. 4.4(D)].

The optical absorption spectra of H_2OEP in CH_2Cl_2 in the presence of p-BQ before and after laser irradiation at 441.6 nm are shown in Fig 4.5(A). Prior to irradiation the spectral positions are the same as in the absence of p-BQ [Fig. 4.5A(a)]. However, after about 30 min. irradiation under aerobic conditions the spectrum becomes similar to that for the diacid $(H_4OEP)^{2+}2Cl^-$ in CH_2Cl_2, except for the appearance of a shoulder at 413 nm [Fig. 4.5A(b)]. Since no such band was observed in a chemically prepared acid product of H_2OEP [Fig. 4.1], the shoulder appearing at 413 nm in the absorption spectra of the photoirradiated sample of H_2OEP is associated with one of the degradation products formed as a result of photochemical reactions in the system. Formation of products other than diacid can also be seen from RR study. In Fig. 4.5B, the RR spectra of H_2OEP (~0.25 mM) in the presence of p-BQ in CH_2Cl_2 at different irradiation times are shown. It can be seen from this figure [Fig. 4.5B(a,c,d)] that under aerobic conditions, increasing the laser irradiation time (~35 mW focused laser power) is accompanied by a progressive shifting of the ν_4 mode wavenumber from 1388 to 1380 cm^{-1} and finally to 1375 cm^{-1} after 30 and 60 min exposure, respectively. However, under anaerobic conditions, the ν_4 mode remains at 1388 cm^{-1} even after 30 min exposure

[Fig. 4.5B(b)]. It is interesting to note that the degradation of RR bands at 1380 and 1375 cm^{-1} were observed only when the concentration of H_2OEP is lower that 1 mM. This is attributed to difference in the optimum concentration of the diacid and the degradation products at 441.6 nm excitation. The 414 nm shoulder also persists in the absorption spectrum of the photoirradiated sample of H_2OEP in the presence of p-BQ under anaerobic conditions [Fig. 4.5A(c)], suggesting that the degradation products observed in RR and optical absorption spectra are not the same. However, despite all these complications, it can be clearly pointed out from our RR and optical absorption studies that laser excitation of H_2OEP in CH_2Cl_2 in the presence of p-BQ results in the formation of the OEP diacid derivative, irrespective of the presence or absence of oxygen.

Similar photo-induced diacid formation was also observed in solvents like $CHCl_3$, $C_2H_4Cl_2$ and $C_2H_2Cl_4$ [Fig. 4.6], but not in CS_2, C_6H_6 and CCl_4 [Fig. 4.7]. However, in CCl_4, simultaneous presence of p-BQ and methanol or ethanol was found essential for the formation of diacid..

The RR spectrum of H_2OEP (ca. 1 mM) in CCl_4 at 441.6 nm excitation is shown in Fig. 4.8 A(a), and is similar to the one in CH_2Cl_2 in the absence of p-BQ. Addition of p-BQ (ca. 8 mM) or methanol (15% v/v) separately also does not result in any spectral change [Fig. 4.8 A(b,c)]. However, in the simultaneous presence of p-BQ and MeOH [Fig. 4.8 A(d)], certain marker bands associated with the ν_4, ν_{11} and ν_{10} modes at 1369, 1545 and 1615 cm^{-1} for H_2OEP shift to 1388, 1560 and 1603 cm^{-1}, respectively, on laser excitation. Replacing MeOH with ethanol also gives similar RR spectral changes (not shown). On the other hand, in contrast to this, the solution of H_2OEP in a CH_2Cl_2 (85%) + MeOH (15%) mixture in the presence of

p-BQ on laser excitation gives RR spectrum [Fig. 4.8 B(b)], that is the same as for neutral OEP in CH_2Cl_2 [Fig. 4.8 B(a)]. But on increasing the MeOH content from 15% to 30% (v/v), formation of monoacid could be seen as evidenced by the characteristic RR bands at 1383 and 1552 cm^{-1} for the ν_4 and ν_{11} modes, respectively [Fig. 4.8 B(c)].

4.4 Discussion

4.4.1 Mechanism

The excited state of OEP directly reached by 441.6 nm excitation is a $^1(\pi,\pi^*)$ singlet state, which is known to relax by an intersystem crossing process to a triplet state with a quantum yield of 0.75.[20] The fact that no ground state chemical reaction occurred between H_2OEP and p-BQ [Fig. 4.5A(a)] indicates that the excited state quenching of H_2OEP by p-BQ initiates the reaction for OEP diacid formation. Since diacid formation was observed independently of the presence or absence of oxygen, apart from degradation [Fig. 4.3(B,C)], it appears that the singlet excited state of H_2OEP plays a major role in the process. Quenching of the OEP excited state may occur either by energy transfer to give p-BQ in an excited state (p-BQ*) or by electron transfer to give a one-electron ring oxidized H_2OEP product. Formation of p-BQ* by energy transfer quenching is unlikely because the process requires overlap of the absorption spectrum of p-BQ with the emission spectrum of H_2OEP, which is not possible since the longest and shortest wavelength absorption[21] and emission[22] bands of p-BQ and H_2OEP are found at 430 nm and 610 nm, respectively. Therefore, the intermediate species responsible for the reaction process is believed to be the

$(H_2OEP)^{+\bullet}$ π-cation radical. However, in our system we did not observe any signal that could be attributed to a $(H_2OEP)^{+\bullet}$ species. But according to recent investigations[12] the π-cation radical is short lived and highly reactive, leading to a follow-up reaction in which the acid derivative of OEP is the final product. Moreover, the π-cation radical of H_2TPP was also proposed to play an intermediate role in the photochemical formation of the corresponding diacid derivative.[13,14] Although we could not detect the $(H_2OEP)^{+\bullet}$ π-cation radical directly in our experiments, its transient formation is believed to initiate the reaction. In this reaction either p-BQ or the solvent can act as proton donor. But RR spectra characteristic of diacid were also found in $CHCl_3$, $C_2H_4Cl_2$ and $C_2H_2Cl_4$ solvents in the presence of p-BQ [Fig. 4.6], but not in CS_2, CCl_4 and C_6H_6 [Fig. 4.7] under otherwise similar conditions, suggesting that the solvent used is the proton source. This is further supported by diacid formation in CCl_4 only in the simultaneous presence of p-BQ and MeOH on laser excitation [Fig. 4.8A]. Diacid formation in CH_2Cl_2 in the presence of Br_2 observed in our case [Fig. 4.2(B)] and similar to reports in the literature[1] also gives further support to cation radical initiated proton removal from the solvent. In the light of the above discussion, the following mechanism for diacid formation is proposed, which is in consonance with proposals in the literature.[13]

$$H_2OEP \overset{h\nu}{\Leftrightarrow} {}^1(H_2OEP) \qquad 4.1$$

$${}^1(H_2OEP)^* + \text{p-BQ} \Rightarrow {}^1[(H_2OEP)\text{---}(\text{p-BQ})]^* \rightarrow (H_2OEP)^{+\bullet} + \text{p-BQ}^- \qquad 4.2$$

$$(H_2OEP)^{+\bullet} + \text{p-BQ}^- \Rightarrow H_2OEP + \text{p-BQ} \qquad 4.3$$

$$(H_2OEP)^{+\bullet} + CH_2Cl_2 \Rightarrow H_2OEP + {}^{\bullet}CHCl_2 + H^+ \qquad 4.4$$

$$p\text{-}BQ^{\cdot-} + CH_2Cl_2 \Rightarrow p\text{-}BQ + {}^{\cdot}CH_2Cl + Cl \qquad 4.5$$

$$H_2OEP + 2\,H^+ + 2\,Cl^- \Rightarrow (H_4OEP)^{2+}2Cl^- \qquad 4.6$$

The photochemical formation of diacid is found to be accompanied by degradation products in the presence of strong electron acceptors like p-BQ. These side-reactions are likely to involve radicals originating from both p-BQ and the solvent.

In CCl_4, our results suggest that CCl_4 could not directly remove an electron from H_2OEP in the excited state, otherwise it should lead to diacid formation in the presence of MeOH, similar to that observed in the H_2TPP[13] system. Even at 406 nm excitation no photooxidation was observed for H_2OEP in the presence of CCl_4 as electron acceptor [Fig. 4.4(D)]. Therefore, observation of diacid formation only in the simultaneous presence of p-BQ and MeOH [Fig. 4.8(A)] leads to a mechanism whereby MeOH acts as proton source in analogy to the suggestion given above.

$$(H_2OEP)^{+\bullet} + CH_3OH \rightarrow H_2OEP + {}^{\cdot}CH_3O + H^+ \qquad 4.7$$

$$p\text{-}BQ^{\cdot-} + CCl_4 \rightarrow p\text{-}BQ + {}^{\cdot}CCl_3 + Cl \qquad 4.8$$

$$H_2OEP + 2\,H^+ + 2\,Cl^- \rightarrow (H_4OEP)^{2+}2Cl^- \qquad 4.9$$

The ${}^{\cdot}CH_3O$ (Eqn. 4.7) and ${}^{\cdot}CCl_3$ (Eqn. 4.8) radicals are expected to finally decay to formaldehyde and chloroform according to the well-documented mechanism [13,23] for oxidation of ethanol.

$${}^{\cdot}CCl_3 + CH_3OH \rightarrow CHCl_3 + {}^{\cdot}CH_2OH \qquad 4.10$$

$${}^{\cdot}CH_3O + CH_3OH \rightarrow CH_3OH + {}^{\cdot}CH_2OH \qquad 4.11$$

$${}^{\cdot}CH_2OH + CCl_4 \rightarrow {}^{\cdot}CCl_3 + Cl^- + HCHO + H^+ \qquad 4.12$$

The lack of signal for π-cation species in the presence of p-BQ alone in CCl_4 is attributed to the highly unstable nature of the $(H_2OEP)^{+\bullet}$ radical, which quickly reverts to the neutral form by a fast back electron transfer process in the absence of protic co-solvent.

The 441.6 nm excitation wavelength used in most of our experiments is also in resonance with the longest wavelength absorption band (430 nm)[21] of p-BQ. It is not clear at this stage how far direct excitation of p-BQ will have implications on the photochemical reaction. However, observation of similar diacid formation with 514.5 nm excitation[19] strongly suggests that the primary process in the reaction involves excited state quenching of H_2OEP by p-BQ (Eqn. 4.2). Therefore, it is proposed that in the initial stage of the process, p-BQ acts only as a catalyst, which appears to be the most consistent with the experimental results.

Another interesting aspect of the photochemical process is the different effect of MeOH in CH_2Cl_2 and CCl_4 solvents [Fig. 4.8]. In CCl_4, presence of MeOH is essential for the formation of diacid since it acts as the proton source (Eqn. 4.7). On the other hand, addition of MeOH greatly inhibits the diacid formation in CH_2Cl_2. However, at higher concentration of MeOH (about 30%), the RR spectra show the presence of monoacid. As in CCl_4, the higher rate of formation of monoacid with increasing concentration of MeOH in CH_2Cl_2 indicates that MeOH also acts as the proton donor in CH_2Cl_2. Therefore, it is most likely that the inhibitory effect of MeOH on OEP diacid formation is due to a lower scavenging power of CH_2Cl_2 for the methoxy radicals produced in the process, resulting in a lower yield of H^+ and Cl^- ions, and hence formation of only monoacid in the presence of a high concentration of methanol.

It is surprising that no photooxidation of OEP is observed in CCl_4 even in the presence of p-BQ [Fig. 4.4 & 4.7], while very clean photooxidation[3b,14] could be obtained for H_2TPP on laser excitation in the Soret absorption region. Since both of these porphyrins have almost the same values for the oxidation potentials[12] and excited state energies,[22] it appears that the observed difference arises mainly from difference in the lifetimes of the excited states, apart from differences in size, shape or solvation effects.

4.4.2 Radical Character

In Table 4.1 the wavenumber of the modes are listed for neutral, monoacid and diacid OEP. It is seen that OEP acid formation is accompanied by large upshifts of the ν_{11} and ν_4 modes by about 8-15 and 16-19 cm^{-1}, respectively. The wavenumber shift pattern of the ν_{11} mode, involving mainly the C_β–C_β bond, is in accord with the antibonding character of the a_u (a_{1u} in D_{4h} symmetry) orbital with respect to the C_β–C_β bond as expected for OEP complexes.[24] However, a large upshift in the wavenumber of the ν_4 (pyrrole half-ring stretch)$_{sym}$ mode in which the C_α–N and C_α–C_β bonds stretch out-of-phase, is inconsistent with these expectations since the a_u orbital is nonbonding and bonding, respectively, with respect to these bonds. From an NMR study,[15] it was shown that protonation of H_2OEP results in deshielding of the N-H protons and hence in a higher electron density on the methine C atoms due to migration of negative charge from the anion counter ions to the positively charged porphyrin core. Therefore, it is most likely that the effect also

increases electron densities in the C_α–N and C_α–C_β bonds of the acid derivatives, as reflected in the observed large upshift of the ν_4 mode.

4.5 Conclusion

From the above observations, we can conclude that in the photochemical reaction of H_2OEP with p-BQ induced by selective laser excitation, diacid is the most stable product of the reaction and the process is very sensitive to the solvent composition. Although formation of OEP π-cation radicals was not detected directly in our experiments, its transient formation as an intermediate in the process is proposed. The abnormal deviation of the ν_4 mode wavenumber of OEP acids from that expected for a_u character suggests that the ring oxidized and protonated species may not be comparable in H_2OEP due to a deshielding effect on the N-H protons.

References

1. (a) Oertling, W.A.; Salehi, S.A.; Chung, Y.C.; Leroi, G.E.; Chang, C.K.; Babcock, G.T. *J. Phys. Chem.*1987, 91, 5887; (b) Oertling, W.A.; Salehi, S.A.; Chang, C.K.; Babcock, G.T. *J. Phys. Chem.*1987, 91, 3114.
2. Wolberg, A.; Manassen, J. *J. Am. Chem. Soc.*1970, 92, 2982.
3. (a) Saini, G.S.S.; Chaudury, N.K.; Verma, A.L. *J. Chem. Soc. Farad. Trans.* 1992, 88, 2853; (b) Saini, G.S.S.; Chaudury, N.K.; Verma, A.L. *Photochem. Photobiol.* 1992, 55, 815.
4. (a) Gasyna, Z.; Browett, W.R.; Stillman, M.J. *Inorg. Chem.*1984, 23, 382; (b) Gasyna, Z.; Browett, W.R.; Stillman, M.J. *Inorg. Chem.* 1985, 24, 2440.
5. Parson, W.W.; Ke, B. in *Photosynthesis: Energy Conservation by Plants and Bacteria*; Grovindiju, Ed.; Academic Press: New York, 1983.
6. Frew, J.E.; Jones, P. *Advances in Inorganic and Bioinorganic Mechanism*; Academic Press: New York, 1984; p. 175.
7. Kadish, K.M. *Progress in Inorganic Chemistry*; Lippard, S.J., Ed.; Wiley: New York, 1986; vol. 34.
8. (a) Davis, D.G. in *The Porphyrins*; Dolphin, D., Ed.; Academic Press: New York, 1978; vol. V, p. 127. (b) Felton, R.H. in *The Porphyrins*, Dolphin, D., Ed.; Academic Press: New York, 1978; vol. V, p. 53.
9. (a) Lexa D.; Reix, M. *J. Chim. Phys.* 1974, 71, 511. (b) Lexa D.; Reix, M. *J. Chim. Phys.* 1974, 71, 517.
10. Fajer, J.; Borg, D.C.; Forman, A.; Felton, R.H.; Vegh, L.; Dolphin, D. *Ann. N.Y. Acad. Sci.* 1973, 206, 349.

11. Fajer J.; Davis, M.S. in *The Porphyrins*; Dolphin, D., Ed.; Academic Press: New York, 1978; vol. IV, p. 197.

12. Inisan, C.; Saillard, J-Y.; Guilard, R.; Tabard, A.; Mest, Y.L *New. J. Chem.* 1998, 22, 823.

13. Varani, G.; Maldotti, A.; Bartocci, C. *New J. Chem.* 1992, 16, 827.

14. Saini, G.S.S.; Mehdi, O.K.; Verma, A.L. *Chem. Phys. Lett.* 2000, 322, 293.

15. Ogoshi, H.; Watanabe, E.; Yoshida, Z. *Tetrahedron* 1973, 29, 3241.

16. Smith, K.M. in *Porphyrins and Metalloporphyrins;* Smith, K.M., Ed.; Elsevier: Amsterdam, 1975; p. 24.

17. Sato, S.; Aoyagi, K.; Haya, T.; Kitagawa, T. *J. Phys. Chem.* 1995, 99, 7766.

18. Perng, J-H.; Bocian, D.F. *J. Phys. Chem.* 1992, 96, 4804.

19. The 488 and 514.5 nm excited samples of H_2OEP in CH_2Cl_2 in the presence of p-BQ under aerobic conditions gave violet color and absorption spectral changes characteristic of OEP diacid. But the RR spectra are poorly resolved due to excitation within the Q-band region and are not presented here.

20. Tobita, S.; Kajii, Y.; Tanaka, I. *ACS Symp. Ser.* 1986, 321, 219.

21. Dani, V.R in *Organic Spectroscopy*; Tata McGraw-Hill Publishing Com. Ltd.: New Delhi, 1995; p. 66.

22. Gouterman, M. in *The Porphyrins*; Dolphin, D., Ed.; Academic Press: New York, 1978; vol. III, p. 34.

23. (a) Bartocci, C.; Maldotti, A.; Varani, G.; Carassiti, V.; Battioni, P.; Mansuy, D. *J. Chem. Soc. Chem. Commun.* 1989, 964; (b) Maldotti, A.; Bartocci, C.; Amadelli, R.; Carassiti, V. *J. Chem. Soc. Dalton Trans.* 1989, 1197.

24. Czernuszewicz, R.S.; Macor, K.A.; Li, X-Y.; Kincaid, J.R.; Spiro, T.G. *J. Am. Chem. Soc.* 1989, 111, 3860.

25. Li, X-Y.; Zgierski, M.Z . *J. Phys. Chem.* 1991, 95, 4268.

Table 4.1 Observed RR spectral shifts (cm^{-1}) for H_2OEP, its acid derivatives and their assignment.

H_2OEP	$(H_4OEP)^{2+}2Cl^-$	$(H_3OEP)^+Cl^-$	**Mode no. and Assignment**
1615[a]	1603	1616	ν_{10}, $\nu(C_\alpha\text{-}C_m)_{asym}$
1590[a]	---	---	ν_{19}, $\nu(C_\alpha\text{-}C_m)_{asym}$
1546[a]	1561	1554	ν_{11}, $\nu(C_\beta\text{-}C_\beta)$
---	---	1515	---
1482[a]	1480	1479	ν_{28}, $\nu(C_\alpha\text{-}C_m)_{sym}$
1467[c]	1467	1468	ν_3, $\nu(C_\alpha\text{-}C_m)_{sym}$
1369[a]	1388	1385	ν_4, $\nu(\text{Pyr.half-ring})_{sym}$
1324[a]	---	---	ν_{20}, $\nu(\text{Pyr.quarter-ring})$
---	1317[b]	1319	$\nu(CH_2)_{wag}$
1257[a]	1257	1257	$\nu(CH_2)_{twist}$
---	1222[c]	1223	δ_{NH}
1210[b]	---	---	ν_{13}, $\delta(C_mH)$
1154[c]	1154	1155	ν_{42a}, $\delta(C_mH)$
---	1133[b]	1133	ν_5, $\nu(C_\beta\text{-}C_1)_{sym}$
1124[b]	---	1123	ν_{22}, $\nu(\text{Pyr. Half-ring})_{sym}$

[a] Ref. 17. [b] Ref. 18. [c] Ref. 25.

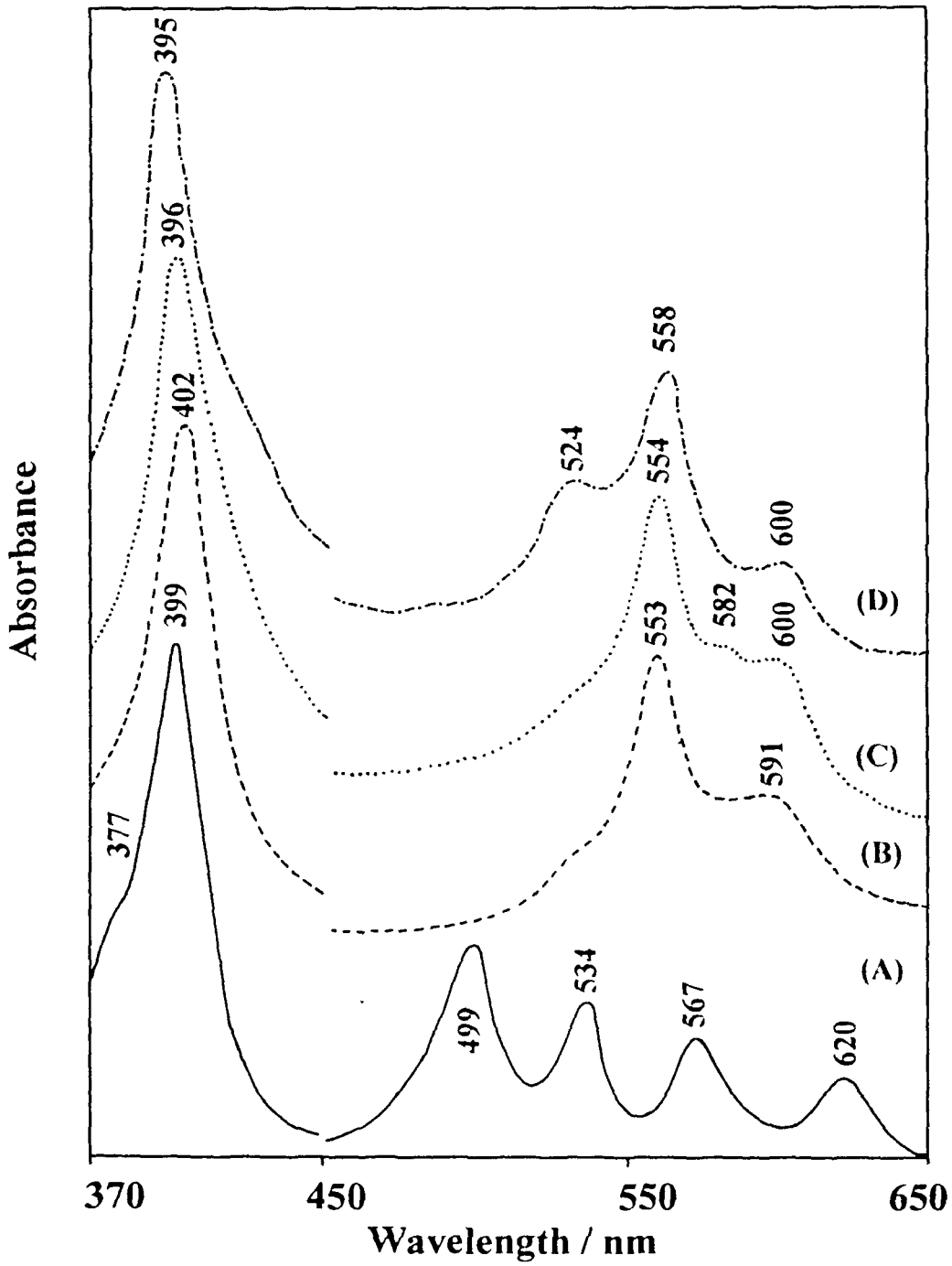

Fig. 4.1 Electronic absorption spectra of H_2OEP and its chemically prepared acid derivatives in CH_2Cl_2: (A) H_2OEP; (B) $(H_4OEP)^{2+}2Br^-$; (C) $(H_4OEP)^{2+}2Cl^-$; (D) $(H_3OEP)^+Cl^-$.

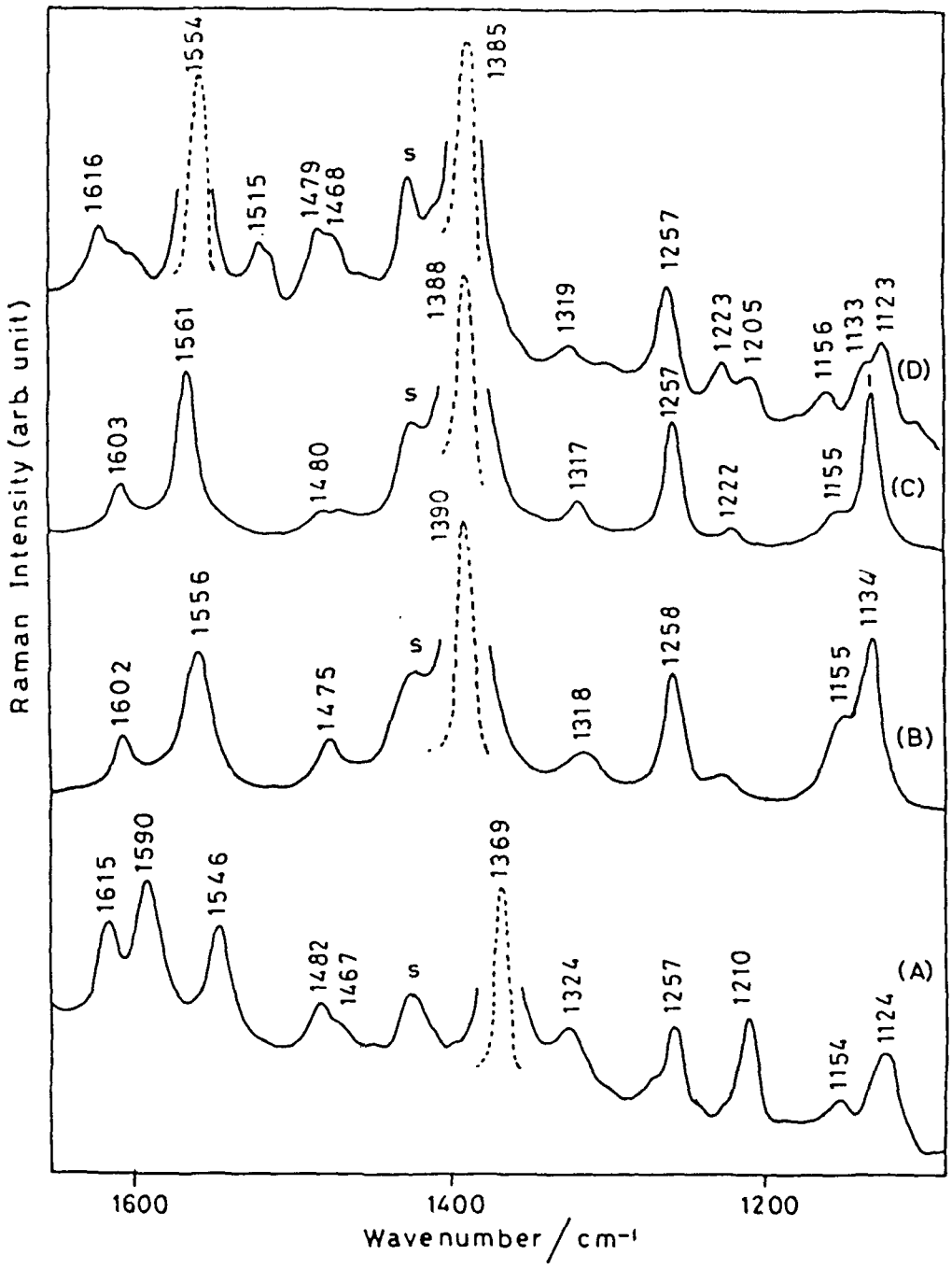

Fig. 4.2 Resonance Raman spectra (1650-1090 cm^{-1}) of H_2OEP and its chemically prepared acid derivatives in CH_2Cl_2 : (A) H_2OEP; (B) $(H_4OEP)^{2+}2Br^-$; (C) $(H_4OEP)^{2+}2Cl^-$; (D) $(H_3OEP)^+Cl^-$. The letter "S" indicates solvent band (λ_{ex} = 441.6 nm).

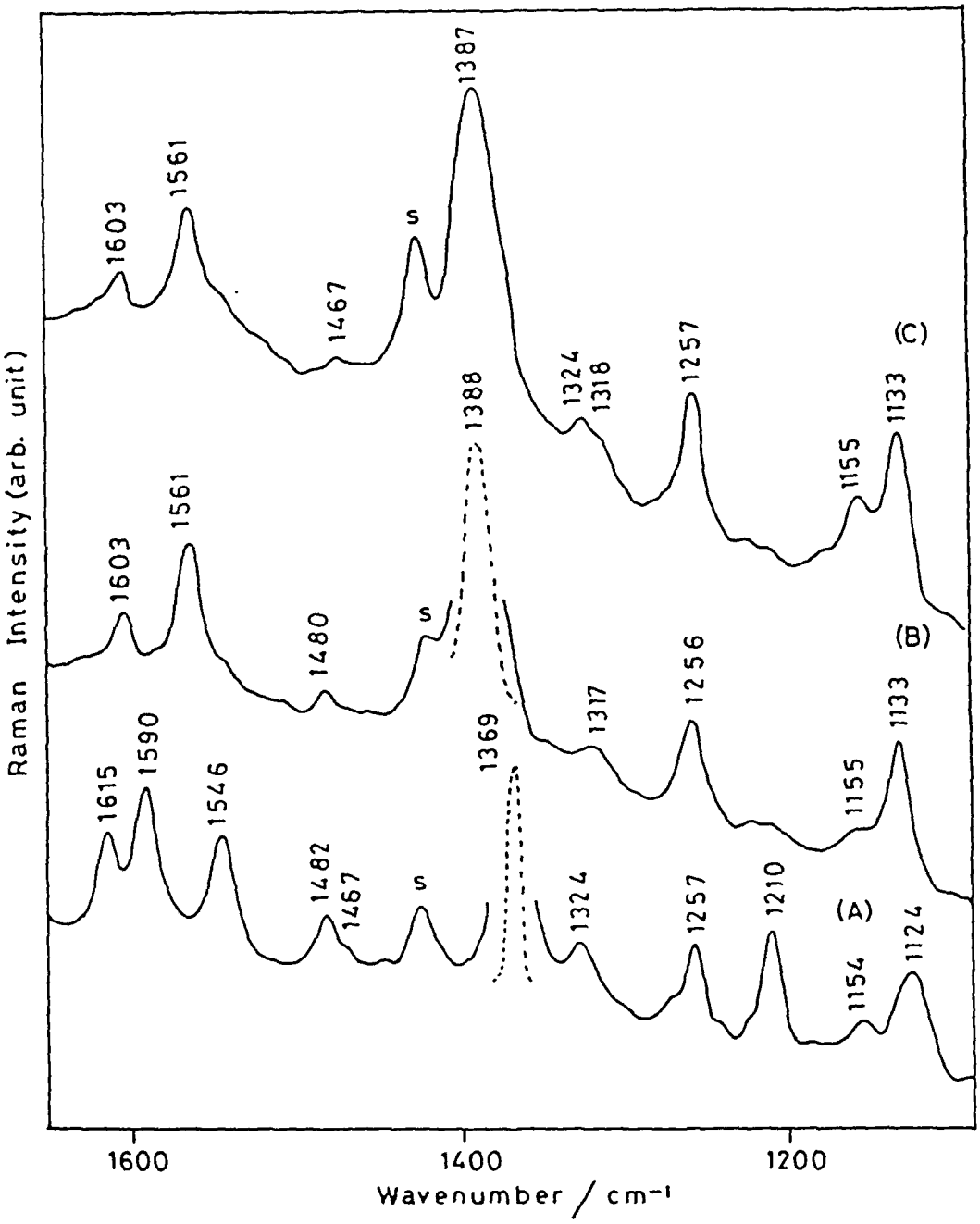

Fig. 4.3 The 441.6 nm excited RR spectra (1090-1650 cm^{-1}) of : (A) H_2OEP (ca. 1 mM) in CH_2Cl_2 ; (B) in the presence of p-BQ (ca. 8 mM) under aerobic condition; (C) in the presence of p-BQ (ca. 8 mM) under anaerobic condition. The letter "S" indicates solvent band.

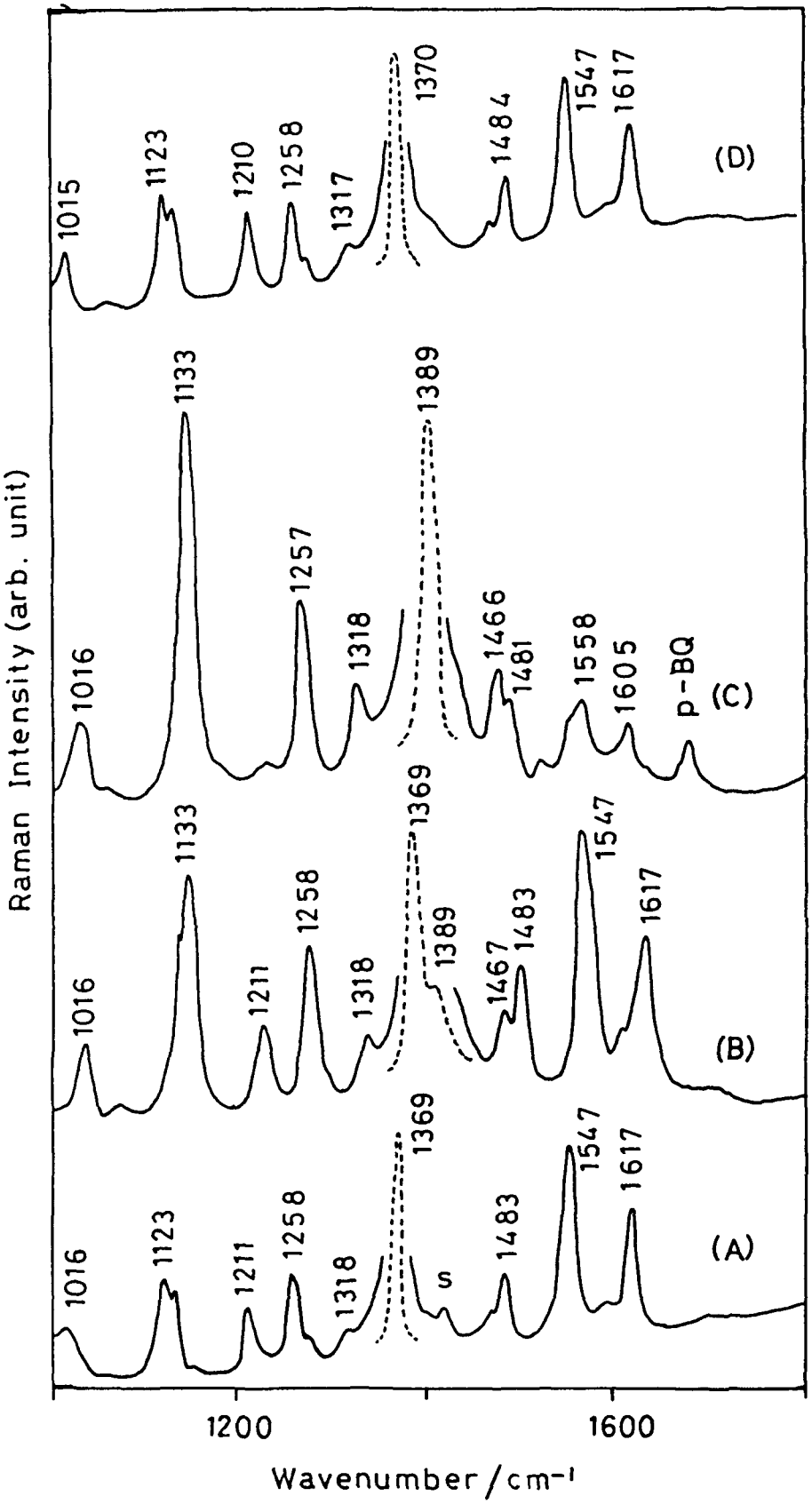

Fig. 4.4 The 406.7 nm excited RR spectra (1000-1800 cm^{-1}) of : (A) H_2OEP in CH_2Cl_2; (B) in the presence of chloranil (aerobic); (C) in the presence of p-BQ (aerobic); (D) H_2OEP in neat CCl_4 (aerobic). The letter "S" indicates solvent band.

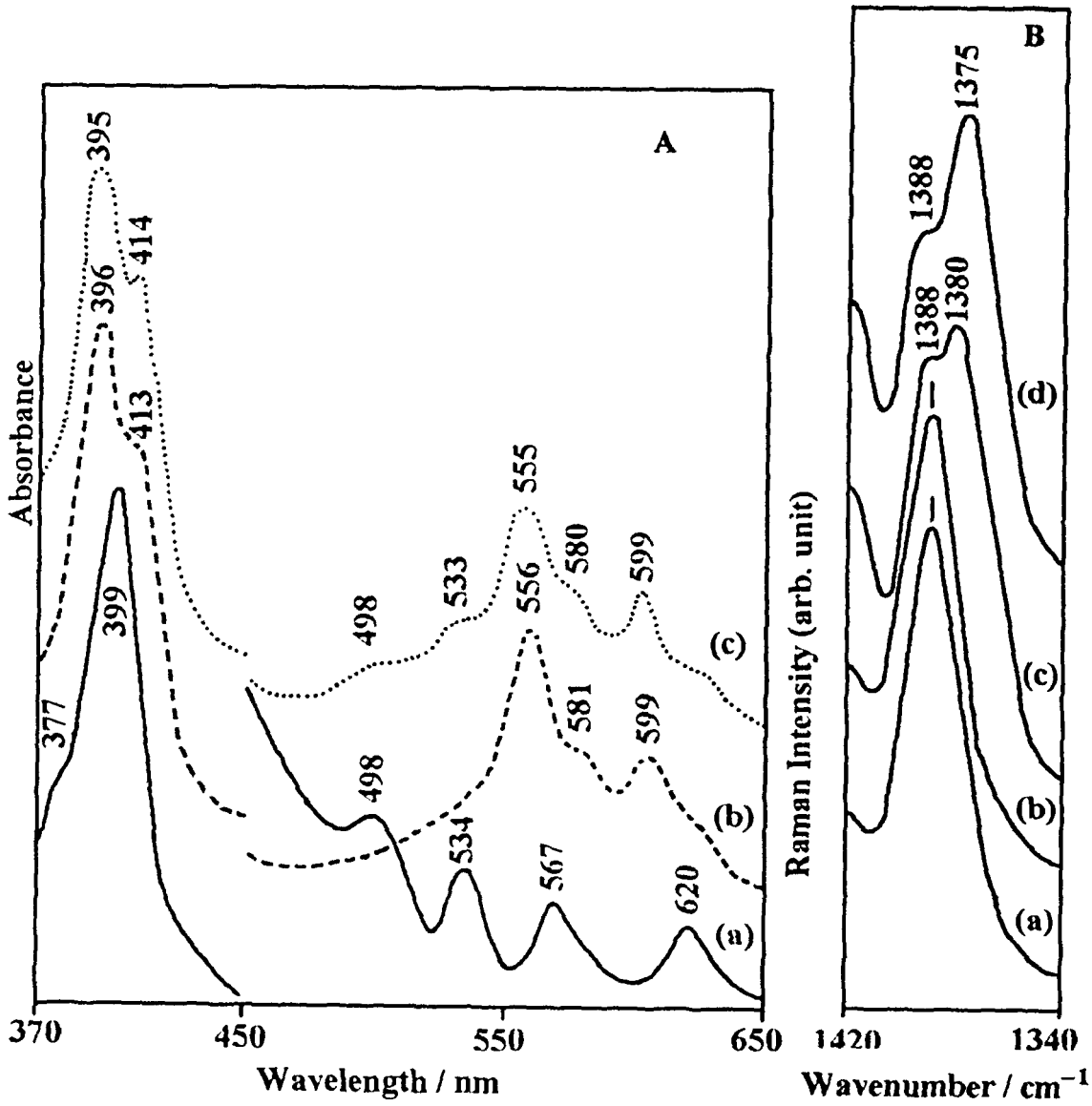

Fig. 4.5 (A) Electronic absorption spectra of H_2OEP + p-BQ (1:8) in CH_2Cl_2: (a) before laser irradiation (aerobic); (b) after 30 min laser irradiation (aerobic); (c) after 15 min laser irradiation (anaerobic). λ_{ex} = 441.6 nm.

(B) The ν_4 mode region in the RR spectra of H_2OEP (~0.25 mM) in CH_2Cl_2 in the presence of p-BQ (~6mM) as a function of irradiation time. (a) after 15 min (aerobic); (b) after 30 min (anaerobic); (c) after 30 min (aerobic); (d) after 60 min (aerobic). λ_{ex} = 441.6 nm (35 mW, focussed laser power).

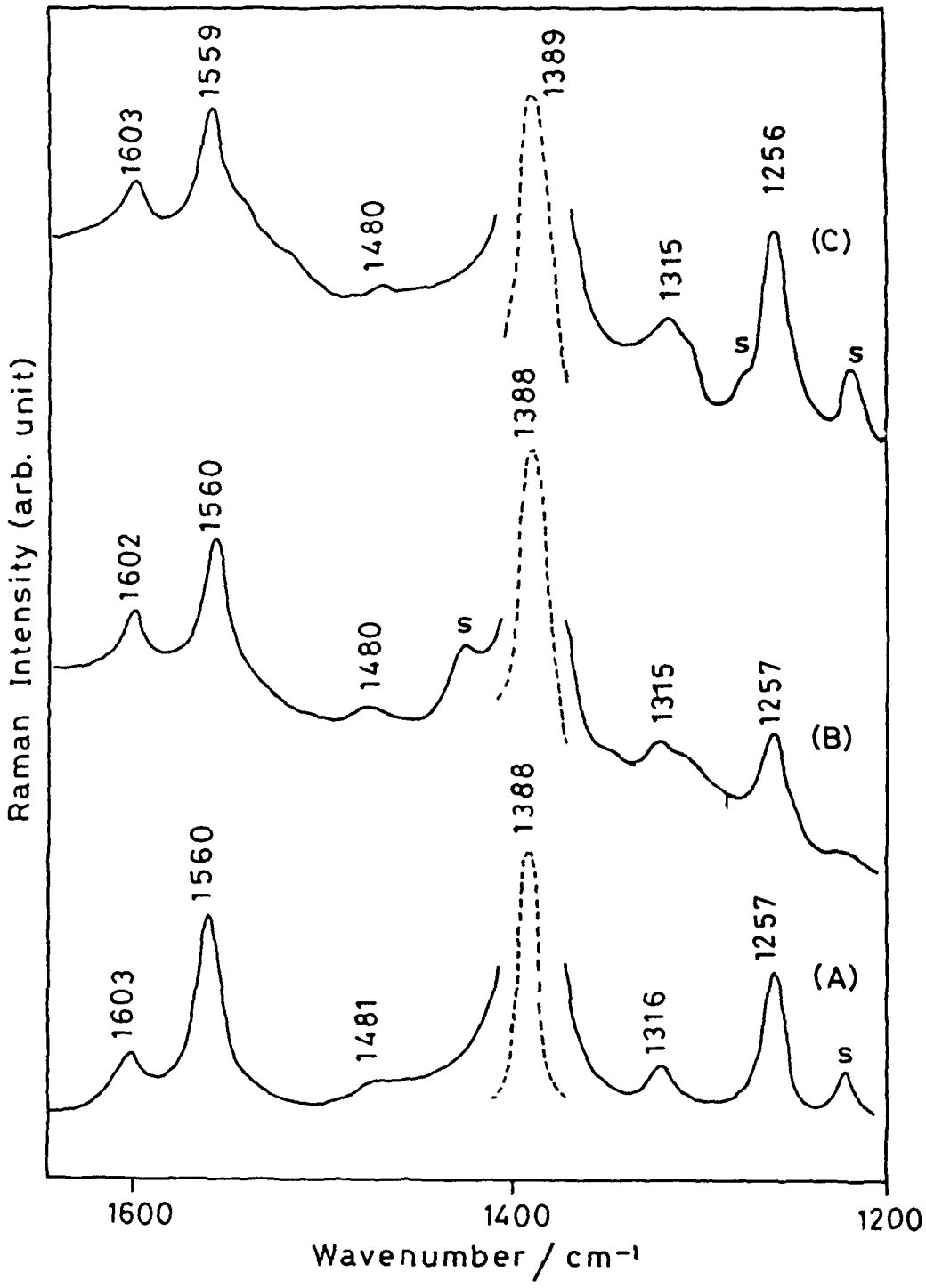

Fig. 4.6 The 441.6 nm excited RR spectra (1200-1650 cm^{-1}) of H_2OEP in in the presence of p-BQ under aerobic conditions: (A) in $CHCl_3$; (B) in $C_2H_4Cl_2$; (C) in $C_2H_2Cl_4$. The letter "S" indicates solvent band.

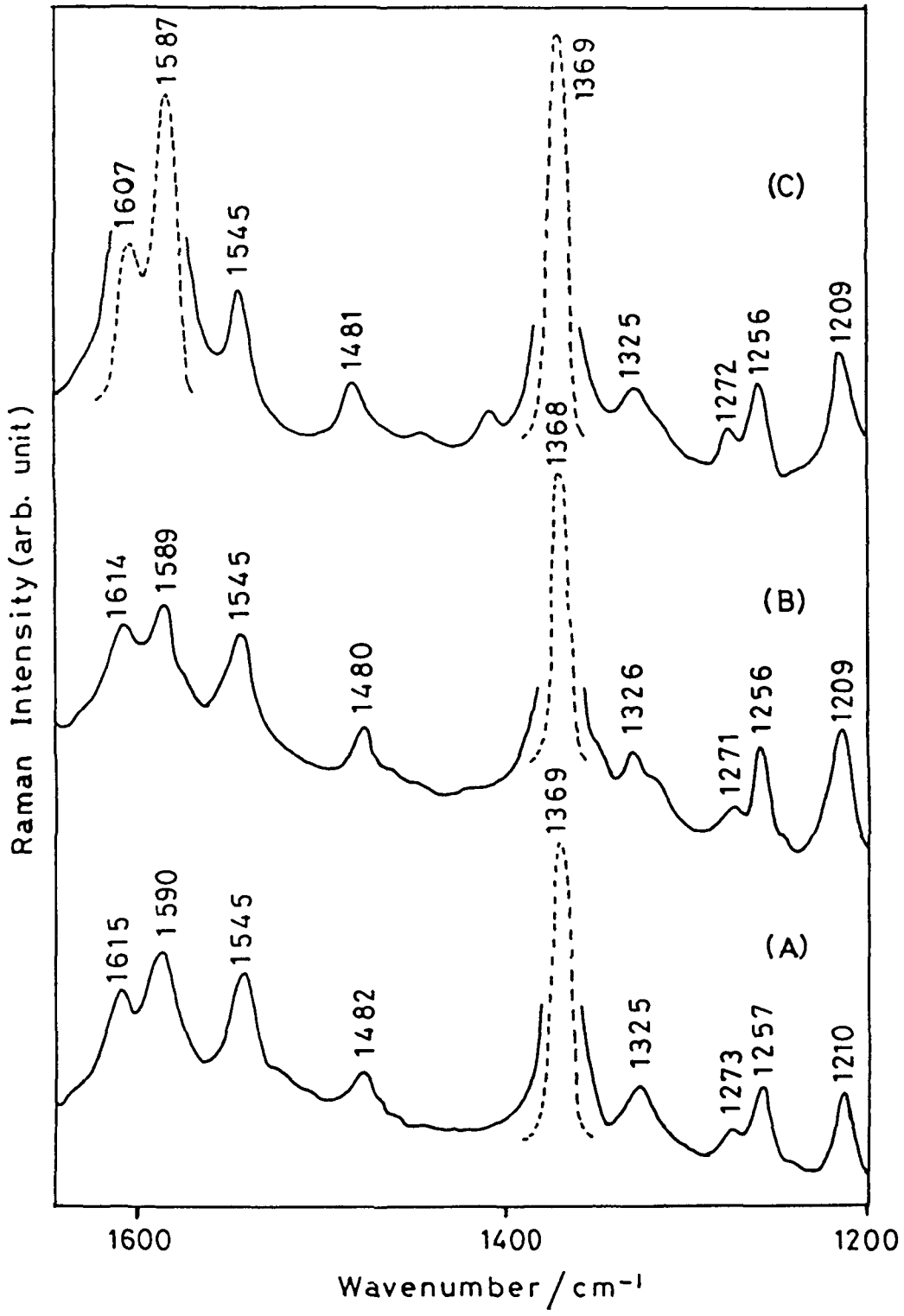

Fig. 4.7 RR spectra (441.6 nm) of H_2OEP (1200-1650 cm^{-1}) in the presence of p-BQ under aerobic conditions: (A) in CCl_4; (B) in CS_2; (C) in C_6H_6.

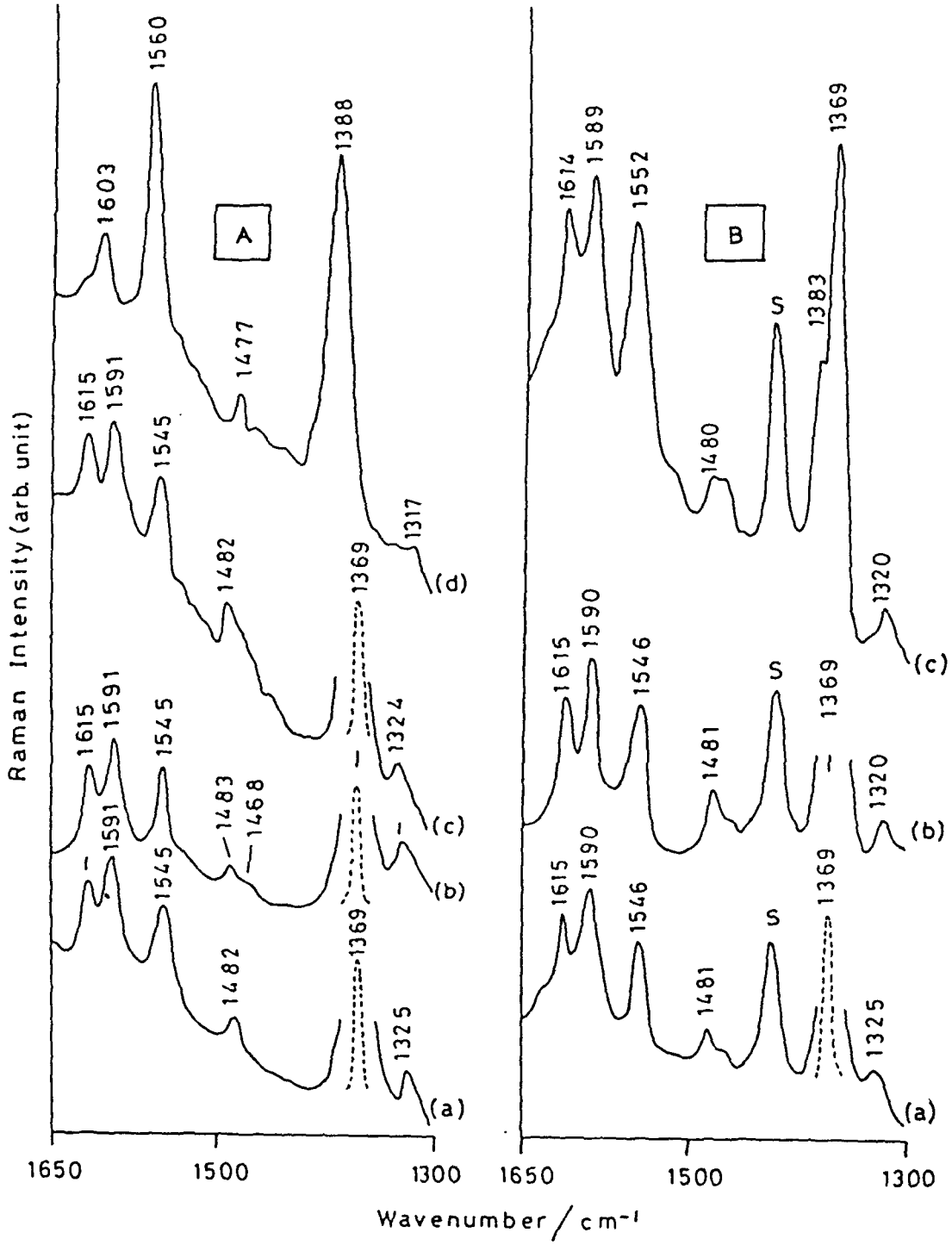

Fig. 4.8 (A) The 441.6 nm excited RR spectra (1300-1650 cm^{-1}) of: (a) H_2OEP (ca. 1 mM) in CCl_4; (b) H_2OEP + CCl_4 + p-BQ (ca. 8 mM); (c) H_2OEP + CCl_4 + 15% (v/v) MeOH ; (d) H_2OEP + CCl_4 + p-BQ (ca. 8 mM) + 15% (v/v) MeOH.

(B) The 441.6 nm excited RR spectra (1300-1650 cm^{-1}) of: (a) H_2OEP (ca. 1 mM) in CH_2Cl_2; (b) H_2OEP + CH_2Cl_2 + p-BQ (ca. 8 mM) + 15% (v/v) MeOH; (c) H_2OEP + CH_2Cl_2 + p-BQ (ca. 8 mM) + 30% (v/v) MeOH. The letter "S" indicates solvent band.

CHAPTER 5

Photooxidation of Cobalt(II) *meso*-Tetraphenylporphyrin Monitored by Optical Absorption and Resonance Raman Spectroscopies

This chapter reports photooxidation of $Co^{II}TPP$ by p-benzoquinone under 441.6 nm laser excitation studied by optical and resonance Raman spectroscopies. The results show that 441.6 nm excitation of $Co^{II}TPP$ in the presence of p-BQ gives rise to oxidation of the porphyrin complex to either $Co^{III}(TPP)^{+}$ or $Co^{III}(TPP)^{2+\bullet}$ depending on the experimental conditions. Under anaerobic conditions, the oxidation takes place at the metal center to produce the cobaltic species. However, in the presence of molecular oxygen formation of two-electron oxidized $Co^{III}(TPP)^{2+\bullet}$ π-cation radical having predominant A_{2u} character has been observed. The photochemical formation of the π-cation radical only under aerobic conditions suggests involvement of peroxy radicals in the process, and a mechanism is proposed. The photooxidation of $Co^{II}TPP$ under aerobic conditions was also studied as a function of solvents.

5.1 Introduction

During the last few decades, porphyrin systems have fascinated researchers in different fields and the interest in these macrocycles is still growing.[1] Among others, the Co-porphyrin complexes have been studied extensively because they act as model systems for the iron-containing native proteins and B_{12} coenzyme.[2,3] Due to their dioxygen binding capacity, Co(II) porphyrins are also found to act as versatile catalysts during the oxidation of wide range of organic substrates under aerobic conditions.[4,5]

Apart from these, the ease of oxidation of Co-porphyrin complexes and relatively stable nature of the corresponding π-cation radicals find another use as models for biological-type radical cations.[6] In this regard, there is a great interest in the preparation and characterization of the oxidized species of porphyrin complexes.[6,7] In particular, photooxidation of the parent porphyrin by an electron acceptor to give π-cation radical species has been the subject of many studies,[8,9] which have helped in understanding several biological reactions, including photosynthetic reaction centers[10,11] and photosynthetic model systems,[12] as well as artificial photocatalytic systems.[13,14] Especially, H_2TPP, ZnTPP and MgTPP have been extensively studied due to their ease of oxidation by light in the presence of organic electron acceptors.[8,9]

Like other MTPP complexes, photooxidation has also been observed in case of CoTPP by exciting within the Soret absorption band in the presence of alkyl chlorides.[8a,15] Due to the lower oxidation potential of the metal center compared to porphyrin ring system,[7,16] photooxidation of Co(II) tetraphenylporphyrin (Co^{II}TPP)

was found to occur at the metal center to give the cobaltic complex, followed by electron removal from the porphyrin π system during subsequent photooxidation.[8a] Although the photooxidation products of the $Co^{II}TPP$ have been characterized successfully by optical, EPR and MCD spectrocopies,[8a,15] the understanding of mechanisms by which the photochemical reactions take place is still insufficient and our experimental results are at variance with information available in literature.

Therefore, in order to have better understanding of the photochemical reactions of $Co^{II}TPP$, optical and RR spectroscopic investigations of the photooxidation of $Co^{II}TPP$ by p-benzoquinone (p-BQ) under laser excitation were carried out in the present study under different conditions. The reaction mechanism, solvent effect and the nature of the cation radical in the ground electronic state have been discussed, which are consistent with available results from previous workers.

5.2 Experimental Techniques

$Co^{II}TPP$ and p-benzoquinone (p-BQ) were commercially purchased from Aldrich Chem. Co., and used without further purification. Dichloromethane (CH_2Cl_2) was purified by washing with concentrated H_2SO_4, 15% solution of potassium carbonate, large volume of water, dried over anhydrous calcium chloride, distilled and then stored over molecular shieves. All other solvents used were of HPLC grade.

Chemical oxidation of $Co^{II}TPP$ was carried out by dropwise addition of dilute solution of bromine in CH_2Cl_2. The $Co^{III}(TPP)^+Cl^-$ complex was prepared by molecular oxygen oxidation of $Co^{II}TPP$ under acidic condition according to the method given in literature.[17]

Raman spectra were recorded with a SPEX Ramalog 1403 double monochromator equipped with a water-cooled RCA 31034 photomultiplier. Liconix 4240 HeCd laser provided excitation line at 441.6 nm. A microprocessor-based SPEX Datamate was used for spectrometer control, data acquisition and processing facilities. The typical laser power at the sample was ~ 35-40 mW and most of the Raman spectra were measured at spectral resolution of 4 to 5 cm^{-1}. The position of Raman peaks was calibrated with indene or the known bands of the solvents used. Minimum of three freeze-pump-thaw cycles were employed whenever anaerobic conditions of the solutions were required.

Electronic absorption spectra were recorded on a Carey 2300 UV-VIS spectrometer using 10 mm path length quartz cuvettes.

5.3 Results

Figure 5.1 compares the optical spectra of $Co^{II}TPP$ and its chemically oxidized complexes in CH_2Cl_2. The absorption spectrum of $Co^{II}TPP$ [Fig. 5.1(A)] is in good agreement with the reported ones,[8a,18] and is characterized by a strong Q_{0-1} band at 528 nm and an intense B band at 408 nm. The $Co^{III}(TPP)^+Cl^-$ complex shows the Soret and Q_{0-1} band's red-shifted respectively to 434 nm and 543 nm, with respect to the neutral form [Fig. 5.1(B)], which is also in conformity with the earlier reports.[7,8a] Dropwise addition of dilute solution of Br_2 to $Co^{II}TPP$ in CH_2Cl_2 results in color changes from, orange red → red → reddish brown. The red color solution is the most stable among the bromine oxidized products and gives RR spectrum similar to $Co^{III}(TPP)^+Cl^-$ in CH_2Cl_2 [Fig. 5.2(B,C)]. The reddish brown product is less

stable and readily converts to the red colored product. The spectrum of the reddish brown compound is characterized by Soret band at 423 nm and a series of weaker bands at 540, 597 and 654 nm in the visible region [Fig. 5.1(C)]. Except for the appearance of a band at 540 nm, the spectrum is very similar to the one reported for electrochemically generated $Co^{III}(TPP)^{2+\bullet}2ClO_4^-$ species[7] which gives the Soret band at 416 nm along with a series of broad features centered around 600 and 650 nm. Therefore, by comparing our results with those reported in literature for oxidation of $Co^{II}TPP$, we can identify the red and reddish brown oxidation products as $Co^{III}(TPP)^+$, $Co^{III}(TPP)^{2+\bullet}$, respectively, and the band appearing at 540 nm in the optical absorption spectrum of the reddish brown complex is attributed to arise from cobaltic species. The Soret and Q- band positions of $Co^{II}TPP$ and its oxidation products observed in this work and those reported in literature are listed in Table 5.1.

The resonance Raman spectra of $Co^{II}TPP$ and the chemically prepared $Co^{III}(TPP)^+$ complex in CH_2Cl_2 at 441.6 nm excitation wavelength are shown in Fig. 5. 2. Since most of the TPP vibrations are shifted only slightly by changing the central metal and normal mode composition is expected not to alter much by changing of the central metal atom, RR spectra of neutral and the oxidized CoTPP obtained for our systems are analyzed in the light of assignments[19] made for MTPP's (M = Ni, Cu and Fe) and their corresponding π-cation radicals. The 441.6 nm line is close to resonance with the $Co^{II}TPP$ B band. In the RR spectrum of $Co^{II}TPP$ [Fig. 5.2(A)] the most intense bands arise from the high-wavenumber skeletal modes ν_2, ν_4, and ν_1 at 1569, 1369 and 1234 cm^{-1}, respectively. The ϕ_4(phenyl), ν_{11}, ν_3 and ν_{27} modes are also seen with moderate intensities at 1600, 1499, 1467 and 1270 cm^{-1},

respectively. This assignment is in agreement with the one reported[20] for $Co^{II}TPP$ at low temperature, except that the low temperature RR spectra show these modes at higher wavenumber compared to our room temperature solutions. Ruffling of CoTPP[21] is attributed to account for the lowering of the wavenumber for these modes at room temperature solution compared to their values at low temperature, because at low temperature coordination of solvent or other molecules to Co atom can reduce the ruffling effect. Depolarization ratio measurement (Table 5.2) also indicates that the symmetry of $Co^{II}TPP$ is lower than D_{4h} because all the modes appearing in the 1200-1650 cm^{-1} region are polarized. The spectrum of $Co^{III}(TPP)^{+}Cl^{-}$ [Fig. 5.2(B)] is marked by enhancement in the relative intensity of the ϕ_4(phenyl) mode at 1600 cm^{-1} along with an upshift of ν_{11} mode wavenumber by about 9 cm^{-1}. For other RR bands in $Co^{III}(TPP)^{+}$ spectrum, the wavenumber shifts do not amount to more than 3 cm^{-1}. This is what is expected for electron removal from the Co d_{z^2} orbital because the d_{z^2} electron does not interact significantly with porphyrin orbitals. The situation is quite similar to the spectral variation between $Ni^{II}TPP$ and $Ni^{III}(TPP)^{+}$,[19b] where also, the molecules differ by one electron in the metal d_{z^2} orbital. The reddish oxidized product of $Co^{II}TPP$ prepared by addition of dilute Br_2 solution also gives identical spectral features [Fig. 5.2(C)]. For other higher oxidized products prepared by chemical method, reliable spectra could not be presented due to labile nature of these products which readily converted to $Co^{III}(TPP)^{+}$ species (as monitored from the color changes) during RR measurements irrespective of the presence or absence of oxygen.

The optical spectrum of $Co^{II}TPP$ in CH_2Cl_2 shows changes when excited with 441.6 nm laser line in the presence of p-benzoquinone (p-BQ), as shown in Fig. 5.3.

Before laser irradiation, the spectrum remains unchanged on addition of p-BQ even when the solution was stored aerobically for 24 hrs at room temperature [Fig. 5.3(A)], indicating ground state complexation between $Co^{II}TPP$ and p-BQ would be very weak, if not totally absent. However, after 441.6 nm laser irradiation two kinds of spectral changes are seen depending on the presence or absence of oxygen [Fig. 5.3(B,C)]. In the absence of oxygen, the photoirradiated sample of $Co^{II}TPP$ in the presence of p-BQ gives spectrum shown in [Fig. 5.3(B)] which can be resolved into a mixture of $Co^{II}TPP$ and $Co^{III}(TPP)^{+}$ complexes by comparing with the known spectra of $Co^{II}TPP$ and $Co^{III}(TPP)^{+}$. Under aerobic conditions laser irradiation gives another spectrum characterized by the appearance of bands at 423, 434 and 541 nm [Fig. 5.3(C)]. Since the 423 nm band is characteristic of $Co^{III}(TPP)^{2+\bullet}$ species and the $Co^{III}(TPP)^{+}$ product is characterized mainly by bands at 434 and 543 nm, the spectrum obtained in the presence of molecular oxygen indicates formation of these two oxidized species in the system. The above observations, therefore, suggest that laser excitation of $Co^{II}TPP$ in CH_2Cl_2 in the presence of p-BQ results in photooxidation of the porphyrin. In the absence of molecular oxygen oxidation occurs at metal center to give the cobaltic complex, while presence of molecular oxygen results in oxidation of the porphyrin π system also.

The photooxidation of $Co^{II}TPP$ by p-BQ was also studied by resonance Raman spectroscopy and the spectra obtained at 441.6 nm excitation under different conditions mentioned above are shown in Fig. 5.4. The RR spectrum of the photooxidation product obtained under degassed conditions containing $Co^{II}TPP$ and p-BQ in CH_2Cl_2 [Fig. 5.4(B)] is similar to the chemically prepared $Co^{III}(TPP)^{+}$ species. On the other hand, the RR spectrum of $Co^{II}TPP$ obtained in the simultaneous

presence of p-BQ and molecular oxygen is characterized by strong enhancement of the ϕ_4(phenyl) mode along with the appearance of additional bands of moderate intensity at 1542 and 1533 cm^{-1} [Fig. 5.4(C)]. Downshifts in the ν_{11} and ν_3 mode wavenumbers by about 4-5 cm^{-1} and slight upshifts of the ν_4 mode and solvent band are also characteristic features of this spectrum. Except for the slight upshift of the solvent band and appearance of a band at 1542 cm^{-1} and, the spectral changes are similar to the ones reported[19b,c] for oxidation of NiTPP and CuTPP to their corresponding π-cation radicals. In other solvents where solvent bands are not appearing in the 1400-1450 cm^{-1} region, $Co^{II}TPP$ shows a weak band at 1429 cm^{-1} in the RR spectra [Fig. 5.7 & 5.8], the intensity of which becomes strongly enhance in the RR spectra of $Co^{III}(TPP)^{2+\bullet}$ [Fig. 5.7]. Similar enhancement of the band at around 1452 cm^{-1} was also observed in the RR spectrum of $Cu(TPP)^{+\bullet}$ radical, and is assigned to ν_{28} mode.[19c] Accordingly, the 1429 cm^{-1} band observed in the RR spectra of $Co^{II}TPP$ can be assigned to ν_{28} mode, and the apparent upshift (~ 4 cm^{-1}) of the CH_2Cl_2 solvent band in the RR spectra of $Co^{III}(TPP)^{2+\bullet}$ radical is attributed to large intensity contribution from the ν_{28} mode. In order to identify the bands at 1542 and 1533 cm^{-1}, a CH_2Cl_2 solution of CuTPP was excited with 441.6 nm in the absence and presence of p-BQ. The RR spectra are shown in Fig. 5.5 (A,B). In the presence of p-BQ, the RR spectrum of CuTPP shows additional bands at 1542 and 1477 cm^{-1}. These new features can not result from photochemical formation of $Cu(TPP)^{+\bullet}$ radical as no bands appear at such positions in the RR spectra of the radical. In the RR spectra of $Cu(TPP)^{+\bullet}$ π-cation radical,[19c] the ν_2 and ν_{11} modes are observed at 1530 and 1469 cm^{-1}, respectively, and no bands appear at 1542 and 1477

cm^{-1} wavenumber. Fig. 5.5(C,D) gives RR spectra of H_2TPP in CH_2Cl_2 in the presence and absence of p-BQ. The RR spectrum of H_2TPP obtained in the presence of p-BQ is identical to that of H_4TPP^{2+},[9a] and the ν_2 and ν_{11} modes are seen at 1541 and 1476 cm^{-1}. Therefore, by comparing the spectra (B) and (D) of Fig. 5.5, we can associate the 1542 cm^{-1} band to the ν_2 mode of free base TPP diacid, while the 1533 cm^{-1} band is assigned to ν_2 mode of $Co^{III}(TPP)^{2+\bullet}$ oxidized product. Table 5.2 gives the mode numberings and assignment along with the depolarization ratios for neutral and the oxidized products.

Addition of 2-MeIm to the photo-irradiated dichloromethane solution of $Co^{II}TPP$ in the presence of p-BQ gives RR spectrum similar to the one obtained by addition of the nitrogenous base before laser irradiation [Fig. 5.6]. In this 2-MeIm complex, the oxidation state marker mode (ν_4) is seen at 1370 cm^{-1}, same position as in its absence. But $Co^{II}TPP$(2-MeIm) complex was reported to show the ν_4 mode at 1363 cm^{-1}.[22] This indicates that the 2-MeIm complex of $Co^{II}TPP$ obtained in our system is $Co^{III}TPP$- imidazole adduct. This provides another support for photooxidation of $Co^{II}TPP$ to $Co^{III}(TPP)^{2+\bullet}$ radical, because addition of 2-MeIm to the photoirradiated sample of $Co^{II}TPP$ will reduce the radical cation and stabilize the Co^{III} complex, as observed in case of CoOEP complexes[6a] where coordination of donor ligand to the metal center of $Co^{III}(OEP)^{2+\bullet}$ stabilizes the Co^{III} complex over the π-cation radicals. Therefore, in agreement with our observations and earlier reports,[7,8a] the two-electron photooxidation of $Co^{II}TPP$ is believed to be first initialized by one electron removal from the metal, followed by porphyrin ring oxidation to give π-cation radical product.

Photooxidation of $Co^{II}TPP$ by p-BQ was also observed in $C_2H_4Cl_2$ and $C_2H_2Cl_4$ solvents similar to the one in CH_2Cl_2 solutions [Fig. 5.7]. But no photooxidation occurs in $CHCl_3$, CCl_4 and CS_2 [Fig. 5.8].

Fig. 5.9 gives the RR spectra of CoTPP obtained with 488 and 406.7 nm excitation wavelengths. The enhancement pattern of 488 nm excited RR spectra of $Co^{II}TPP$ and $Co^{III}(TPP)^+$ are quit similar to the ones obtained with 441.6 nm excitation except for the appearance of ϕ_5(phenyl) mode at 1511 cm^{-1} in the RR spectrum of $Co^{III}(TPP)^+$. Spectral changes shown in Fig. 5.9(C) are obtained in the presence of p-BQ under aerobic conditions. The spectrum is dominated by bands at 1601(ϕ_4), 1581(ν_{10}), 1556(ν_{19}), 1493 (ν_{11}), 1464(ν_3) and 1427 cm^{-1}. The enhancement pattern is quit different form the 441.6 nm excited spectra under otherwise similar conditions. But from the band positions of ν_{11} and ν_3 modes at 1493 and 1494 cm^{-1}, we can infer that the spectrum (C) originates from $Co^{III}(TPP)^{2+\bullet}$ oxidized product. Trace (D) gives the RR spectrum of $Co^{II}TPP$ in neat CCl_4 recorded with 406.7 nm excitation. The spectral feature is similar to that of 441.6 nm excited spectra, except that an additional band appears at 1485 cm^{-1} with an enhancement of the ν_{12} mode at 1304 cm^{-1}.

5.4 Discussion

5.4.1 Mechanism

From the above observations, it can be seen that solution of $Co^{II}TPP$ in CH_2Cl_2 is quite stable under 441.6 nm laser excitation. In the ground electronic state no appreciable complexation or oxidation was found on addition of p-BQ [Fig.

5.3(A)]. However, in the presence of p-BQ and under 441.6 nm laser excitation, the degassed solution of $Co^{II}TPP$ in CH_2Cl_2 shows occurrence of photooxidation of Co^{II} to Co^{III} porphyrin [Fig. 5.3(B) & 5.4(B)]. The excitation wavelength used in these experiments is in resonance with the B band (409 nm) of $Co^{II}TPP$ and the 430 nm band of p-BQ. But complication from p-BQ excited states reaction can be ruled out by observation of similar type of photooxidation at 488 nm excitation in the systems [Fig. 5.9(C)]. Therefore, the one-electron metal center photooxidation of $Co^{II}TPP$ is suggested to involve mainly the (π-π^*) excited states of TPP. From time-resolved ESR study[23] of photooxidation of ZnTPP by p-BQ under anaerobic conditions, formation of both $p\text{-}BQ^-$ anion and $Zn(TPP)^{+\bullet}$ cation radicals have been detected. Therefore, the photooxidation of $Co^{II}TPP$ by p-BQ under anaerobic conditions can be safely represented as,

$$Co^{II}TPP \overset{h\nu}{\Leftrightarrow} [Co^{II}TPP]^* \qquad 5.1$$

$$[Co^{II}TPP]^* + p\text{-}BQ \Rightarrow Co^{III}(TPP)^+ + p\text{-}BQ^- \qquad 5.2$$

$$p\text{-}BQ^- + CH_2Cl_2 \Rightarrow {}^{\bullet}CH_2Cl + Cl^- \qquad 5.3$$

$$Co^{III}(TPP)^+ + Cl^- \Rightarrow Co^{III}(TPP)^+Cl^- \qquad 5.4$$

In the presence of molecular oxygen, porphyrin ring oxidation also takes place in addition to the metal center oxidation. Since formation of $Co^{III}(TPP)^{2+\bullet}$ cation radical was not observed under anaerobic conditions, molecular oxygen appears to play crucial role in the above process. In pulse radiolysis study of oxidation of NiTPP, methyl chloride's peroxy radicals were used to oxidize the TPP complexes.[24] Moreover, ESR and optical absorption study also revealed oxidation of $Co^{III}TPP$ to $Co^{III}(TPP)^{2+\bullet}$ by ${}^{\bullet}CH_2ClO_2$ radical in the photoinduced homolytic

cleavage of C-Cl bond of CH_2Cl_2.[15] Methylene chloride peroxy radical is, therefore, suggested to be the oxidant of CoTPP π-system oxidation in the present case. Accordingly, the following mechanism is proposed in addition to the above equations.

$$^{\bullet}CH_2Cl + O_2 \Rightarrow {}^{\bullet}CH_2ClO_2 \qquad 5.5$$

$$^{\bullet}CH_2ClO_2 + Co^{III}(TPP)^{+} \Rightarrow Co^{III}(TPP)^{2+\bullet} + \text{products} \qquad 5.6$$

$$Co^{III}(TPP)^{2+\bullet} + 2Cl^{-} \Rightarrow Co^{III}(TPP)^{2+\bullet}2Cl^{-} \qquad 5.7$$

As excited states of p-BQ is reduced by dioxygen to give superoxide ion,[25] the fate of p-BQ^{-} anion radical can also be predicted to degrade as:

$$p\text{-}BQ^{-} + O_2 \Rightarrow p\text{-}BQ + O_2^{-} \qquad 5.8$$

The superoxide ion will in turn react with the solvent molecule to give peroxy radicals,[26] which will finally result in reaction similar to Eqn. 5.6.

5.4.2 Solvent dependence

It is interesting to note that photooxidation of $Co^{II}TPP$ was not observed in neat CCl_4 or $C_2H_2Cl_4$ solutions [Fig. 5.7 & 5.9]. Even at 406 nm laser excitation, the CCl_4 solution did not show photooxidation, while some workers reported[8a] photooxidation in these solvents with 417 nm excitation. This is attributed to low quantum yield of formation of the oxidized product by focussed laser beam which becomes undetectable by RR technique since the excited state lifetime of $Co^{II}TPP$ is very short (<15 ps)[27] and, CCl_4 and $C_2H_2Cl_4$ are not as strong as p-BQ in their oxidizing power. In the presence of p-BQ and at 441.6 nm laser excitation, photooxidation of $Co^{II}TPP$ occurred in solvents like CH_2Cl_2, $C_2H_4Cl_2$ and $C_2H_2Cl_4$

[Fig. 5.4 & 5.7], but not in CCl_4, $CHCl_3$ and CS_2 solutions [Fig. 5.8]. The above solvent dependence of photooxidation, on one hand, can be understood from the decrease in radical reactivity with increasing number of chloride substituents in the molecules.[28] Polarity of the solvents can also be another factor, because it will enhance the charge separation processes in reactions (5.2) and (5.6).[29] The dielectric constants of CS_2, CCl_4, $CHCl_3$, CH_2Cl_2, $C_2H_4Cl_2$ and $C_2H_2Cl_4$ are respectively, 2.60, 2.24, 4.80, 8.93, 10.36 and 8.20.[27,30] Therefore, the non-photooxidability of $Co^{II}TPP$ in CS_2, CCl_4 and $CHCl_3$ in the presence of p-BQ can also be attributed to their low dielectric constants.

5.4.3 Radical character

In Table 5.2 wavenumber shifts associated with different modes are listed for $Co^{II}TPP$ and radical TPP complex of Co^{III} (chloride adduct). The pattern of wavenumber shifts upon radical formation is very similar to that of the $Ni^{II}(TPP)^{+\bullet}$ and $Cu^{II}(TPP)^{+\bullet}$ complexes.[19b,c] Large downshift of 34 cm^{-1} is found for the ν_2, while smaller downshifts, 4-6 cm^{-1} are found for the ν_{11} and ν_3 modes. The remaining mode shifts are small, 0-3 cm^{-1}. The key point in the interpretation of the RR wavenumber shifts upon radical formation is that the a_{2u} orbital has a bonding interaction between the C_β atoms of a given pyrrole ring, while the a_{1u} interaction is antibonding. The wavenumber shift pattern of ν_2 and ν_{11} modes involving mainly the C_β–C_β bond, is in accord with the bonding character of the A_{2u} orbital with respect to the C_β–C_β bond as expected for TPP complexes.[19c] The A_{2u} character of $Co^{III}(TPP)^{2+\bullet}2ClO_4^-$ and $Co^{III}(TPP)^{2+\bullet}2Cl^-$ species had also been established from EPR[7] and MCD[8a]

studies. The small upshift of 2 cm^{-1} for the ν_4 mode seen for $Co^{III}(TPP)^{2+\bullet}$ is, however, in contrast to other reported MTPP π-cation radicals[19c] (M = Ni^{II}, Cu^{II}, Fe^{III}), for which downshifts of about 4-18 cm^{-1} have been reported. The ν_4 mode contains mainly C_α–N stretch,[31] but according to later normal mode analysis,[19d] a more apt description is the pyrrole symmetric half-ring stretch, in which the C_α–N and C_α–C_β bonds stretch out of phase. In the A_{2u} orbital both the C_α–N and C_α–C_β interactions are nearly nonbonding, and the ν_4 shifts are expected to be small and variable.[19c]

5.5 Conclusion

From the above observations and discussion, it can be concluded that 441.6 nm excitation of Co^{II}TPP solution in the presence of p-benzoquinone results in photooxidation of the cobalt porphyrin complex. The oxidation products were characterized with optical and RR spectroscopies by comparison with the chemically prepared ones. The results show that under anaerobic only metal centered oxidation occurs, while in the simultaneous presence of oxygen and p-benzoquinone porphyrin π system also gets oxidized in addition to the metal centered oxidation to give radical cation of A_{2u} character. Peroxy radicals originating from the solvent were suggested to facilitate electron removal from the porphyrin ring, and the reactions are very sensitive to the nature of the solvents used.

References

1. Milgrom, L.R. *The Colour of Life: An Introduction to the Chemistry of Porphyrins and Related Compunds*; Oxford University Press: Oxford, 1997.
2. Doorslaer, S.V.; Bachmann, R.; Schweiger, A. *J. Phys. Chem A.* 1999, 103, 5446.
3. Rovira, C.; Kunc, K.; Hutter, J.; Parrinello, M. *Inorg. Chem.* 2001, 40, 11.
4. Mandal, A.K.; Iqbal, J. *Tetrahedron* 1997, 53, 7641.
5. Sugamoto, K.; Matsushita, Y.-I.; Matsui, T. *J. Chem. Soc. Perkin Trans. 1* 1998, 3989.
6. (a) Oertling, W.A.; Salehi, A.; Chung, Y.C.; Leroi, G.E.; Chang, C.K.; Babcock, G.T. *J. Phys. Chem.* 1987, 91, 5887. (b) Sandusky, P.O.; Oertling, W.A.; Chang, C.K.; Babcock, G.T. *J. Phys. Chem.* 1991, 95, 4300.
7. Wolberg, A.; Manassen, J. *J. Am. Chem. Soc.* 1970, 92, 2982.
8. (a) Gasyna, Z.; Browett, W.R.; Stillman, M.J. *Inorg. Chem.* 1984, 23, 382. (b)Gasyna, Z.; Browett, W.R.; Stillman, M.J. *Inorg. Chem.* 1985, 24, 2440.
9. (a) Saini, G.S.S.; Medhi, O.K.; Verma, A.L. *Chem. Phys. Lett.* 2000, 322, 293. (b) Saini, G.S.S.; Chaudhury, N.K.; Verma, A.L. *J. Chem. Soc. Farad. Trans.* . 1992, 88, 2853.
10. Fajer, J.; Davis, H.S. In *Porphyrins*; Dolphin, D., Ed.; Academic Press: New York, 1979; Vol. 4, p. 197.
11. Deisenhofer, J.; Epp, O.; Miki, K.; Huber, R.; Michel, H. *J. Mol. Biol.* 1984, 180, 385.
12. McIntosh, A.R.; Siemiarczuk, A.; Bolton, J.R.; Stillman, M.J.; Ho, Fe-Te.; Weedon, A.C. *J. Am. Chem. Soc.* 1983, *105*, 7215.

13. Darvent, J.R.; Douglas, P.; Harriman, A; Porter, G.; Richoux, M.-C. *Coord. Chem. Rev.* 1982, 44, 83.

14. Harriman, A.; Richoux, M.C.; Neta, P. *J. Phys. Chem.* 1983, 87, 4957.

15. Yamamoto, K.; Hoshino, M.; Kohno, M.; Ohya-Nishiguchi, H. *Bull. Chem. Soc. Jpn.* 1986, 59, 351.

16. Mu, X.H.; Schultz, F.A. *Inorg. Chem.* 1990, 29, 2877.

17. Sakurai, T.;Yamamoto, K.; Naito, H.; Nakamoto, N. *Bull. Chem. Soc. Jpn.* 1976, 49, 3042.

18. Reddy, D.; Reddy, N.S.; Chandrashekar, T.K.; van Willigen, H. *J. Chem. Soc. Dalton Trans.* 1991, 2097.

19. (a) Li, X.-Y.; Czernuszewicz, R.S.; Kincaid, J.R.; Su, Y.O; Spiro, T.G. *J. Phys. Chem.* 1990, 94, 31. (b) Kim, D.; Miller, L.A.; Spiro, T.G. *Inorg. Chem.* 1986, 25, 2468. (c) Czernuszewicz, R.S.; Macor, K.A.; Li, X.-Y.; Kincaid, J.R.; Spiro, T.G. *J. Am Chem. Soc.* 1989, 111, 3860. (d) Li, X.-Y.; Czernuszewicz, R.S.; Kincaid, J.R.; Stein, P.; Spiro, T.G. *J. Phys. Chem.* 1990, 94, 47.

20. (a) Kozuka, M.; Nakamoto, K. . *J. Am Chem. Soc.* 1981, 103, 2162. (b) Kozuka, M.; Iwaizumi, M. *Bull. Chem. Soc. Jpn.* 1983, 56, 3165.

21. Prendergast, K.; Spiro, T.G. *J. Am Chem. Soc.* 1992, 114, 3793.

22. Parthasarathi, N.; Hansen, C.; Yamaguchi, S.; Spiro, T.G. *J. Am. Chem. Soc.* 1987, 109, 3866.

23. van Willigen, H.; Voulle, M.; Dinse, K.P. *J. Phys. Chem.* 1989, 93, 2441.

24. Nahor, G.S.; Neta, P.; Hambright, P.; Robinson, L.R. *J. Phys. Chem.* 1991, 95, 4415.

25. Lang, K.; Wagnerova, D.M.; Stopka, P.; Damerau, W. *J. Photochem. Photobiol. A Chem.* 1992, 67, 187.

26. Wilshire, J.; Sawyer, D.T. *J. Am. Chem. Soc.* 1979, 101, 105 and refs. therein.

27. Tait, C.D.; Holten, D.; Gouterman, M. *Chem. Phys. Lett.* 1983, 100, 268.

28. Bansal, R.K. *Oganic Reaction Mechanism*, Second Ed.; TATA McGraw-Hill Publishing Co. Ltd.: New Delhi, 1986, pp. 207.

29. O'Driscoll, E.; Simon, J.D.; Peters, K.S. *J. Am. Chem. Soc.* 1990, 112, 7091.

30. Delaney, J.K.; Mauzerall, D.C.; Lindsey, J.S. *J. Am. Chem. Soc.* 1990, 112, 957.

31. Abe, M.; Kitagawa, T.; Kyogoku, Y. *J. Phys. Chem.* 1978, 69, 4526.

Table 5.1 UV-VIS absorption band positions for $Co^{II}TPP$ and its oxidized products.

Complex	Solvent	Absorption band (nm) Soret	Q-band	Ref.
$Co^{II}TPP$	CH_2Cl_2	408	528, 617	This work
$Co^{III}(TPP)^+$	CH_2Cl_2	434	543	This work
$Co^{III}(TPP)^{2+\bullet}$	CH_2Cl_2	423	540, 597	This work
$Co^{II}TPP$	Benzonitrile	415	529[a]	7
$Co^{III}(TPP)^+$	Benzonitrile	438	549[a], 586[a]	7
$Co^{III}(TPP)^{2+\bullet}$	Benzonitrile	416	610[a], 661[a]	7
$Co^{II}TPP$	CH_2Cl_2	410	528, 860	15
$Co^{III}(TPP)^+$	CH_2Cl_2	406	545, 900	15
$Co^{III}(TPP)^{2+\bullet}$	CH_2Cl_2	NA	620, 680	15
$Co^{III}(TPP)^+$	CH_2Cl_2	405	542, 510	8a
$Co^{III}(TPP)^{2+\bullet}$	CH_2Cl_2	420	608[a], 688[a]	8a
$Co^{II}TPP$	$CHCl_3$	411	528	18
$Co^{II}TPP$	$CHCl_3$	430	544, 584	18

[a] Calculated from the figure.

Table 5.2 Wavenumbers (cm^{-1}) of Resonance Raman Bands for $Co^{II}TPP$, $Co^{III}(TPP)^{+}$ and $Co^{III}(TPP)^{2+\bullet}$ Complexes (Chloride Adduct).[a]

$Co^{II}TPP$	$Co^{III}(TPP)^{+}$	$Co^{III}(TPP)^{2+\bullet}$	**Mode no. and Assignment**
1600 (0.37)[b]	1600	1600 (0.37)	ϕ_4(phenyl)
——	——	1581	ν_{10}, $\nu(C_\alpha C_m)_{asym}$
1569 (0.19)	1569	1533 (0.44)	ν_2, $\nu(C_\beta C_\beta)$
——	——	1556	ν_{19}, $\nu(C_\alpha C_m)_{asym}$
1510	1511	——	ϕ_5(phenyl)
1499 (0.47)	1505	1493 (0.46)	ν_{11}, $\nu(C_\beta C_\beta)$
1485	——	——	
1467 (0.37)	1466	1464	ν_3, $\nu(C_\alpha C_m)_{sym}$
1429 (0.41)	1429	1430 (0.41)	ν_{28}, $\nu(C_\alpha C_m)_{sym}$
1369 (0.22)	1368	1372 (0.37)	ν_4, ν(Pyr.half-ring)$_{sym}$
1304 (0.53)	1305	1304 (0.40)	ν_{12}, ν(Pyr.half-ring)$_{sym}$
1270 (0.42)	1270	1269	ν_{27}, $\nu(C_m Ph)$
1234 (0.30)	1234	1237 (0.32)	ν_1, $\nu(C_m Ph)$

[a]From ref. No. 19. [b]Depoalrization ratio measured in CS_2 and $C_2H_2Cl_4$.

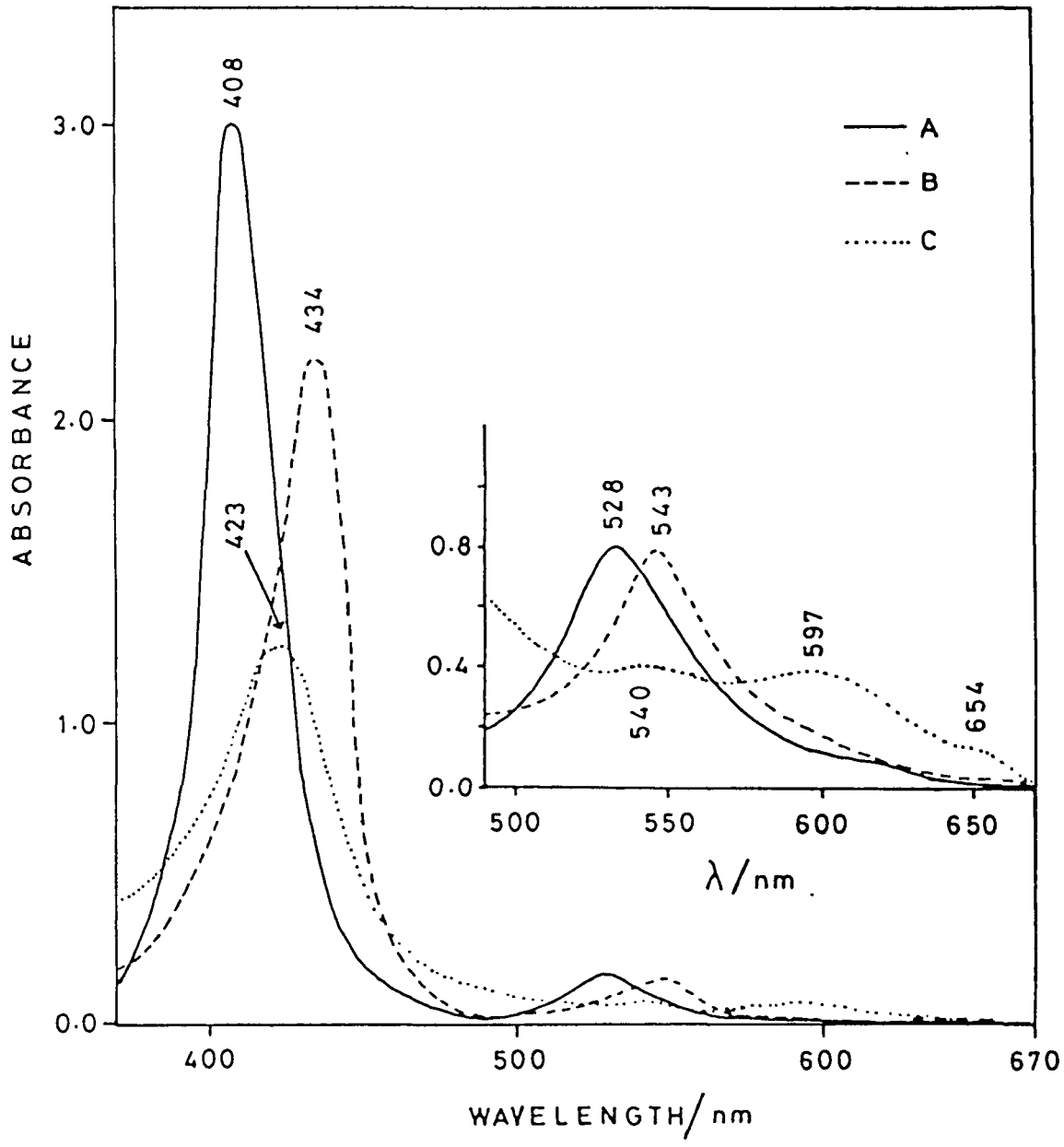

Fig. 5.1 Absorption spectra of $Co^{II}TPP$ and its chemically oxidized products in CH_2Cl_2: (A) $Co^{II}TPP$; (B) $Co^{III}(TPP)^+Cl^-$; (C) $Co^{III}(TPP)^{2+\bullet}2Br^-$ (reddish brown). Scan rate: 2 nm/s.

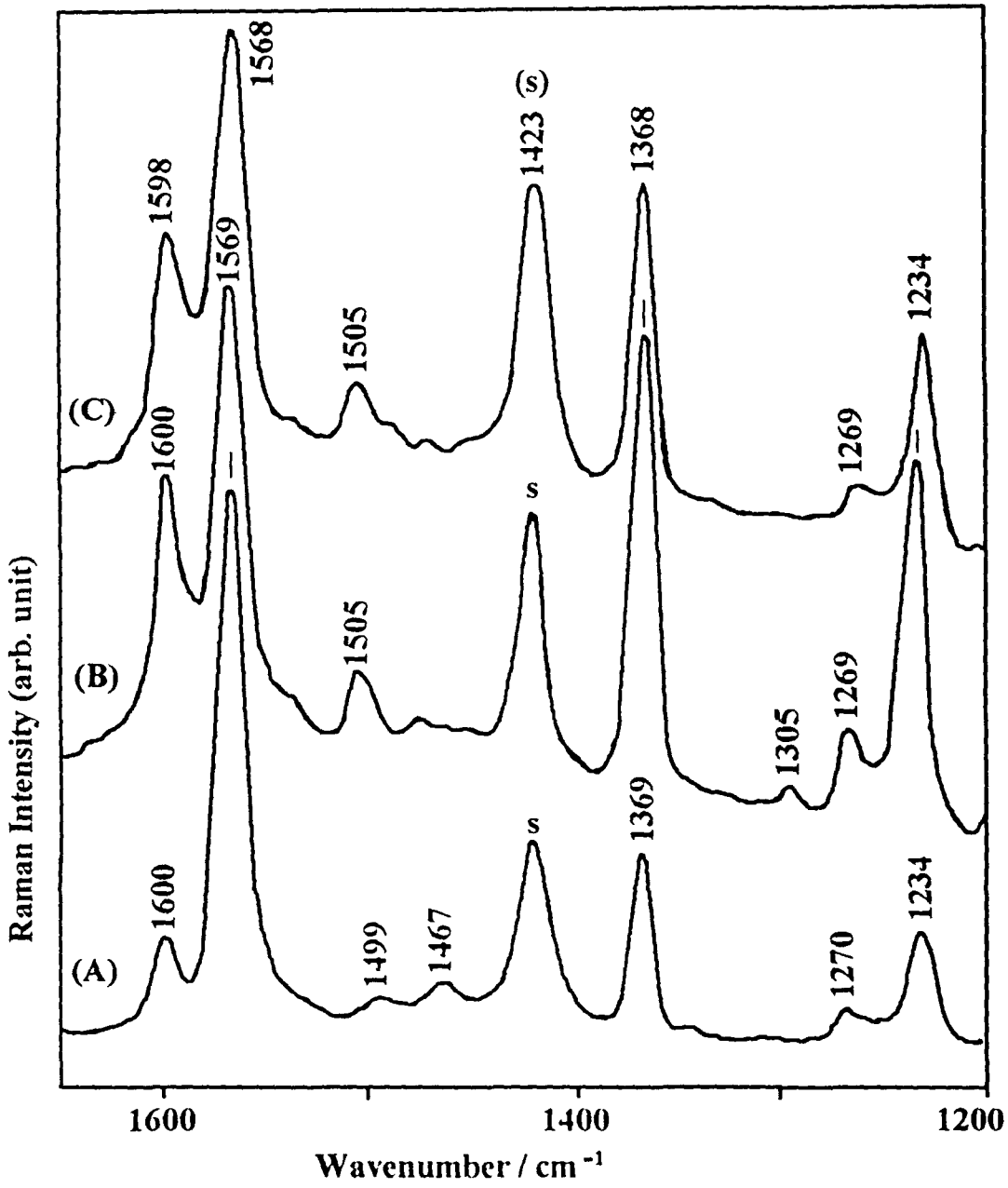

Fig. 5.2 Resonance Raman spectra (1200-1650 cm^{-1}) of (A) $Co^{II}TPP$ in CH_2Cl_2; (B) $Co^{III}(TPP)^+Cl^-$ in CH_2Cl_2; (C) $Co^{III}(TPP)^+Br^-$ in CH_2Cl_2. λ_{ex} = 441.6 nm. The letter "S" indicates solvent band.

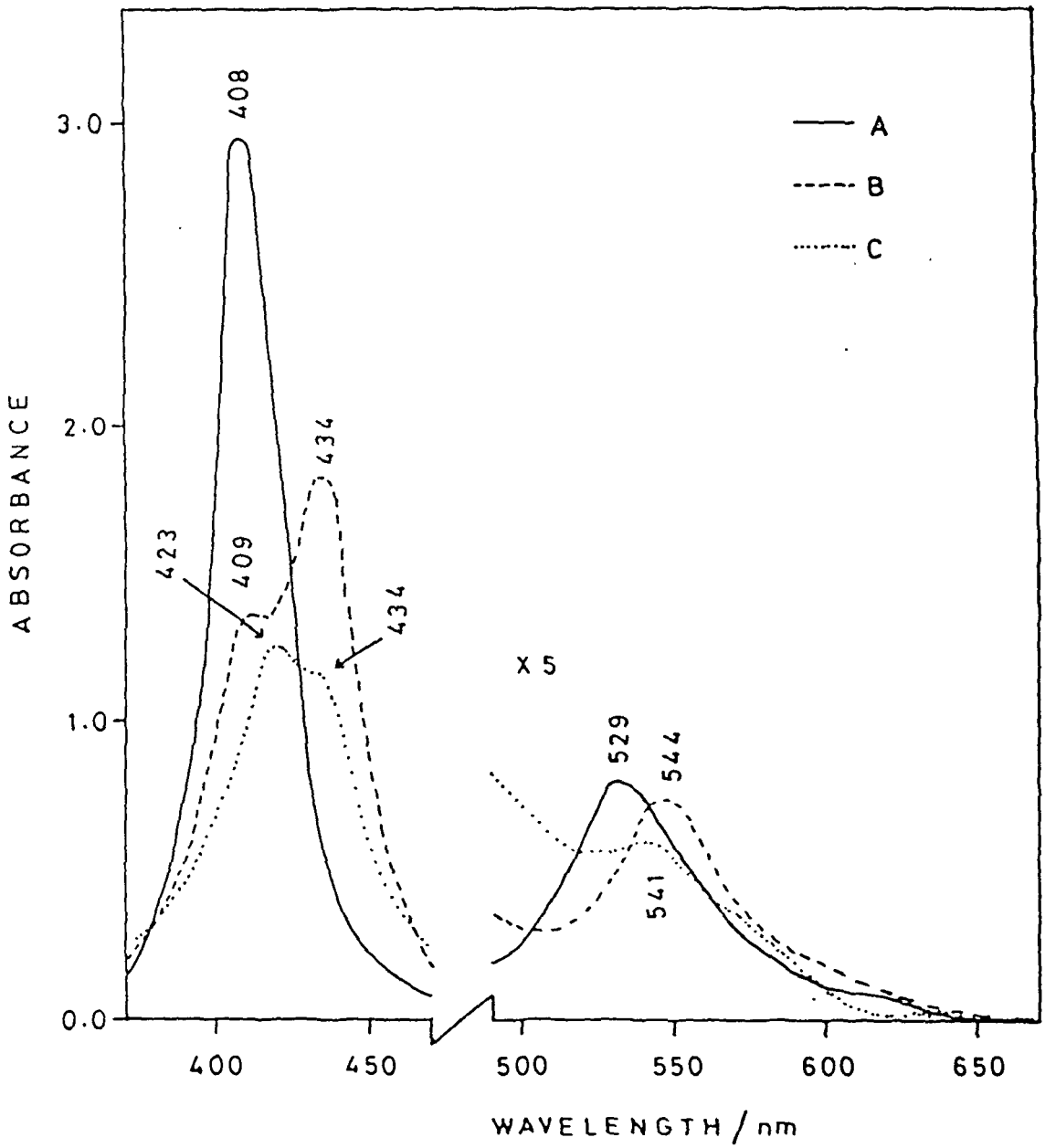

Fig. 5.3 Absorption spectra of $Co^{II}TPP$ (1.5 mM) in CH_2Cl_2: (A) after storing in dark for 24 hr in the presence of p-BQ (aerobic); (B) after 45 min excitation with 441.6 nm (35 mW, focussed) in the presence of p-BQ under anaerobic condition; (C) same as 'B' but under aerobic condition. Scan rate: 2 nm/s. Conc. of p-BQ = 100 mM.

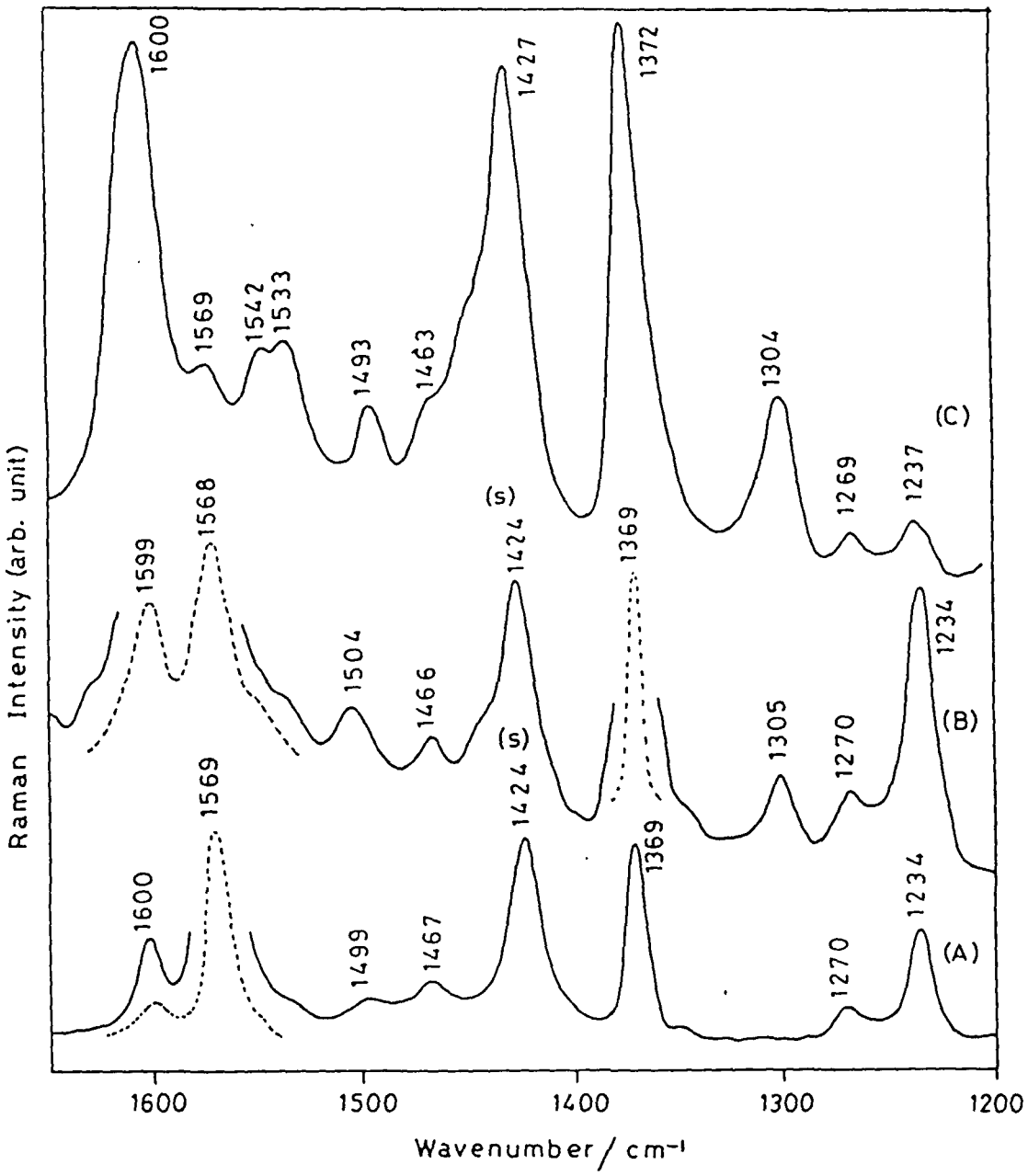

Fig. 5.4 The 441.6 nm excited resonance Raman spectra (1200-1650 cm^{-1}) of (A) $Co^{II}TPP$ (1.5 mM) in CH_2Cl_2 ; (B) in the presence of p-BQ (anaerobic); (C) in the presence of p-BQ (aerobic). The letter "S" indicates solvent band. Conc. of p-BQ = 100 mM.

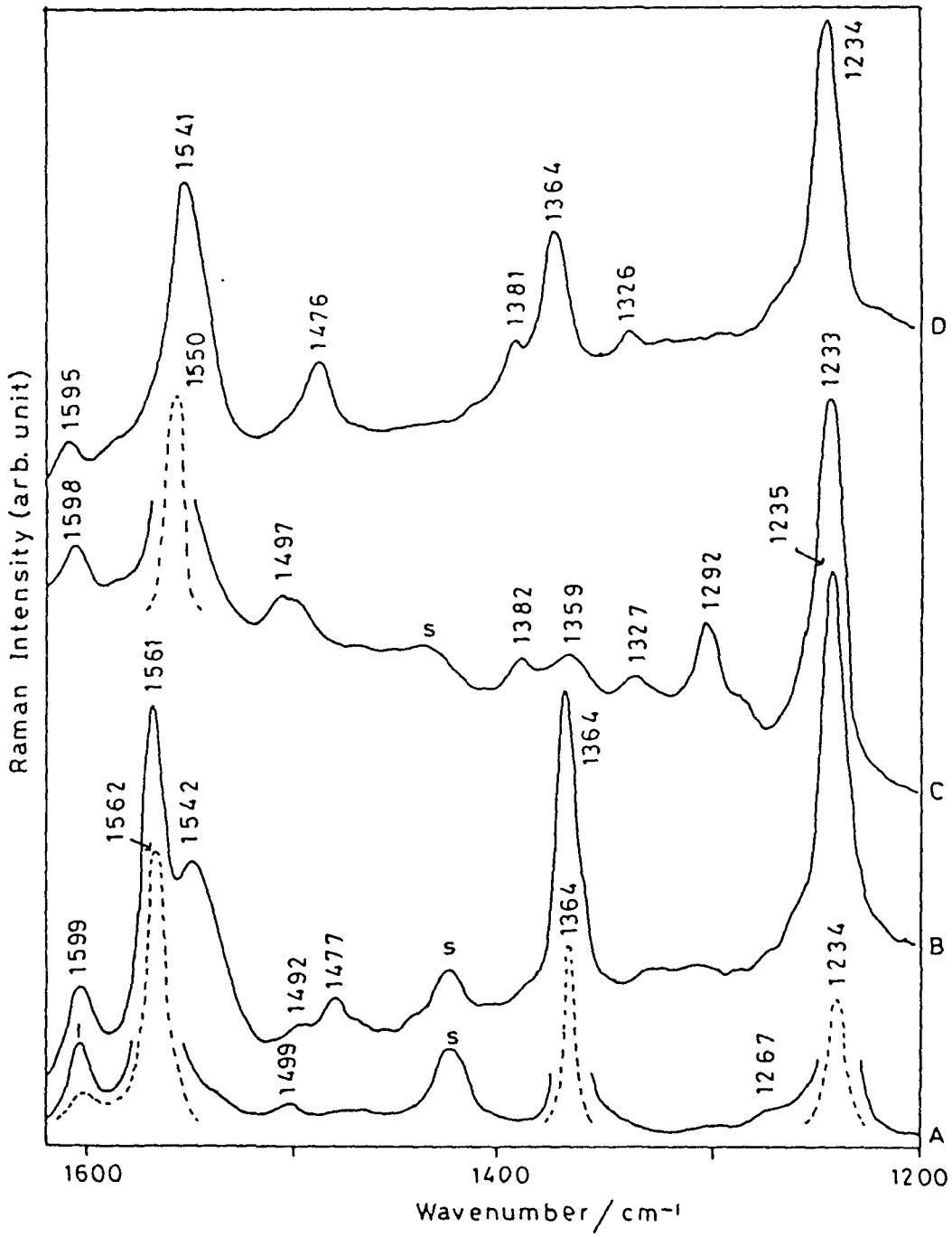

Fig. 5.5 RR spectra (1200-1620 cm^{-1}) of CuTPP and H_2TPP in CH_2Cl_2 under aerobic conditions. (A) CuTPP; (B) CuTPP + p-BQ; (C) H_2TPP; (D) H_2TPP + p-BQ. λ_{ex} = 441.6 nm. The letter "S" indicates solvent band.

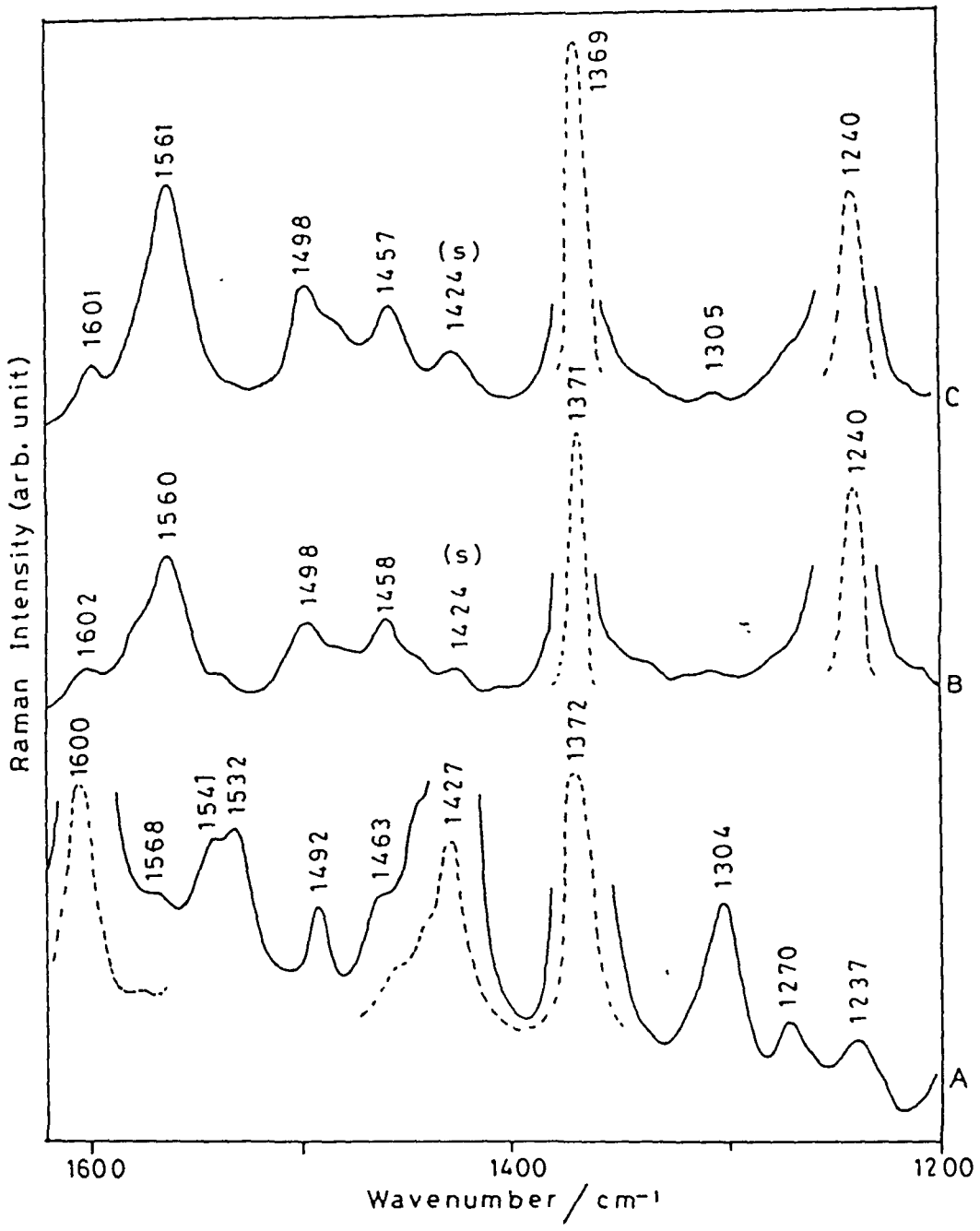

Fig. 5.6 RR spectra (1200-1620 cm^{-1}) of CoTPP in the presence of 2-MeIm in CH_2Cl_2. (A) $Co^{II}TPP$ + p-BQ (aerobic); (B) after addition of 2-MeIm to sample "A"; (C) $Co^{II}TPP$ + 2-MeIm. . λ_{ex} = 441.6 nm. The letter "S" indicates solvent band.

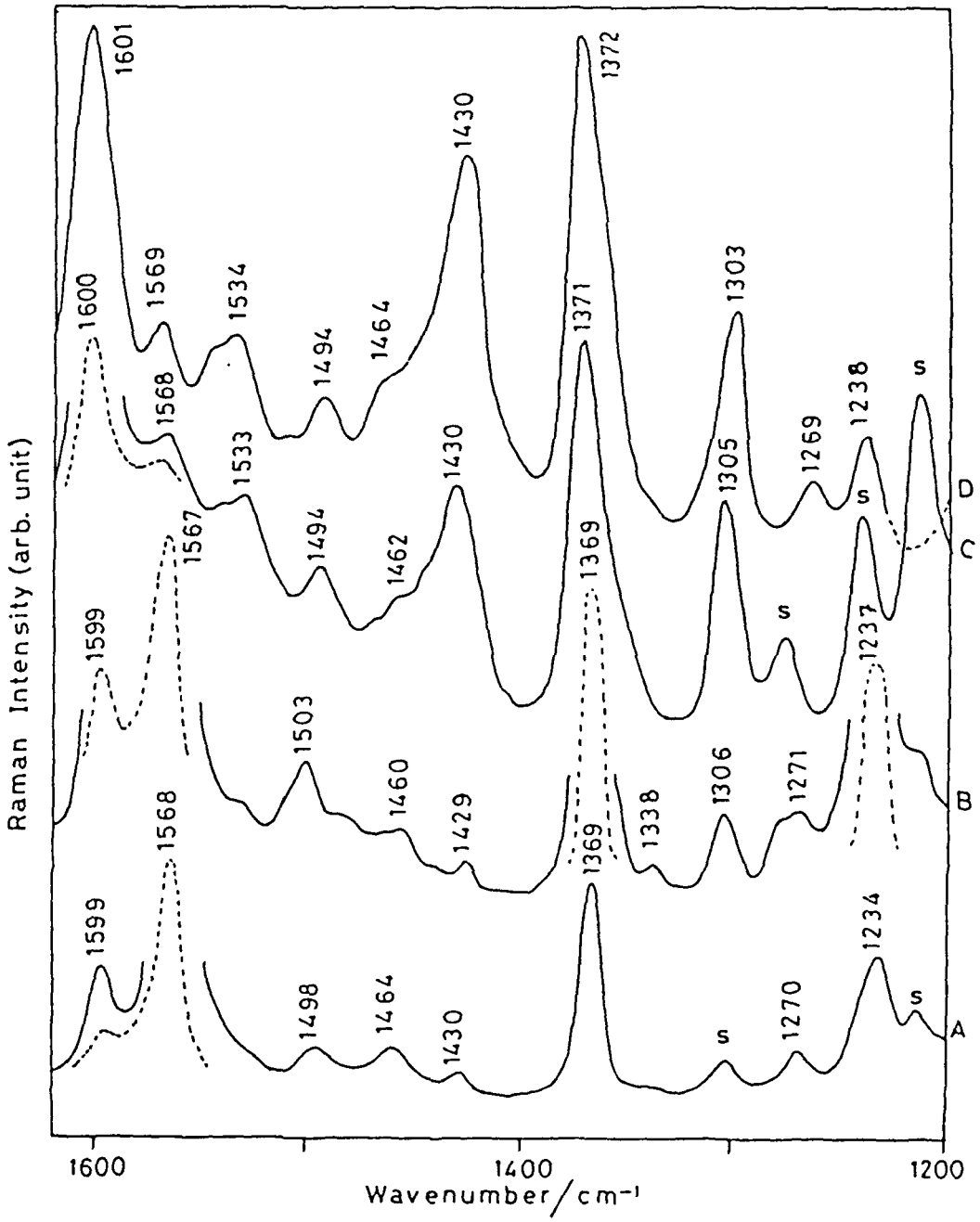

Fig. 5.7 The 441.6 nm excited RR spectra (1200-1620 cm^{-1}) of $Co^{II}TPP$ (1.5 mM) under different conditions. (A) in $C_2H_2Cl_4$; (B) in $C_2H_2Cl_4$ + p-BQ (anaerobic); (C) in $C_2H_2Cl_4$ + p-BQ (aerobic); (D) in $C_2H_4Cl_2$ + p-BQ (aerobic). Conc. of p-BQ = 100 mM. The letter "S" indicates solvent band.

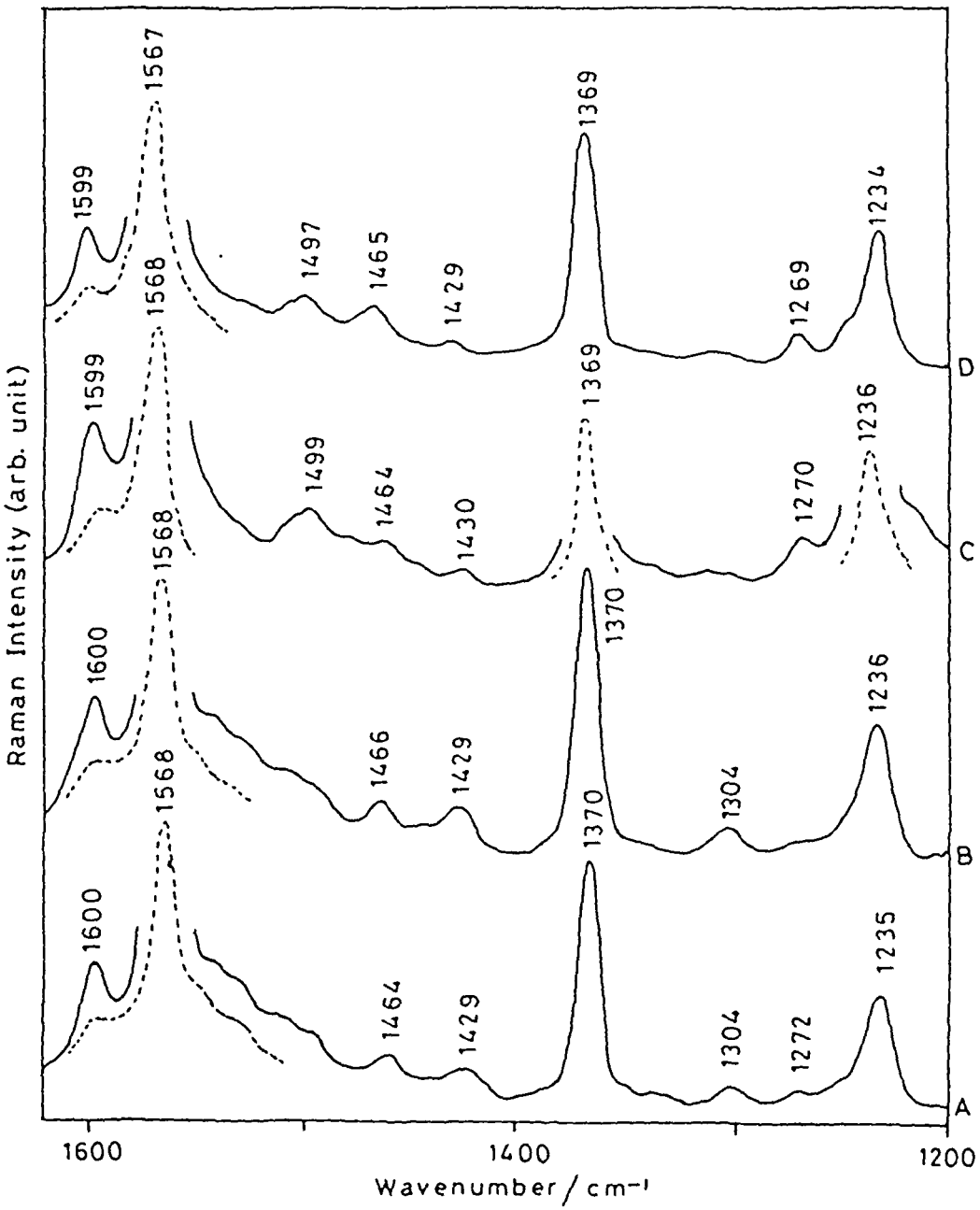

Fig. 5.8 The 441.6 nm excited RR spectra (1200-1620 cm^{-1}) of $Co^{II}TPP$ in different solvents under aerobic conditions. (A) in CCl_4; (B) in CCl_4 + p-BQ; (C) in CS_2 + p-BQ; (D) in $CHCl_3$ + p-BQ.

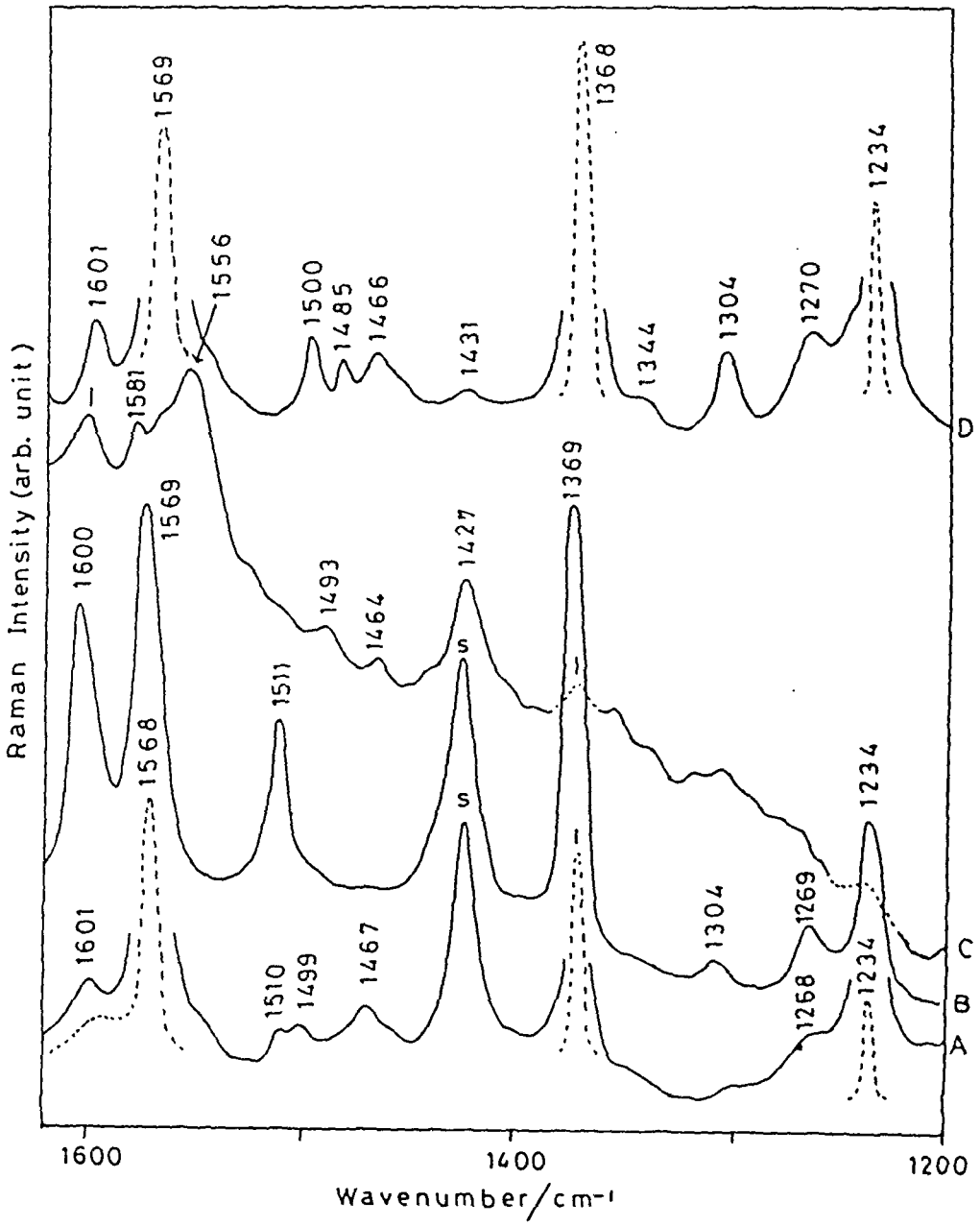

Fig. 5.9 RR spectra (1200-1620 cm^{-1}) of CoTPP at 488 and 406.7 nm excitations. (A) $Co^{II}TPP$ in CH_2Cl_2 (488 nm); (B) $Co^{III}(TPP)^+Cl^-$ in CH_2Cl_2 (488 nm); (C) $Co^{II}TPP$ + *p*-BQ in CH_2Cl_2 (488 nm); (D) $Co^{II}TPP$ in CCl_4 (406.7 nm). All the spectra were recorded under aerobic conditions. The letter "S" indicates solvent band.

CHAPTER 6

Excitation Wavelength Dependence of Photoreduction of Cytochrome-c and Its Mechanism Monitored by Resonance Raman Spectroscopy

---

In this chapter we report photoreduction of cytochrome-c (cyt-c) as a function of pH, excitation wavelengths, laser power and salt/buffer concentrations studied by resonance Raman (RR) spectroscopy. During the course of our RR studies, we noticed that highly purified monomeric cytochrome-c at neutral pH exhibited extensive photoreduction under anaerobic conditions (a fore pressure of 10^{-5} Torr) upon laser irradiation in the 400-450 nm region and the resonance Raman (RR) spectrum of the photoreduced species was identical with that of the chemically reduced species. However, only partial photoreduction occurred at pH 10.1 where the axial methionine ligand is replaced probably by lysine, and no photoreduction took place after the transitions with pK_a = 12.76 and 2.5 where the axial histidine ligand is replaced by other residue. The photoreduction was completely inhibited in the presence of oxygen suggesting active participation of a triplet state in this process. The relative quantum yield for photoreduction of cyt-c at neutral pH as a function of excitation wavelengths shows a weak maximum centered around 410 nm while it increases almost exponentially when excitation wavelength is moved from 380 to 330 nm and then tends to saturate from 330 to 260 nm. Immediate electron donors to the heme and plausible mechanisms of the photoreduction are discussed.

6.1 Introduction

Cytochrome-c (cyt-c) is a water soluble heme protein with M_r = 12,4000 and shuttles electrons between two membrane-bound proteins, cytochrome-bc_1 complex and cytochrome-c oxidase, of the mitochondrial electron transfer chain. The active site is a mesoheme, which is covalently bound to the protein via two thioehter linkages. Under physiological pH the heme iron adopts the F^{2+}- or Fe^{3+} -low spin state and its two axial positions are occupied by methionyl sulfur (Met-80) and histidyl nitrogen (His-18) .[1a]

The molecular structure of cyt-c has been revealed at the level of 1.5 Å resolution by Takano and Dickerson, [1b] and there are only minor structural differences between the reduced and oxidized forms.[1c] Since the heme group is buried within the protein, numerous physicochemical studies have been conducted to delineate various pathways for movement of the electrons to the heme . Met-80 has been considered to play a crucial role in the redox process[2] while according to other views, electrons may tunnel to the heme through some aromatic residues[2,3] or through the exposed front portion of the heme edge.[4,5] A mixing of the iron t_{2g} orbitals with the porphyrin π orbitals may extend the effective metal redox orbital density to the heme edge which may facilitate electron transfer to the metal, but the situation is still far from clear.

Ferri cyt-c undergoes five distinct pH-dependent structural changes[6] with pK_a values of 0.42, 2.50, 9.35, and 12.76 and they are named as Forms I, II, III, IV, and V from the acidic side.[4,7a] When the pH is raised above 9.35 for ferri cyt-c, the NMR

methyl signal of the coordinated methionine [6b] as well as the absorption band at 695 nm disappear, but the heme iron remains in the low-spin state and the axial Met-80 ligand is replaced by Lys-79.[8] Raising the pH beyond 12.8 (Form V) produces another low-spin form with unfolded protein conformation in which the axial ligands are suggested to be His-18 and OH^- ion.[2] Acidification of ferri cyt-c causes the heme crevice to open and leads to a partially unfolded structure (Form II) in which the heme iron adopts the high-spin form and is coordinated presumably by two solvent water molecules.[1,2]

During the course of our resonance Raman (RR) studies,[9] we noticed that highly purified ferri cyt-c at neutral pH undergoes photoreduction under anaerobic conditions upon laser irradiation in the 400-440 nm region. Later on, Gu et al.,[10] have reported detailed studies of photoreduction in many heme proteins including cyt-c by illumination at discrete wavelengths and characterized the photoreduced products using optical absorption and resonance Raman spectroscopies. They also measured photoreduction cross-section as a function of excitation wavelengths and suggested that heme axial ligands play important role and the process may involve multiple electron donors. Occurrence of photoreduction had also been noticed long back in many heme proteins upon laser excitation,[11] though not much is still known about its mechanism and the nature of electron donors. However, RR studies on photoreduction of model iron-porphyrins in the presence of external electron donors suggest that the photoreduction is a ligand aided process where a coordinated ligand is detached in the electronically excited state of porphyrin donating its charge to produce reduced species.[12] In spite of many efforts, a clear understanding and

elucidation of the photoreduction mechanism of cyt-c and other heme proteins is lacking. As the cyt-c undergoes a series of reversible conformational transitions involving replacement of axial ligands with change of pH, it is expected that pH dependent studies may help in clarifying the role of axial ligands and other amino acids in the photoreduction process. Therefore, in order to gain information about an access route of electrons to the redox center either within or from the surroundings of the protein, we undertook the present study of photoreduction of cyt-c as a function of pH, excitation wavelengths, laser power, salt and buffer concentration. We find that the photoreduction in the 450-390 nm excitation range involves active participation of excited heme while the process in the 380 to 260 nm excitation range is more complicated due to occurrence of photooxidation also. Almost exponential yield of photoreduction suggests direct participation of aromatic amino acid residues of the protein and may involve contributions from multiple electron donors.

6.2 Experimental Procedures

The horse heart cyt-c (Sigma type VI) was dialyzed against 0.01 M phosphate buffer at 0° C for several hours and subjected to the column chromatography on CM-52 (Whatman) just before use. The absorption spectrum showed the characteristic features of highly purified cyt-c having an absorption ratio at 280/410 nm of less than 0.20. The pH of the solution was adjusted by HCl or NaOH. The cyt-c solution with a concentration of 30 μM was placed in a quartz cell having a Teflon stopcock (to avoid contact with grease) and evacuated thoroughly in repeated cycles without freezing the solution with a fore-pressure of 10^{-5} Torr. The

absorption spectra were monitored before and after each Raman measurement with the same cell. A fresh sample was used for each pH-dependent study.

The wavelength dependence of photoreduction was measured from 450 to 260 nm at intervals of 10 nm using high photon flux from Okazaki large spectrograph. The thoroughly degassed solution (30 μM conc.) was placed in the same quartz cell of 2 mm thickness used for Raman measurements and illuminated for 10 minutes at different wavelengths by adjusting the photon flux to $5x10^{14}$ photons/s-cm^2 over the entire cross-section of the sample cell using appropriate neutral density filters from Hoya Co., Tokyo. The fluence rates were measured with a photon density meter Model HK-1 made by Institute for Physical and Chemical Research, Saitama, Japan. The optical absorption spectra were recorded on a Hitachi 124S spectrophotometer before and after illumination of the sample and the extent of photoreduction was monitored from changes in the α–β absorption bands of cyt-c. A fresh sample was used for irradiation at each wavelength. Since the absorption bands due to the oxidized and reduced forms overlap, the fraction Φ of the photoreduced species at any wavelength of illumination was determined using the relation.[13]

$$\Phi = \frac{[\text{Ferro cyt-c}]}{[\text{Total cyt-c}]} = \frac{[A_\lambda - A_{o\lambda}]}{[A_{R\lambda} - A_{o\lambda}]}$$

Where A_λ is the absorbance of the sample at the peak of the α-band at 550 nm due to irradiation at wavelength λ, $A_{o\lambda}$ and $A_{R\lambda}$ are the absorbances of the fully oxidized and fully reduced species at the peak of the α-band of cyt-c.

Raman scattering was excited with a Kr (Spectra-Physics, model 164), He/Cd (Kinmon Electronics, model CDR80MGE), and Ar lasers (NEC, model GLG3200)

and recorded on a JEOL-400D Raman spectrometer equipped with a cooled RCA 31034 photomultiplier and photon counting electronics. The Raman shifts were calibrated with indene for each excitation line.

6.3 Results

The visible absorption spectrum of monomeric and polymeric forms of ferri cyt-c at pH 6.95 are shown in Fig. 6.1. The polymeric form is characterized by the absence of the absorption band at 695 nm, typical blurring of the absorption features around 280 nm.[6] The spectra of monomer were obtained just after purification and they remained unaltered after 24 hours, whereas the polymeric form under anaerobic conditions exhibited, rather unexpectedly, dark reduction. The spectral changes in the $\alpha-\beta$ bands region of the anaerobic polymeric form are illustrated in Fig. 6.1(B) as a function of time. The protein was almost completely reduced within 24 hr.

A rather unexpected observation was that the freshly purified monomeric cyt-c at neutral pH placed under anaerobic conditions exhibited strong luminescence peaking around 552 nm and its band shape was nearly mirror image of the absorption band. Because of this, RR bands were not detectable upon excitation at 514.5 nm while no emission was observed with the 441.6 and 406.7 nm excitations. In contrast, the solution of cyt-c as received from Sigma Co. did not exhibit luminescence upon excitation at 514.5 nm whereas it gave strong background upon excitation at 441.6 nm. So far such emission had been reported for reduced cyt-c only upon 514.5 nm excitation.[14] and we confirmed it in this study. This emission may arise due to

changes in electronic dephasing in comparison to vibrational decay rates[14b] and may be suppressed by formation of polymeric species.

The RR spectra of the ferri cyt-c at pH 6.95 under aerobic conditions in a static cell excited at 406.7 or 441.6 nm were similar to the reported spectra,[15a] and all the bands are assignable to the ferric low-spin form. The 441.6 nm excited RR spectra in the ν_4 band region for the monomeric and polymeric forms under aerobic and anaerobic conditions are shown in Fig. 6.2. The ν_4 band appears usually around 1360-1363 cm^{-1} and 1370-1375 cm^{-1} for the ferrous and ferric heme proteins, respectively.[15b-d] A weak feature appearing at 1367 cm^{-1} is not due to the reduced species, and has also been detected both in the oxidized and reduced forms of cyt-c as well as in cyt-c_3. When the polymeric form at neutral pH was excited at 441.6 nm, the protein was photoreduced even under aerobic conditions [Fig. 6.2(C)]. However, the monomeric form did not show any photoreduction under aerobic conditions. Excitation of Raman scattering at 406.7 nm converted more efficiently the polymeric ferri cyt-c to ferro cyt-c. The 406.7 nm excited RR spectrum of polymeric cyt-c under anaerobic conditions matches very well with that of the chemically reduced monomeric species and other reported spectra except for the relative intensity of the RR band pair at 348-356 cm^{-1} and wavenumber shifts for a few others bands (see Table 6.1).

Since most of the oxidation-, ligation- and spin-state sensitive bands[16] lie above 1200 cm^{-1}, we give the RR spectra of cyt-c in this region at different pH values in Fig. 6.3, where all the spectra except the spectrum (A) were obtained under anaerobic conditions. It is evident from Figs. 6.3(A) and (B) that ferri cyt-c at neutral

pH does not undergo photoreduction under aerobic conditions, but it is converted completely to the reduced form under anaerobic conditions when excited at 406.7 nm with moderate laser power (10-15 mW at the sample). When the laser power was higher than 60 mW at the sample, it appears that thermal denaturation started and we obtained only partial photoreduction. Therefore, most of the measurements were carried out with a power level of 10-15 mW where there was no indication of denaturation of the protein even after prolonged laser irradiation. Plot of the I_{1362} /I_{1372} intensity ratio Vs laser power (mW) at 406.7 nm excitation is shown in Fig. 6.4. The linear relationship continues up to around 60 mW, but beyond 60 mW power at the sample, photo-oxidation occurs and at around 120 mW power, all the sample is photo-oxidized. With decrease in the power again, photoreduction takes place and the process appears reversible in the beginning and then becomes irreversible giving only the oxidized spectra, most likely due to conformational changes resulting in irreversible secondary photochemical reactions under steady-state irradiation.

When the RR spectrum of ferri cyt-c at pH 10.1 (Form IV) was measured under anaerobic conditions [Fig. 6.3(C)], major fraction of the protein was photoreduced, giving rise to RR bands characteristic of a ferrous low-spin form.[16] However, weak features at 1376 (ν_4), 1502 (ν_3), and 1636 (ν_{10}) cm^{-1} indicate the presence of the ferri cyt-c also. Therefore, at this pH the protein exists as a mixture of reduced (major) and oxidized (minor) low-spin forms while the 695 nm absorption band is completely absent. When the pH was further raised to 12.98 or 13.1 (Form V), the RR spectrum [Fig. 6.3(D)] was characteristic of a ferric low-spin form but the

band positions were slightly different from those of Fig. 6.3(A). Form V was not photoreduced at all even under anaerobic conditions.

At pH 1.81 (Form II), cyt-c gave a mixture-type RR spectrum [Fig. 6.3(E)] which consists of a few sets of band pairs. Upon lowering pH to 0.91 [Fig. 6.3(F)] where the protein still remains in Form II, the shoulder at 1377 cm^{-1} and strong bands at 1504 and 1585 cm^{-1} decreased in intensity drastically compared to those in the spectrum at pH 1.81, and these features persisted in the RR spectra of aerobic solution also. According to the NMR study,[16] the protein at pH 2.0 adopts the high-spin state with H_2O molecules at two axial positions, but it is likely that the protein at pH 1.8 is a spin mixture; the high-spin form gives RR bands at 1632, 1576, 1489, and 1373 cm^{-1} while the low-spin form gives the corresponding bands at 1636, 1585, 1504, and 1377 cm^{-1}. Anyway, both forms were not photoreduced. The observed RR bands at different pH along with their assignments are given in Table 6.1.

Apart from the pH dependent behavior of cyt-c photoreduction, detailed experiments were also conducted on the photoreduction as a function of excitation wavelengths with constant photon flux as well as salt and buffer concentrations and monitored by absorption spectroscopy. We found that illumination of ferri cyt-c by light with wavelength at 380 nm or higher wavelengths, the 695 nm band remained intact in the photoreduced form after chemically oxidizing it (data not shown). However illumination by light below 370 nm showed drastic changes in the spectrum and the yield of photoreduction increased almost exponentially. The relative quantum yield of photoreduction represented in terms of fraction of reduced species manifests different ways of wavelength dependence in the 260-440 nm range of excitation. In

going from visible towards UV region, the yield of photoreduction first attains a weak maximum near 410 nm [Fig. 6.5 and the inset] and then increases almost exponentially when the excitation wavelength is moved from 370 to 330 nm. Below 330 nm the yield tends to get saturated.

Salt/buffer concentration dependence of photoreduction yields at neutral pH are given in Table 6.2 and in the inset of Fig 6.5. The relative quantum yield of photoreduction decreases with increase in the concentration of NaCl or Sodium phosphate buffer. Although both the salts used have the same type of cation, the effect is stronger with phosphate buffer than with NaCl for a given concentration, indicating that the inhibiting effect of salt is related to the type of anion rather than the cation. It was reported that[10] the photoreduction cross-section of cyt-c in citrate/phosphate buffer is larger than in phosphate buffer alone. We believe that the higher dissociation constant of citric acid (~ 10^{-5}) over phosphate (~10^{-8}) suppresses the ionization of the latter into its ions. But due to its large size citrate ion may not enter into the protein matrix, and hence interacts only with the cationic charges on the protein surface. Consequently, presence of citric acid decreases the concentration of phosphate ion inside the protein leading to higher rate of photoreduction in citrate/phosphate buffer than in the phosphate buffer alone.

In order to elucidate the inhibitory action of oxygen in the photoreduction of cyt-c, a degassed solution (phosphate buffer pH 7) of the ferric form was first photoreduced by irradiating with a 100 W lamp for 15 hr. The extent of photoreduction was checked with the relative intensity of the ν_4 mode in the RR spectra of the sample using 441.6 nm excitation [Fig. 6.6 (a)]. The sample was then

thoroughly equilibrated with oxygen and re-excited with 441.6 nm laser line. We did not find any appreciable growth of the characteristic ν_4 band at 1372 cm^{-1} for the oxidized form [Fig. 6.6 (b,c)], implying that the reduced form of cyt-c is not significantly oxidized by oxygen in the excited states.

6.4 Discussion

6.4.1 Electron Donors

The coincidence of the RR spectrum of the photoreduced cyt-c with that of the chemically reduced form rules out a possibility of the reduction of the porphyrin ring to an anion radical or chlorin form as these systems have distinct RR features.[16b] Many suggestions have been advanced in the literature about the possible electron donors in the redox cycle of cyt-c. Met-80 and His-18 axial ligands are considered to play crucial role in the redox process by some[2] while others believe that electrons may tunnel through some amino acids,[2,3] or through the exposed portion of the heme edge.[4,5] Overlapping of the π-orbitals of amino acids and heme may be other effective channel for electron transfer. Since we did not incorporate any external-reducing reagent during the pH changes, it is clear that the photoreduction process involves an active role of some amino acid residues and specific conformation of the protein.

Monomeric cyt-c by excitation at 406.7 or 441.6 nm was photoreduced at pH 6.95 and 10.1 where His-18 was present as the fifth ligand.[1,17] The lack of the 695 nm band at pH 10.1 indicated the absence of Met-80 at the sixth coordination position. Since the RR spectrum at pH 10.1 was of low-spin type, a strong field ligand such as ε-amino group of Lys-79 must occupy the sixth coordination position.[8,17] Therefore,

methionine can be ruled out as possible electron donor for the photoreduction. Cyt-c at pH 13 was not photoreduced at all by excitation in the 400-450 nm region. For alkaline pH greater than 12.0, the sixth ligand is suggested to be OH^- ion[6,13b] with His-18 as the other axial ligand. However, the prominent RR bands at pH 13 [Fig. 6.3(D)] are characteristic of ferric low-spin form,[15,16] but their wavenumbers are slightly different from those of the native [Fig. 6.3(A)] and weak alkaline forms [Fig. 6.3(C)] due to axial ligation changes and unfolding of the protein. The non-photoreducibility of this form where His-18 is present as axial ligand suggests against His-18 acting as direct electron donor, though non-photoreducibility may partly be a result of shift in reduction potential of the protein on changes of axial ligands as well as unfolding of the protein. However, axial histidine may still act as potential electron donor in forms III and IV where protein is in the folded form.

Acidification of cyt-c opens the heme crevice, allowing intrusion of solvent water into the heme crevice. Accordingly, it is considered that below pH 2.5 two water molecules are bound to the heme iron and undergo exchange with bulk water[2b,c] yielding the hexa-coordinated high-spin state. However, RR spectrum at pH 1.81 indicated a thermal mixture of the high- and low-spin forms. Non-photoreducibility of the acidic forms with more open portion of heme in the unfolded protein argues against electron transfer through the exposed portion of the heme. Even in folded conformation (pH 7), the higher rate of photoreduction of cyt-c in citrate/phosphate buffer over phosphate buffer alone[10] suggests that electron donors originate from somewhere within the protein and not from the outside environment.

On the other hand, there is another possibility that aromatic rings like Phe-82 and Tyr-67 come into contact with the porphyrin ring during their thermal vibrations and donate electrons to the heme directly via overlap of their π-orbitals.[2,3] These two residues lie at around 4 A from the nearest carbon atom of porphyrin in the equilibrium structure at neutral pH.[1] Then a slight conformational change of the protein due to pH changes may alter the π-overlap and thus the photoreducibility. The replacement of the sixth ligand from Met-80 to Lys-79 does not require a large conformational change in other parts of the protein[4] but removal of the amino acid residue from the sixth coordination position at extreme alkaline pH may induce a large conformational change and, as a result the π-overlap between the aromatic residue and the heme group would be reduced significantly. Accordingly, the idea of aromatic electron donor can also explain the present observations satisfactorily. Since ionization potential of such aromatic residues is much higher than the energy of the light at 400-440 nm, special mechanism involving a hole-induced electron transfer, as described below, will be required to understand this process in this excitation range. However, the aromatic acids may play important role during irradiation below 370 nm due to their absorption in the 280 nm region.

As the acidic forms of cyt-c have greater part of their hemes exposed to solvent, these might be expected to show enhanced rate of photoreduction compared to the neutral form if electrons have access to the heme through the exposed front edge. In contrast, the contact between the heme and the nonbonding aromatic residues such as Phe-82 and Tyr-67 is greatly reduced in the open structure of the heme pocket and thus the electron transfer between the two groups would be

inhibited. The non-photoreducibility of the acidic forms argues against the mechanism of electron transfer through the exposed part of the heme but favors that through nonbonding aromatic residue.

6.4.2 Role of Oxygen:

As observed in the present work and earlier reports[9,10,18] on photoreduction of ferri cyt-c in the absence of external electron donors, presence of oxygen in the system can completely inhibit the process of photoreduction, whatever is the excitation wavelength. Since oxygen can not reoxidize the reduced cyt-c in the ground electronic state, the non-photoreducibility of the hemeprotein under aerobic condition can result from (1) electron transfer quenching of re-excited photoreduced product or (2) quenching of excited oxidized form by energy transfer to the oxygen molecule. The first possibility is ruled out from the high stability of reduced cyt-c under aerobic conditions and laser excitation [Fig. 6.6]. Therefore, the non-photoreducibility of ferri cyt-c can not result from electron-transfer quenching of re-excited photoreduced product during Raman measurement, but to the energy-transfer quenching of oxidized from in the excited states by O_2.

6.4.3 Mechanisms of Photoreduction

From the discussion so far, it is obvious that heme excited state plays important role for excitation in the 390-440 nm range while below 370 nm illumination, the photophysical and photochemical properties of amino acids may be directly involved in the photoreduction process of cyt-c. Moreover, photooxidation

also starts competing with photoreduction by excitation below 350 nm. We shall try to understand the experimental results in the framework of excited state electron transfer following photoexcitation of the donor (D) and acceptor (A) system. Since photooxidation also occurs, the donor (D) must be regarded to have separate donor and acceptor sites for charge transfer to and from heme chromophore as acceptor A. From different experimental results and the discussion, it emerges that aromatic amino acids may be potential candidates as D, some of which may have donor and some acceptor sites depending upon their pK_α values.

The donor-acceptor (DA) system is excited by photons which may decay or relax to a photoreactive state (DA)*. The photoreactive state then decays to either to ground state or transfers electron from D to A to form transient $(D^+A^-)^*$ excited state which may either undergo back electron transfer to produce (DA)* or may undergo charge separation to give D^+ and A^- species. Schematically,

$$(DA) \xrightarrow{h\nu} (DA)^* \Leftrightarrow (D^+A^-)^* \qquad 6.1$$

$$(D^+A)^* \Leftrightarrow D^+ + A^- \Leftrightarrow D + A \qquad 6.2$$

where D^+ neutralizes its charge with solvent or surroundings in the last step. The charge separation would be favored in polar aqueous environment and under anaerobic conditions. The dependence of photoreduction on the nature of anion of salt present in the system is expected to be a consequence of the binding of the anion to some specific cationic amino acids like lysines on the surface and in the proximal part of the protein,[10,20] thereby exerting inhibitory effect either by interacting with the

charge-separated complex formed during photoreduction or by weakening the overlap of electron clouds between acceptor A and donor B orbitals.

The reverse process of photooxidation may occur where acceptor site in D abstracts an electron from chromophore A as per the scheme:

$$(DA) \xrightarrow{h\nu} (DA)^* \Leftrightarrow (D^-A^+)^* \qquad 6.3$$

$$(D^-A^+)^* \Leftrightarrow D^- + A^+ \Leftrightarrow D + A^+ \qquad 6.4$$

In this framework, it is expected that excited state electron transfer is coupled to some major optical transition of heme and/or of some amino acids. Observation of maximum in photoreduction yield coinciding with Soret absorption of heme is fully consistent with this scheme. However, nearly exponential rise in photoreduction yield on excitation from 370 to 330 nm and then nearly constant yield below 330 nm suggests some sort of chain reaction and the process may result as a combination of increased rate of photooxidation and contribution from other amino acids like axial histidine in the photoreduction process. There is also a possibility of generation of hydrated electrons by irradiation in the absorption region of aromatic amino acids,[21] which may contribute for such high yield of photoreduction below 370 nm excitation. Therefore the process in this excitation region appears complicated and may involve multiple electron donors and combination of many processes. We shall therefore concentrate our discussion of photoreduction by excitation above 370 nm where the results are not complicated by photooxidation and other processes.

Coincidence of the photoreduction yield maximum with that of the Soret band of the heme group suggests that the excited heme may play a dominant role in the photoreduction process. The fact that presence of oxygen in the system cannot

significantly reoxidize ferro cyt-c in the heme excited state further gives support to this idea. Usually oxygen molecules promote the intersystem crossing from the singlet to the triplet in exited states and also the relaxation of the excited triplet state to the ground singlet state. The former is effective in the psec to nsec time region but the latter is effective at much longer time scales. The relaxation time of ferri cyt-c in the excited singlet state is deduced to be 0.5 psec from the psec absorption experiment.[22] Absence of luminescence upon the Soret excitation implies a rapid deactivation of the (π,π^*) state via short-lived low-lying ring-metal CT states such as $[d_\pi, e_g\ (_{\pi^*})]$ and $[a_{2u}(_\pi), d_{z2}]$ and a ligand field state such as (d_π, d_{z2}). The (d_π, d_{z2}) and $[a_{2u}(\pi), d_{z2}]$ states are expected to be dissociative with regard to the axial ligands as the electron density is transferred to the σ-type anti-bonding orbital. Relative energies of all these orbitals have not yet been well established, but for convenience in discussion, appropriate molecular orbital diagram for a Fe^{3+} -low spin heme is drawn in Fig. 6.7.

Out of the various possible relaxation routes, it is most likely that the excited singlet (π,π^*) state (S_1) first relaxes to the lowest triplet (π,π^*) state (T_1) or an energetically closer T_n state due to the intersystem crossing. Afterwards, the $T_1(\pi,\pi^*)$ or $T_n(\pi,\pi^*)$ state relaxes to the ground state [route A in Fig. 6.7] and this would be accelerated by molecular oxygen. In this case the excited electron returns to the original orbital and no photoreduction takes place. However, in the absence of oxygen, the $T_1(\pi,\pi^*)$ or $T_n(\pi,\pi^*)$ state may have a lifetime of μsec order and accordingly, a hole will be present in the low lying a_{2u} orbital for a while. We suggest that an electron is donated to the half-filled a_{2u} orbital directly from an aromatic ring of amino acid residues in contact or from the axial imidazole of His-18

without any significant activation energy [route C]. In other words, this process competes with the relaxation through route A. This electron transfer may occur through direct interaction between the donor and acceptor orbitals or through a molecular orbital including metal orbitals in the case of the axial ligand donor. This would not be unrealistic since HOMO of the axial ligand or aromatic residues are considered to have nearly the same energy as the a_{2u} orbital. Then the excited electron looses the orbital to return. The higher half-filled π orbital of $T_n(\pi,\pi^*)$ state is expected to contain an appreciable amount of the iron d_{z2} character and therefore, the matrix element between the d_π and the half-filled π orbital of $T_n(\pi,\pi)$ would be finite. Since there is a hole in the d_π orbital, the excited electron would relax to the d_π orbital [route B in Fig. 7.6], giving rise to the ferrous low-spin state. The residue that donated an electron may neutralize its charge by exchange with solvent ions, and thus the photoreduction completes without destruction of the protein. This mechanism is plausible either to nonbonding aromatic donor or to the axial histidine donor as the electron transfer processes follow paths of low activation energy, which is an essential condition for the photochemical reaction to compete successfully with the rapid deactivation processes of the heme excited states.

In the case of axial histidine donor, there is another possibility. The π electron of imidazole may be directly excited to the iron d_{z2} orbital, and the triplet ferrous iron (so called intermediate-spin state) is generated as a transient state. Since the ferrous intermediate -spin complex is very unstable in the presence of oxygen,[23] it returns to the original ferric state. However, in the absence of oxygen, the ferrous intermediate-spin state has much longer lifetime. Since the d_{z2} orbital is anti-bonding about Fe-His

bond, the bound histidine cation would be dissociated from the Fe^{2+} ion, neutralize its charge by exchange with solvent ions or other residues and finally rebind to the Fe^{2+} and the photoreduction is completed. This mechanism is plausible because recent subpicosecond studies on some heme proteins and iron porphyrins indicated very fast recombination rates of photodissociated ligands,[24] but there is no observed charge transfer band assignable to the axial imidazole to iron d_{z2} orbital.[25] It is rather suggested that a CT transition from the porphyrin a_{2u} orbital to the iron d_{z2} orbital is present and overlaps with the Soret band.[25] In this case, the process after the formation of hole in the a_{2u} orbital and resultant ferrous intermediate-spin state would be the same as mentioned above.

The photoreduction of a model porphyrin complex was interpreted in terms of the CT transition from the axial 2-methylimidazole to the iron d_{z2} orbital.[12a]. However, since the photoreduction of heme proteins is occasionally conformation sensitive,[11] the photoreduction mechanism might be different between the protein and model systems.

6.4.4 pH Dependence of Photoreduction

In the Soret excited resonance Raman spectra of cyt-c under anaerobic conditions, an extensive photoreduction was observed at neutral pH while only partial reduction occurs at pH 10.1. No photoreduction takes place in the extreme acidic (below pH 4) and alkaline (pH 12.8 and above) forms. Since the protein moiety of cyt-c is known to have inhibiting effect on photoreduction process,[10,26] intrusion of the solvent molecules could not be the main cause for the pH dependent behavior, and

the non-photoreducibility of the hemeprotein in the pH Forms I, II and V can be best understood, as discussed before, in terms of loss of specific interactions of the donor and the acceptor orbitals with the replacement of the axial ligands and opening of the protein structure. The inability of methionine residue to bind to the ferrous center for its stabilization below pH 4 and above pH 12 may also be a reasonable factor. On the other hand the variation of photoreduction yield during the transition from Forms III to IV can be explained with the help of the proposed induced-hole mechanism. As mentioned above, the heme excited state in native cyt-c undergoes rapid radiationless decay through low-lying excited states. The decay process is oxidation state dependent and found to be much faster in the ferric state due to increased interaction between the iron and the porphyrin a_{1u} and a_{2u} orbitals.[27] In the hole-induced mechanism with the donor donating its electron through the metal orbitals, the electron transfer process would be very sensitive to this orbital interaction and hence to the relative energy of the $e_g(d_\pi)$ orbitals. As π-acidic ligand lowers the relative energy of $e_g(d_\pi)$,[28] replacement of the π-acidic methionine ligand with a strong σ-donating Lys-79 in the pH Form IV would certainly destabilize the $e_g(d_\pi)$ orbital leading to decreased orbital interaction and hence the decreased yield of photoreduction of ferri cyt-c compared to Form III. Moreover, binding of the strong σ-bonding lysine ligand produces a cathodic shift in the reduction potential of the iron center[8,19] and increases the net activation energy of non-bonding and axial ligand donors for electron transfer to the heme iron.

6.5 Conclusion

From controlled experiments on photoreduction of cyt-c as a function of pH, excitation wavelength, laser power and salt and buffer concentration, we have been able to exclude Met-80 and the exposed front portion of the heme as the participants in the photoreduction process. The process by excitation in the 390-450 nm range involves active participation of electronically excited heme with aromatic amino acids and/or His-18 as potential electron donors. The process in the 380-260 nm excitation range is more complicated due to occurrence of photooxidation also and may involve contributions from multiple electron donors and processes including reduction by hydrated electrons generated by irradiation in the absorption region of aromatic amino acids. The pH-dependent studies clearly demonstrate that the photoreduction process involves active role of amino acid residues and the protein in only the folded conformation is photoreducible.

References

1. (a) Moore, G.R..; Pettigrew, G.W. *Cytochrome c - Evolutionary, Stuctural and Physicochemical Aspects*; Springer-Verlag: Berlin, 1990. (b) Takano, T.; Dickerson, R.E. *J. Mol. Biol.* 1981, 153, 95. (c) Berghuis, A.M.; Brayer, G.D. *J. Mol. Biol.* 1992, 223, 959.

2. (a) *Structure and Bbonding - Long Range Electron Transfer in Biology*; Palmer, G., Ed.; Springer-Verlag: Berlin, 1991; Vol. 75. (b) Lanir, A.; Aviram, I.; *Arch. Biochem. Biophys.* 1975,166, 439. (c) In *Enzymes*; Dickerson, R.E.; Timkovick, R.; Boyer, P.D., Ed.; Academic Press: New York, 1975; Vol XI.

3. Isied, S.S.; Vassilian, A. *J. Am. Chem. Soc.* 1984, 106, 1726.

4. Wilson, M.T.; Greenwood, C. *Cytochrome c - Multidisciplinary Approach;* Scott, R.A.; Mauk, A.G., Eds.; University Science Books: Mill Valley, CA, 1996.

5. F.A. Amstrong, H.A.O. Hill, N.J. Walton, Quart. Rev. Biophys., 1 (1986) 261.

6. (a) Schejter, A. ; Glauser, S.C.; George, P.; Margoliash, E. *Biochim .Biophys. Acta* 1963, 73, 641. (b) Theorell, H.; Akesson, A. *J. Am .Chem. Soc.* 1971, 93, 1812.

7. Theorell, H.; Akesson, A. *J. Am. Chem. Soc.*1941, 63, 1804. (b) Redfield, A.G.; Gupta, R.K. *Gold Spring Harbor Symp. Quant. Biol.* 1971, 36, 405.

8. Dopner, S.; Hildebrandt, P.; Rosell, F.L.; Mauk , A.G. *J. Am. Chem. Soc.* 1998, 120,11246.

9. Verma, A.L.; Chaudhury, N.K.; Saini, G.S.S. *Raman Spectroscopy*; Banerjee, S.B.; Jha, S.S., Eds.; World Scientific Publishing Co.: Singapore, 1989; pp. 192-209.

10. Gu, Y.; Li, P ; Sage, J.T.; Champion, P.M. *J. Am. Chem. Soc.* 1993, 115, 4993.

11. (a) F. Adar, P.M.; Yonetani, T. *Biochim. Biophys. Acta* 1978, 502, 80. (b) Kitagawa, T.; Nagai, K. *Nature(London)*, 1979, 281, 504. (c) Kitagawa, T.; Chihara, S.; Fushitani, K.; Moirimoto, H. *J. Am. Chem. Soc.* 1984, 106, 1860. (c) Bartocci, C.; Maldotti, A.; Varani, G.; Battioni, P.; Carassitti, V. *Inorg. Chem.* 1991, 30, 1255.

12. (a) Ozaki, Y.; Iriyama, K.; Ogoshi, H.; Kitagawa, T. *J. Am. Chem. Soc.* 1987, 109, 5583. (b) Verma, A.L.; Chaudhury, N.K. *J. Raman Spectrosc.* 1991, 22, 427. (c) Sato, S.; Kamogawa, K.; Aoyagi, K.; Kitagawa, T.; *J. Phys. Chem.* 1992, 96, 10676.

13. Collman, J.P.; Brauman, J.L.; Collins, T.J.; Iverson, B.L.; Lang, G.; Pettman, R.B.; Seccier, J.L.; Walters, M.A. *J. Am. Chem. Soc.* 1983, 105, 3038.

14. (a) Friedman, J.M.; Rousseau, D.L. *Chem. Phys. Lett.*1978, 55, 488. (b) Champion, P.M.; Lange, R.. *J. Chem. Phys.*1980, 73, 5947.

15. (a) Hu, S.; Morris, I.K.; Singh, J.P.; Smith, K.M.; Spiro, T.G. *J. Am. Chem. Soc.*, 1993, 115, 12446. (b) Schomacker, K.T.; Bangcharoenpaurpong, O.; Champion, P.M. *J. Chem. Phys.* 1984, 80, 4701. (c) Kitagawa, T.; Ozaki, Y.; Kyogoku, Y.; Horio, T. *Biochim. Biophys. Acta* 1977, 495, 1. (d) Lanir, A.; Yu, N.T.; Felton, R.H. *Biochemistry* 1979, 18, 1656.

16. Spiro, T.G.; Czernuszewicz, R.S.; Li, X.Y. *Coord. Chem. Rev.* 1990, 100, 541. (b) Kitagawa, T.; Ozaki, Y. *Structure and Bonding* 1987, 64, 71.

17. Hon, X.L.; Dixon, D.W. *FEBS Lett.* 1989, 246, 105. (b) Rosell, F.I.; Ferrer, J.C.; Mauk, A.G. *J. Am. Chem. Soc.*, 1998, 120, 11234.

18. Bartocci, C.; Maldotti, A.; Carassitti, V. ; Traverso, O.; Ferri, A. *Inorg. Chim. Acta* 1985, 107, 5.

19. K.L. Bren, H.B. Gray, J. Am. Chem. Soc. 1993, 115, 10382.

20. Araki, K.; Takeuchi, H. *Biopolymers (Biospectroscopy)* 2000, 57, 169.

21. (a) Bent, D.V.; Hayon, E. *J. Am. Chem. Soc.* 1975, 97, 2599. (b) Steen, H.B. *J. Chem. Phys.* 1974, 61, 3997. (c) McGimpsey, W.G.; Gorner, H. *Photochem. Photobiol.* 1996, 64, 501.

22. Huppert, D.; Straub, K.D.; Rentzepis, P.M.. *Proc. Natl. Acad. Sci. USA* 1977, 74, 4139.

23. Kitagawa, T.; Teraoka, J. *Chem. Phys. Lett.* 1979, 63, 443.

24. (a) Houde, D.; Petrich, J.W.; Rojas, O.L.; Poyart, C.; Antonetti, A.; Martin, J.L. *Ultrafast phenomenon*; Fleming, G.R.; Siegman, A.E., Eds.; Springer-Verlag: Berlin, 1986; p. 419. (b) Traylor, T.G.; Magde, D.; Taube, D.; Jongeward, K. *J. Am. Chem. Soc.* 1987, 109, 5864.

25. . Makinen, M.W; Churg, A.K. In *Iron Porphyrins*; Lever, A.B.P.; Gray, H.B., Eds.; Addison-Wesley: Reading MA, 1983; Part I, pp. 213-214.

26. Vorkink, W.P.; Cusanovich, M.A. *Photochem. Photobiol.* 1974, 19, 205.

27. Cartling, B. *Biological Applications of Raman Spectroscopy*; Spiro, T.G., Ed.; Wiley-Interscience: New York, 1988; Vol. 3, pp. 217-248.

28. Safo, M.K.; Walker, F.A.; Raitsimring, A.M.; Walters, W.P.; Dolata, D.P.; Debrunner, P.G.; Scheidt, W.R. *J. Am. Chem. Soc.* 1994, 116, 7760.

Table 6.1. Observed RR bands in different conformational states of cyt-c with 406.7 nm excitation (15 mW power)

Mode Number, Symmetry, Type[a]	pH 6.95 Aerobic	pH 6.95 Anaerobic	pH 10.1 Anaerobic	pH 12.98 Anaerobic	pH 1.81 Anaerobic	pH 0.91 Anaerobic	Polymeric cyt-c pH 6.95 Anaerobic
	----	----	----	1217 w[b]	1214 vw	1214 vw	1211 vw
ν_{13}, B_{1g}, δC_mH	1232 w	1226 mw	1228 m	----	1232 vw	1231 vw	1230 m
$\nu_5+\nu_9$, A_{1g}	1249 vw 1282 vw	1244 sh ----	1240 sh ----	1240 vw ----	1247 vw ----	---- ----	---- ----
	1302 vw	1299 vw	1299 w	1300 vw	1304 vw	---	1299 vw
ν_{21}, A_{2g}, δC_mH	1318 w	1313 w	1313 w	1321 w	1317 w	1325 w	1313 vvw
ν_4, A_{1g}, νC_aN	----	1362 vvs	1361 vvs	----	----	----	1362 vvs 1367 sh
ν_4, A_{1g}, νC_aN	1372 vs	----	1376 sh	1377 vs	1373 vs 1377 sh	1373 vs	----
ν_{29}, B_{2g}, νC_aC_b	1404 vw	1399 w	1403 w	1409 w	1408 w	1408 w	1397 sh
ν_{28}, B_{2g}	----	1455 vw	----	1437 w 1460 w	1455 vvw	----	----
ν_3, A_{1g}, νC_aC_m	----	1493 m	1493 m	----	1489 m	1489 m	1493 m
ν_3, A_{1g}, νC_aC_m	1503 m	1503 sh	1502 m	1504 m	1504 m	1503 sh	----
ν_{38}, E_u, νC_aC_m	1551 sh	----	----	----	1549 sh	1549 sh	----
ν_{11}, B_{1g}, νC_bC_b	1561 mw	1547 w	1544 mw	1562 mw	----	1568 sh	1547 m 1558 vw
ν_2, A_{1g}, νC_bC_b	----	----	----	1584 sh	1573 s	1576 s	----
ν_2, A_{1g}, νC_bC_b	1586 s	1590 s	1590 s	1590 s	1585 s	1585 s	1590 s
ν_{37}, E_u, νC_bC_b	1602 vw, sh	1602 vw, sh	1603 vw, sh	1603 sh	----	----	1606 sh
ν_{10}, B_{1g}, νC_aC_m	----	1623 w	1622 vw	1612 vw	1616 vw	1617 vw	1623 vw
ν_{10}, B_{1g}, νC_aC_m	1636 w	----	1636 w	1639 w	1636 w	1632 w	----
Observed Spin State	Low spin	Low spin	Low spin	Low spin	High+Low (Thermal mixture)	High+Low (Thermal mixture)	Low spin
Observed Oxidation State	Fe^{3+}	Fe^{2+}	Fe^{2+} +Fe^{3+}	Fe^{3+}	Fe^{3+}	Fe^{3+}	Fe^{2+}

(a) The mode numbering is as per ref. No. 15a

(b) Abbreviations: w=Weak, vw=very weak, mw=medium to weak, s=strong, sh=shoulder

Table 6.2. Effect of NaCl and NaH_2P_4 on the yield of photoreduction of cyt-c

Conc. of NaCl (M)	Conc. of NaH_2PO_4 (M)	Relative Yield of Photoreduction
0.0	0.001	1.2
0.0	0.01	1
0.0	0.2	0.06
0.2	0.01	0.7
2	0.01	0.1

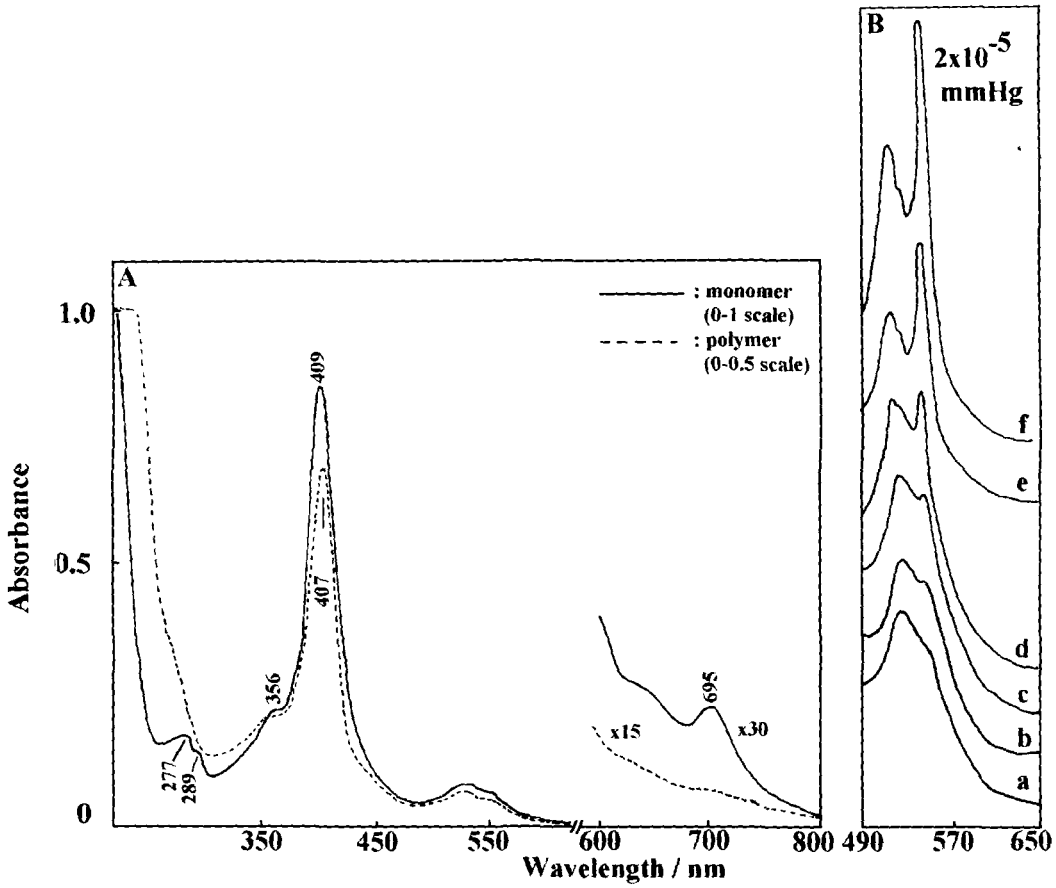

Fig. 6.1 (A) Absorption spectra of purified cytochrome c monomer (solid line) and polymer (broken line) in the presence of air. Absorbance scales : Monomer (0-1A), polymer (0-0.5A) in the 600-200 range; 0-0.03A scale in the 800-600 nm range for both the monomer and polymer. (B) Spectral changes of polymeric cyt-c in the dark as a function of time; (a) aerobic solution; (b)-(f), after evacuating the cell containing the sample until a fore pressure of ~ 10^{-5} Torr; (b) just after evacuation, (c) after 2 hr, (d) after 6 hr, (e) after 10 hr, (f) after 24 hr.

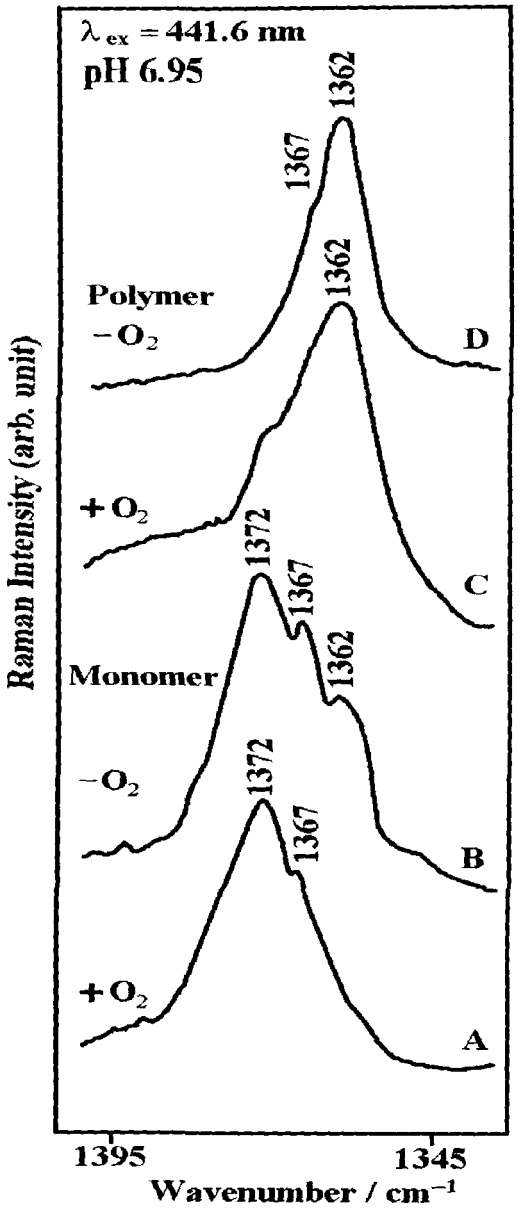

Fig. 6.2 The 441.6 nm excited RR spectra in the ν_4 region of cyt-c under different conditions; laser power, 7.5 mW at the sample; static cell; sample concentration; ~ 10^{-4} M. The spectra A and C correspond to monomeric and polymeric forms under aerobic conditions while B and D are for the monomeric and polymeric forms under anaerobic conditions. Instrumental conditions; sensitivity, 250 counts/sec; scan speed, 5 cm^{-1}/min; time constant, 6.4 sec; spectral resolution, 4 cm^{-1}.

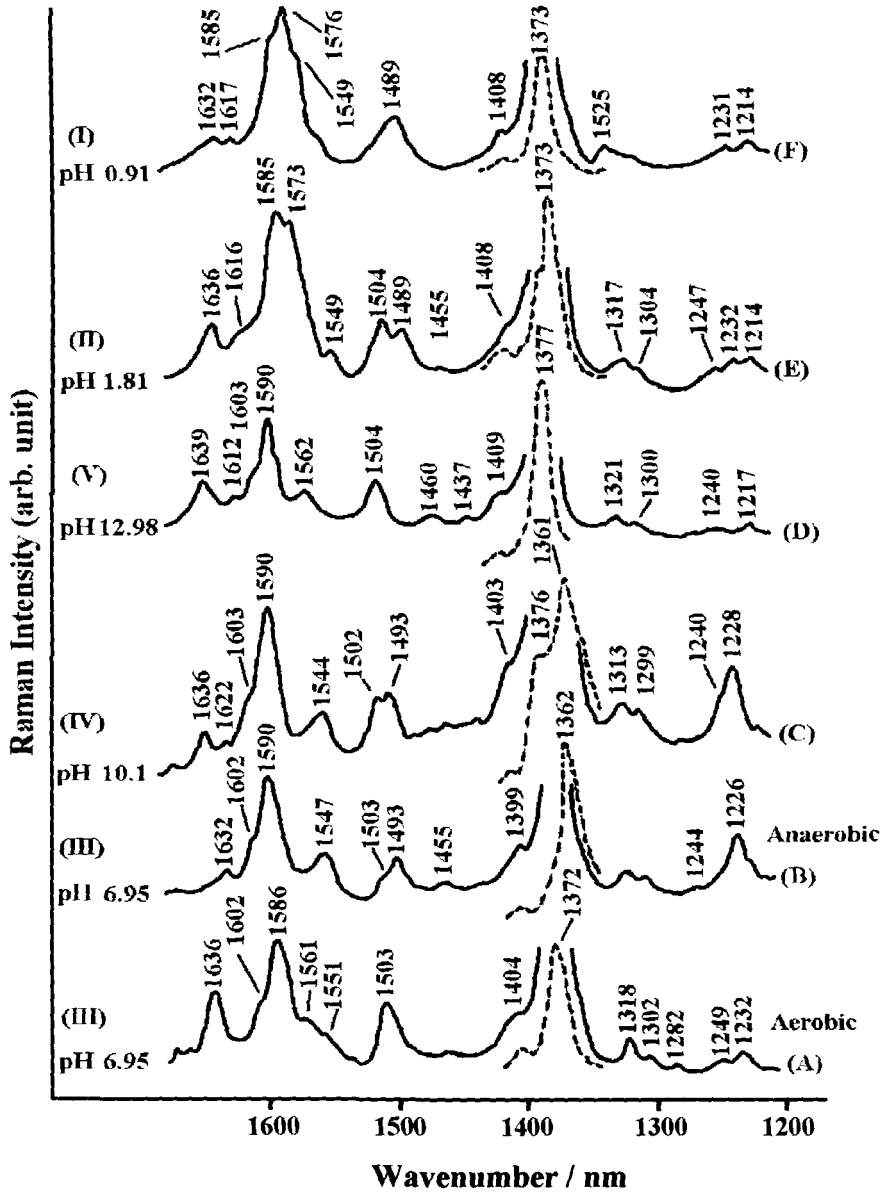

Fig. 6.3 The 406.7 nm-excited RR spectra in the 1200-1700 cm^{-1} region of purified cyt-c at different pH values. Laser power at the sample is 15 mW. Sample concentration is 30 μM for all the spectra. (A) pH 6.95, and under aerobic conditions; (B) pH 6.95, and evacuated until a fore pressure of 10^{-5} Torr (anaerobic); (C) pH 10.1 and anaerobic; (D) pH 12.98 and anaerobic; (E) pH 1.81 and anaerobic; (F) pH 0.91 and anaerobic. Spectrometer: sensitivity, 500 counts/sec; scan speed, 10 cm^{-1} /min; time constant, 3.2 sec; spectral resolution, 4.5 cm^{-1} for all the spectra except B for which the sensitivity was 1000 counts/sec.

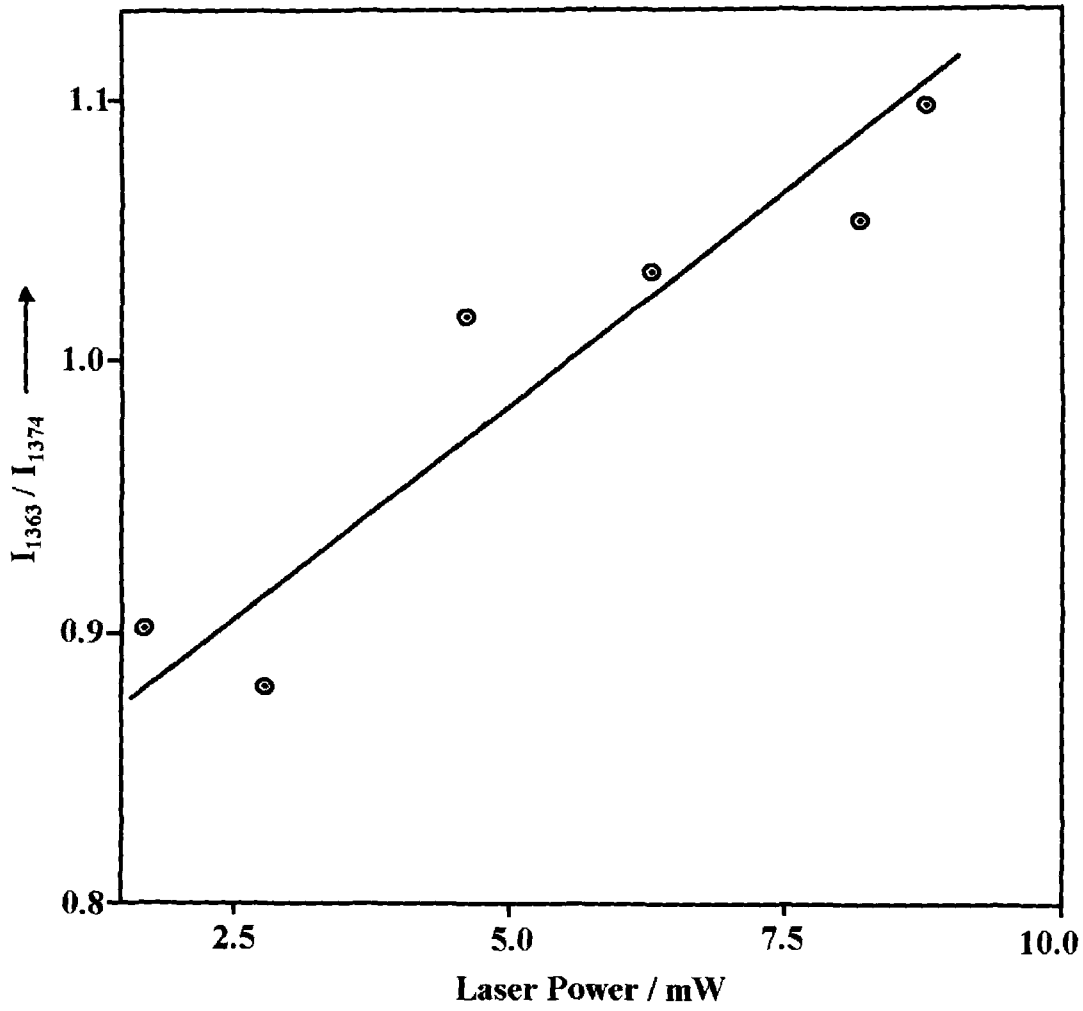

Fig. 6.4 I_{1363}/I_{1374} intensity ratio dependence of cytochrome-c as a function of 406.7 nm laser power at pH 7.02 under anaerobic conditions.

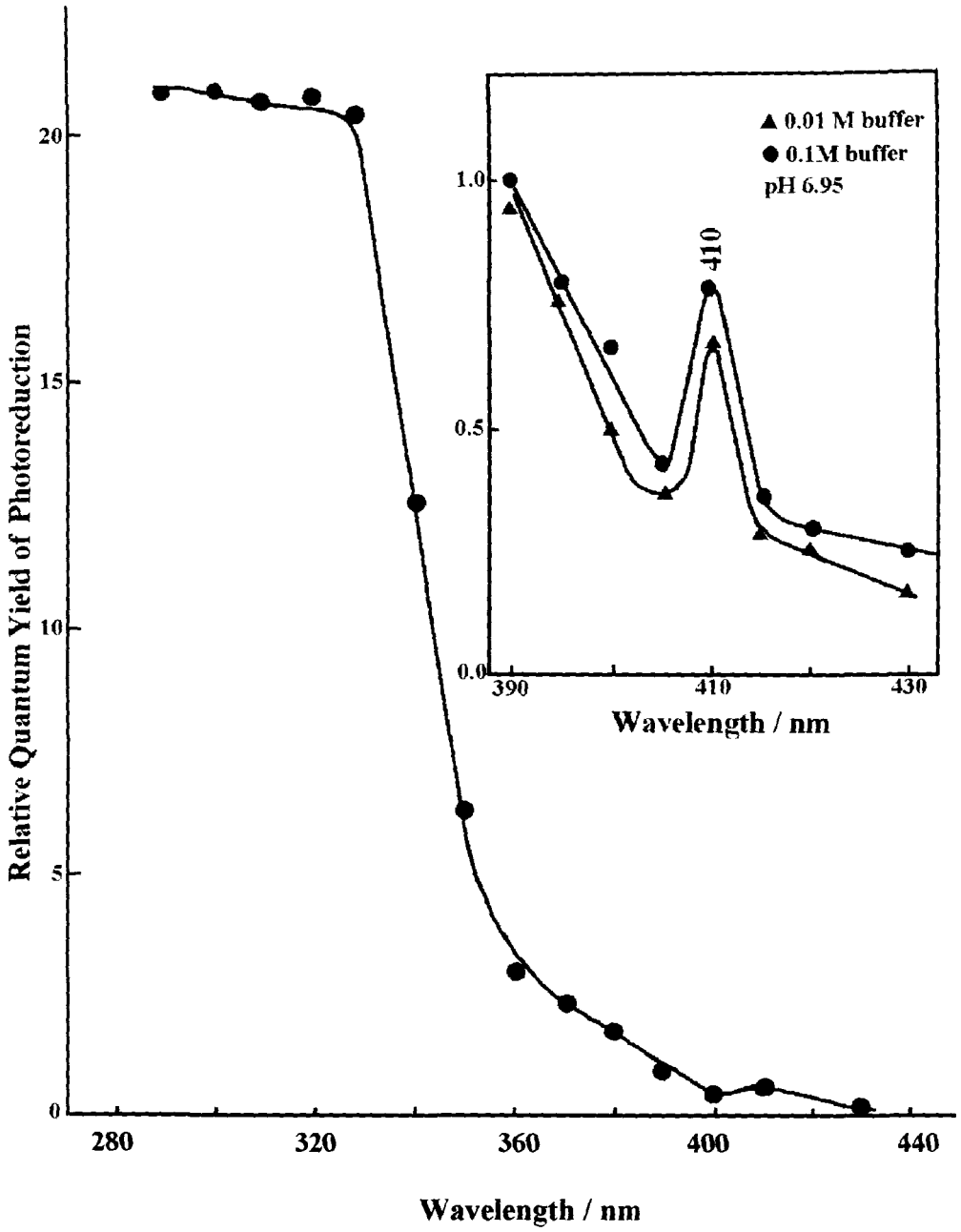

Fig. 6.5 Relative quantum yield of cytochrome-c photoreduction in the 260-430 nm range of excitation wavelengths at pH 6.95 in 0.1 M phosphate buffer. Inset: The 390-430 nm region of the relative quantum yield at two different buffer concentration, 0.01 M and 0.1 M.

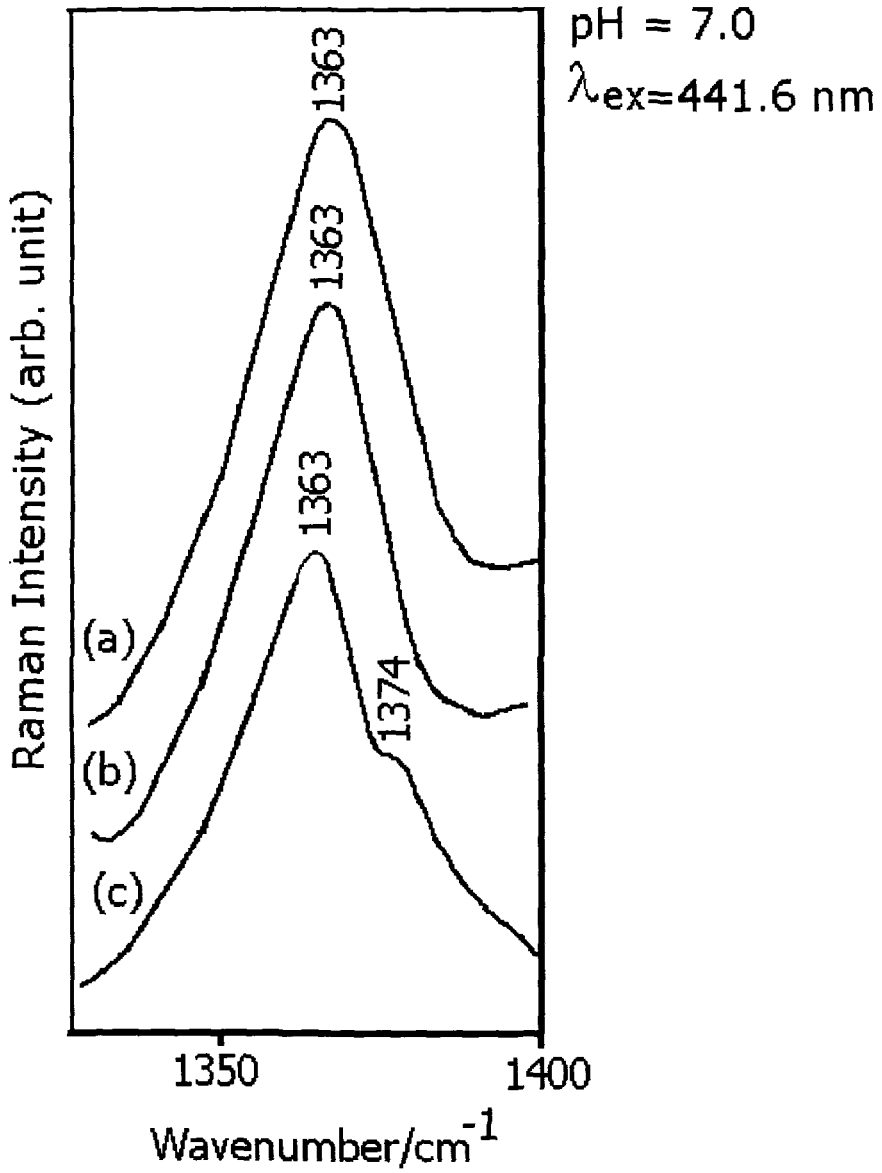

Fig. 6.6 The 441.6 nm excited RR spectra of cytochrome-c in the ν_4 mode region under different conditions at pH 7: (a) just after 16 hrs irradiation with *tungsten light source (100 W) under* N_2 *atmosphere; (b) after shaking the* photoirradiated sample aerobically for 30 min; (c) the same sample after allowing to stand aerobically for 3 hrs.

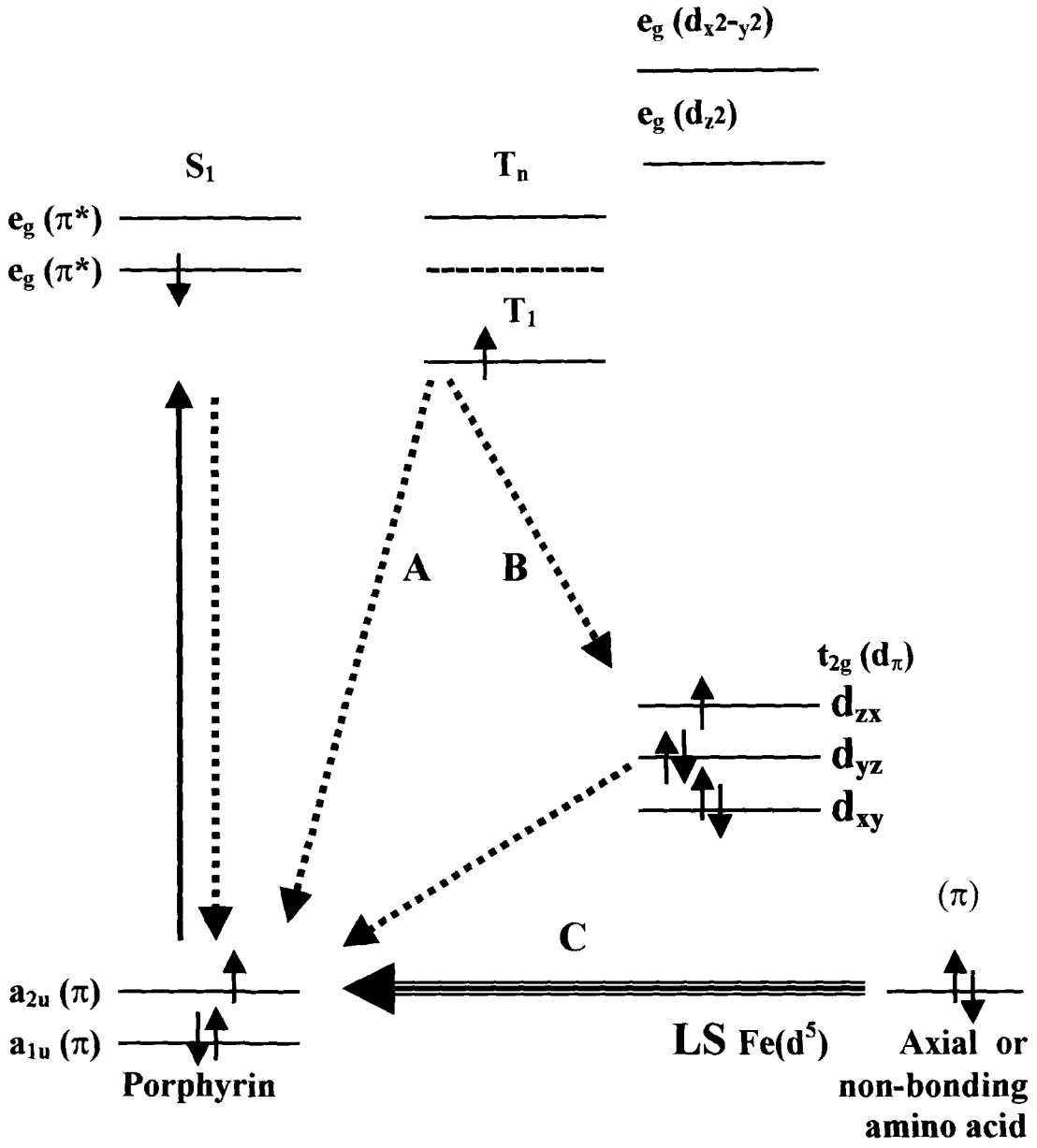

Fig. 6.7 Molecular orbital diagram for a Fe^{III} low-spin porphyrin showing approximate relative energies of porphyrin, metal and axial ligand orbitals. For the convenience in discussion, T_1 and T_n denote the lowest and other π orbitals with triplet configuration of electrons, respectively, although they are normally used to represent the triplet states. Accordingly, energy difference between S (π,π^*) and T (π,π^*) levels implies an energy difference between the same π orbital with the singlet and triplet configurations of electrons.

CHAPTER 7

SUMMARY AND CONCLUSIONS

The present thesis has discussed the basic steps involved in the mechanism of photooxidation of free base octaethylporphyrin and cobalt (II) *meso*-tetraphenylporphyrin as well as photoreduction of cytochrome-c using resonance Raman and optical absorption techniques as probes. These studies on simple model systems and hemeprotein may be of great help in understanding the photocatalytic action of porphyrins in some reactions, the redox reaction process of porphyrins in photochemical splitting of water into hydrogen for solar energy conversion as well as the photosynthetic reactions in green plants, etc.

We have therefore initiated systematic resonance Raman and optical absorption studies on H_2OEP and $Co^{II}TPP$ in the presence of external electron acceptors, and on cytochrome-c under various conditions in order to have better knowledge of the mechanism of photoredox reactions of porphyrins, which may be of great help in gaining insight on electron transfer processes in artificial and biological systems.

Chapter 1 provides a general introduction to the importance of studies of porphyrins and their metal derivatives. Extensive review of earlier studies on the oxidation and reduction processes in porphyrins has been dealt with in this chapter. The importance of resonance Raman technique for studies on these systems compared to other conventional techniques has been described. The basis for employing photo-oxidation/reduction technique and in situ monitoring of the redox process probed by resonance Raman technique has also been emphasized with

various inherent advantageous over conventional chemical and electrochemical techniques.

Sufficient and pertinent theoretical background to understand the absorption and resonance Raman spectra of porphyrins in general is presented in Chapter 2. Essential qualitative description of the principle of photophysical processes was also incorporated in this chapter.

Details of different experimental techniques used in this study for recording the resonance Raman and absorption spectra along with sample preparation and degassing of solutions are given in Chapter 3.

In Chapter 4, we discuss details of our RR and optical absorption studies on the mechanism of photo-induced diacid formation of free base octaethylporphyrin in the presence of external electron acceptors such as chloranil and p-benzoquinone. From our solvent dependent study, we are able to infer that the diacid formation of H_2OEP occurs as a result of photooxidation of the porphyrin to the corresponding π-cation radical, which being highly reactive and unstable, oxidizes the solvent molecule with the generation of proton. Unlike the free base TPP, CCl_4 could not oxidize H_2OEP under laser excitation at 406 or 441.6 nm. However, in the simultaneous presence of p-benzoquinone and methanol or ethanol similar diacid formation could be achieved in CCl_4. In CH_2Cl_2, presence of slight traces of methanol or ethanol greatly inhibits the reaction for OEP acid formation. But on increasing the concentration of methanol or ethanol to about 30%, formation of monoacid derivative of H_2OEP is observed. The large upshifts of the ν_{11} mode wavenumber in the acid derivatives are consistent with predominant a_{1u} character of OEP complexes. However, the unexpected large upshift of the ν_4 mode upon

protonation is inconsistent with expectation for a_{1u} radical type species, and is attributed to arise from deshielding of the N-H protons in the acid derivatives.

Our RR and optical absorption studies do not provide direct evidence for formation of OEP π-cation radical. Since π-cation radical of H_2OEP is known to be very reactive and short lived, its existence as intermediate species is suggested in our discussion. We believe that experiments in rigid matrix at low temperature may help in stabilization of the radical. Time-resolved absorption and resonance Raman techniques using ps set-up would be of great help in detecting the short-lived transient species.

We have extended our studies of photooxidation to cobalt(II) tetraphenylporphyrin in some known non-coordinating alkylchloride solvents in the presence of p-benzoquinone as electron acceptors, as discussed in Chapter 5. It was observed that $Co^{II}TPP$ was photooxidized to $Co^{III}TPP^{+}$ by electron acceptors under anaerobic conditions at 441.6 nm excitation. The two-electron oxidation product, i.e., $Co^{III}(TPP)^{2+\bullet}$ π-cation radical, was formed only when the solution contained molecular oxygen. We infer from these studies that alkylchloride peroxy radicals are responsible for second electron removal form the porphyrin ring. Photooxidation of $Co^{II}TPP$ by p-BQ under aerobic conditions was also found to be very sensitive to the nature of the solvents. The solvent dependent behavior of the photooxidation process was attributed to arise from two factors: (a) different reactivity of the peroxy radicals, and (b) different dielectric constant of the solvents.

Identification of the radical species formed on photooxidation following electron transfer by ESR radical spin traps technique would be of great help in establishing the nature of the transient species involved in the reaction, especially to

understand the mechanism of formation of the two-electron oxidation product of $Co^{II}TPP$.

In Chapter 6, detailed account of RR studies of photoreduction of cytochrome-c as a function of pH, excitation wavelength, laser power, salt and buffer concentrations has been presented. From our controlled experiments on photoreduction of cytochrome-c in the absence of added external electron donor, we have been able to exclude axial Met-80 and the exposed front portion of the heme as the electron donors in the photoreduction process. The photoreduction process by excitation in the 390-450 nm range involves active participation of the excited triplet state of heme with aromatic amino acids/ or axial His-18 as potential electron donors. However, the photoreduction process in the 380-260 nm excitation range is more complicated due to occurrence of photooxidation also and may involve contributions from multiple electron donors and processes including reduction by hydrated electrons generated by irradiation in the absorption region of aromatic amino acids. The pH-dependent studies clearly demonstrate that the photoreduction process involves active role of amino acid residues and the protein in the folded conformation only is photoreducible.

Further studies by other spectroscopic techniques such as time resolved resonance Raman spectroscopy may help in understanding the mechanism of photoreduction in greater details, especially to establish the inhibiting effect of molecular oxygen. Studies on appropriate model compounds such as microperoxidases may also be helpful in clarifying the role of the axial ligands as electron donor in the photoreduction process. pH-dependent studies on photoreduction on excitation from 480 to 300 nm using laser photon flux may further

help in understanding the role of side chains and other amino acids in the photoreduction process of cyt-c and other hemeproteins.

Bio-Data of the Candidate

1.	Name:	HRANGHMINGTHANGA
2.	Father's Name:	LALRINLIANA
3.	Date of Birth:	25th Sept. 1972
4.	Present Address:	Department of Physics North Eastern Hill University Shillong- 793022
5.	Email:	hthanga@rediffmail.com
6.	Permanent Address:	S/o Lalrinliana Chanmari (Ramhlun Road) Aizawl –796007 Mizoram Phone 0389-340091
7.	Nationality:	Indian
8.	Category:	Scheduled Tribe
9.	Sex:	Male

10. Educational Qualifications:

Degree	Year	Institution	Board /University	Subjects	Division	Remarks
Class X	1988	Serchhip Govt. High School.	MBSE	Eng, Science, Soc Sc, Mizo, Maths, etc.	1st div (72.55%)	Obtained Letter Mark in Science
Pre. University (Sc.)	1991	Pachhunga University College	North Eastern Hill University	Eng, Mizo, Maths, Phys, Chem, Stat.	1st div (69.11%)	
B. Sc (Pass)	1993	Pachhunga University College	North Eastern Hill University	Eng, Maths, Phys, Chem.	1st div (62.18%)	
B. Sc (Hons)	1994	Pachhunga University College	North Eastern Hill University	Physics	1st div (65.15%)	6th rank in the University.
M. Sc	1996	North Eastern Hill University	North Eastern Hill University	Physics (Laser Physics)	1st div (73.28%)	1st rank in the University.

11. Details of Fellowships Awarded:

(i) Junior Research Fellow w.e.f. from 1.9.97 to 31.10.98 in a DST sponsored research project entitled "Laser-Induced Photophysical and Photochemical Studies on Some Porphyrins Probed by Resonance Raman Technique".

(ii) Junior Research Fellow w.e.f. from 1.11.98 to 31.10.2000 and Senior Research Fellow w.e.f. 1.11.2000 under CSIR. Fellowship Schemes.

12. List of Publications

(a) Research Papers Published/Communicated in cited International Journals:

(i) Photoreduction of Fe(TPP)Cl in CH_2Cl_2 and DMSO in the presence of and in neat 1,2-dimethylimidazole without alcohol: Evidence for a photoreactive state from resonance Raman and optical absorption studies.
Journal of Raman Spectroscopy, 1998, 29, 997-1001.
P.K. Shantha, H.H. Thanga and A.L. Verma

(ii) Photoreduction of iron protoporphyrin IX chloride in non-ionic triton X-100 micelle studied by electronic absorption and resonance Raman spectoscopies.
Journal of Raman Spectroscopy, 2001, 32, 159-165.
P.K. Shantha, G.S.S. Saini, H.H. Thanga and A.L. Verma

(iii) Photo-induced diacid products of octaethylporphyrin probed by resonance Raman and absorption techniques.
New Journal of Chemistry, 2002, 26, 1-6.
H.H. Thanga and A.L. Verma

(iv) Excitation wavelengths dependence of photoreduction of cytochrome-c and its mechanism monitored by resonance Raman spectroscopy.
Asian Journal of Spectroscopy (in press)
A.L. Verma, H.H. Thanga and T. Kitagawa

(v) Photooxidation of Cobalt (II) meso-tetraphenylporphyrin monitored by optical absorption and resonance Raman spectroscopies.
H.H. Thanga and A.L. Verma (communicated).

(vi) Photoreduction of iron protoporphyrin IX chloride in ionic detergent micelles studied by electronic absorption and resonance Raman spectroscopies.
P.K. Shantha, G.S.S. Saini, H.H. Thanga and A.L. Verma (communicated).

(b) Research Papers Published in Symposium/Conference

(i) Photoreduction of iron protoporphyrin IX chloride in non-ionic triton X-100 micelle studied by electronic absorption and resonance Raman spectoscopies.
P.K. Shantha, G.S.S. Saini, H.H. Thanga and A.L. Verma.
Tenth National Conference on Surfactants, Emulsions and Biocolloids (held at NEHU, Shillong, October 3-5th, 2001)

(ii) Photo-induced diacid products of octaethylporphyrin probed by resonance Raman and absorption techniques.
H.H. Thanga and A.L. Verma.
DAE-BRNS National Laser Symposium (held at Centre for Advanced Technology, Indore, December 19-21st, 2001).

13. Conference Attended:

(i) Tenth National Conference on Surfactants, Emulsions and Biocolloids, held at North Eastern Hill University, Shillong, Meghalaya, India (October, 3-5, 2001).

Date: 9.04.02
Place: Shillong

(HRANGHMINGTHANGA)
Department of Physics
North Eastern Hill University